Effect of cucurbit[6]uril on the structure and dynamics of NaDC gels

by

Sree Gayathri Talluri
Integrated M.Sc, Indian Institute of Technology Kharagpur, 2016
Ph.D, University of Victoria, 2021

A Dissertation Submitted in Partial Fulfillment
of the Requirements for the Degree of

DOCTOR OF PHILOSOPHY

in the Department of Chemistry

Effect of cucurbit[6]uril on the structure and dynamics of NaDC gels

by

Sree Gayathri Talluri
Integrated M.Sc, Indian Institute of Technology Kharagpur, 2016
Ph.D, University of Victoria, 2021

Supervisory Committee

Dr. Cornelia Bohne (Department of Chemistry)
Supervisor

Dr. Alexandre G. Brolo (Department of Chemistry)
Departmental Member

Dr. Irina Paci (Department of Chemistry)
Departmental Member

Dr. Richard Keeler (Department of Physics)
Outside Member

Abstract

Gels are colloidal states of matter in which a solid matrix is dispersed in a liquid phase. Supramolecular gels are formed due to the self-assembly of small gelator molecules in a suitable solvent as a result of specific weak non-covalent interactions between the gelators. The last several decades have witnessed an upsurge in research activities in the area of supramolecular gels not only for academic interests but also for applications in material science. Gels have been investigated as potential avenues for drug delivery and oil recovery applications. Despite their huge potential, the properties of gels are discovered through trial-and-error approaches, which makes control of properties a challenging task. The control becomes extremely hard in a multicomponent gel system, which is a common model for applications in material science.

The aim of this thesis is to design a pathway to gain a fundamental understanding on how multiple components in the gel contribute to new properties. This pathway is an attempt to move away from trial-and-error approaches for the development of gels and allows us to make correlations between structure, dynamics and function.

The studies reported in this thesis were performed on a two-component gel system comprising a gelator and an additive. The gelator, sodium deoxycholate (NaDC), is a bile salt known for its ability to form a supramolecular gel within a certain pH range. NaDC gels are made up of aggregates distributed between the aqueous phase and the gel structure. NaDC gels are reversible and considered as promising candidates from a functional point of view. The additive, cucurbit[6]uril (CB[6]), is a macrocycle and is known to affect the mechanical properties of NaDC gels at the macroscopic level.

In the first project, I studied the effect of CB[6] on the NaDC gel at the microscopic level using dynamic light scattering and fluorescence microscopy experiments. These techniques were used to determine the effect of CB[6] on the gel's morphology, size of NaDC aggregates, thermo-reversible properties of NaDC gels and the kinetics of NaDC gel formation. My results showed that the effect of CB[6] on NaDC aggregates begins in solutions and is translated to sols and gels. Thermo-reversibility and kinetic studies showed that the effect of CB[6] on NaDC gels goes beyond changes to the gel's structure and CB[6] was also shown to affect both the gel-sol transition temperatures and time of the gel formation.

In the second project, I studied how the release of dyes of different hydrophobicities from NaDC gels was affected by the addition of CB[6]. The release of the dyes pyrene and rhodamine 6G was investigated using a static diffusion method, which was referred to as the top layer method. My results showed that CB[6] has a different effect on the release kinetics of a hydrophilic dye compared to the release of a hydrophobic dye. The observed difference in the release kinetics was attributed to differences in the localization of the dyes in NaDC gels and the role of CB[6] in affecting the distribution of dyes in different regions in the gel.

In the third project, I studied the colocalization of a hydrophobic and a hydrophilic dye in NaDC-CB[6] gels with the goal to confirm my hypothesis from the release studies. Dynamics of diffusion of dyes within NaDC-CB[6] gels was investigated using the fluorescence recovery after photobleaching (FRAP) technique. Results from colocalization experiments showed that the

addition of CB[6] changes the distribution of hydrophilic dye in the gel. Through colocalization experiments, I was able to showcase the active role of CB[6] in incorporating aggregates from the aqueous phase into the gel structure. Results from FRAP studies showed that, in the presence of CB[6], recovery after bleaching of a hydrophobic dye in the gel structure is slower compared to the dye in the NaDC gel structure.

Table of Contents

List of Tables

List of Figures

List of Charts

List of Schemes

List of Abbreviations

Asp	Aspartate
K_a	Acid dissociation constant
ANS	8-Anilinonapthalene-1-sulfonic acid
AU	Airy unit
API	N-(4-aminophenyl)imidazole
BAMB	1-aminium 4-methylbenzenesulphonate
BSA	Bovine serum albumin
CB[*n*]	Cucurbit[n]uril
CB[5]	Cucurbit[5]uril
CB[6]	Cucurbit[6]uril
CB[7]	Cucurbit[7]uril
CB[8]	Cucurbit[8]uril
CGC	Critical gelation concentration
CLSM	Confocal laser scanning microscopy
DLS	Dynamic Light Scattering
DNA	Deoxyribonucleic acid
DC^-	Deoxycholate anion
DCA	Deoxycholic acid
Na_2HPO_4	Disodium hydrogen phosphate
D_2O	Deuterium oxide
°C	Degrees Celsius
DSC	Differential scanning calorimetry
DR	Dye release
DAH	Diamino hexane
D_{eff}	Diffusion coefficient
ΔH	Enthalpy change
ΔS	Entropy change
K	Equilibrium constant
FCS	Fluorescence correlation spectroscopy

FRET	Fluorescence resonance energy transfer
FRAP	Fluorescence recovery after photobleaching
T_{gs}	Gel-sol transition temperature
GO	Graphene oxide
ΔG	Gibbs free energy change
GUMBOS	Group of uniform materials based on organic salts
GaAsP	Gallium arsenide phosphide
HPLC	High performance liquid chromatography
HCl	Hydrochloric acid
$T_{1/2}$	Half-life time period
ITC	Isothermal calorimetry
IC_{50}	Inhibitor concentration
LE	Loading efficiency
Lys	Lysine
LWD	Long working distance
LMWG	Low Molecular Weight Gelator
MWCO	Molecular weight cutoff
NaH_2PO_4	Monosodium dihydrogen phosphate
M	Molar
M_f	Mobile fraction
mM	Millimolar
μM	Micromolar
μL	Microliter
mL	Milliliter
mg	Milligram
MB	Mass balance
MCC	Manders correlation coefficient
NA	Numerical aperture
NMR	Nuclear Magnetic Resonance
NMRd	Nuclear magnetic resonance diffusometry

OEGMA10	Poly(2-(2-methoxyethoxy)ethyl methacrylate-co-oligo-(ethylene glycol) methacrylate)
CDPDPM	Poly(2-(dimethylamino)ethyl methacrylate-b-2-(2-methoxyethoxy)ethyl methacrylate)
PCC	Pearsons Correlation coefficient
ROI	Region of interest
siRNA	Short interference ribonucleic acid
SPT	Single particle tracking
NaDC	Sodium deoxycholate
NaTC	Sodium taurocholate
NaTDC	Sodium deoxy taurocholate
NaCh	Sodium cholate
SDS	Sodium dodecyl sulfate
NaCl	Sodium chloride
SEM	Scanning electron microscopy
SAXS	Small angle x-ray scattering
SANS	Small angle neutron scattering
T_{gs}	Gel-sol transition temperature
TEM	Transmission electron microscopy
DSMI	Trans-4-[4-(dimethylamino)styryl]-1-methylpyridinium iodide
TRIS	Tris(Hydroxymethyl)aminomethane
UV-Vis	Ultraviolet-Visible
WAXS	Wide angle x-ray scattering

Acknowledgements

The most important lesson I have learned during my PhD is that the true art in science is figuring out which ideas are good and should rise to the top and which ideas to discard to move science forward. Although I have been the executor of this thesis, a PhD is definitely not an alone effort. It takes a community to support an individual in science. The community of individuals in my PhD journey played an important role in defining my attitude on how I approach science and also how I manage the constant uncertainty around me.

I would like to use this opportunity to thank my parents for teaching me the importance of being independent right from childhood. Although the picture they had in their minds about my life is very different from mine, they slowly adapted to my out-of-the-box life choices. My deepest gratitude to my brother, Dr. Bharath Chandra Talluri for being my strongest advocate and a constant source of inspiration in my life. Despite being separated by time zones, he always remained as the first person I would go to when I need support. I would like to thank my sister-in-law for being a positive influence in my life. I would like to thank my new born nephew, Athulya who besides being a source of entertainment at the peak stages of my thesis writing, taught me how to constantly adapt to changing circumstances. I would like to thank my friends from undergrad Nikhila, Harika, Madhav who despite not being fully aware what a scientific journey entitles to, been a constant support throughout my PhD.

My sincere gratitude to my supervisor Prof. Cornelia Bohne for playing a major role in my decision towards pursuing a PhD and serving as a mentor all the years. She encouraged me to maintain high spirits and been very supportive with my initiative to introduce new techniques to the group. She always amazed me with the way she approaches a research problem and will remain as one of the best scientists I met in my life. I would like to extend the gratitude to my undergraduate research advisor Prof. N.D. Pradeep Singh who helped to shape my scientific journey in the initial stages and for introducing me to the field of photochemistry. My humble respect to Prof. V. Ramamurthy, Prof. John Bower and their research groups for broadening my research interests which helped to pick my niche.

I would like to thank my current and past colleagues of Bohne Group, Dr. Suma Thomas, Dr. Mehraveh Seyedalikhani, Dr. Kevin Vos, Elisa Medeiros dos Santos, Alessandra Menandro, Ankur Awasthi, Helia Hosseini Nejad, Guanqiao Wang, Gustavo Lopas Camelo for

providing me with different perspectives and broadening my point of view in my research projects. My deepest gratefulness to Luis Netter, Jessy Oake and Dr. Stanislav Konorov for all the technical assistance and support. I would like to thank my housemates Priya Angara and Joanna Chen for making me feel Victoria as home. My humble respect to my landlady Jennifer Munro and her family for being very inviting and offering mental health support during the difficult times.

My sincere gratitude to my colleagues at Precision Nanosystems, Dr. Anitha Thomas, Dr. Suraj Abraham, Helena Son, Andrea Bernardo, Logan Ingalls for being a positive influence in my PhD journey. I would like to extend my thanks to the organizations I am part of, ComSciCon CAN, ComSciCon CANWEST, BC girl guides and UVic Women in Science for providing me access to wonderful mentors that are otherwise not possible.

Finally, I would like to thank NSERC CREATE PoND program, NSERC, CAMTEC and UVic for the financial and technical support.

Dedication

To my Brother, Dr. Bharath Chandra Talluri

for always being the wind beneath my wings

Chapter 1 Introduction

1.1 Supramolecular chemistry

Supramolecular chemistry termed as chemistry beyond the molecule, is a science of molecular assemblies.[1] The field of supramolecular chemistry acts as a bridge that connects molecular and macromolecular structures. Unlike the covalent bonds playing a major role in forming molecular structures, supermolecules are complex structures held together by weak non-covalent interactions. Basic functional characteristics of supramolecular systems are recognition, reactivity and transport.[2]

1.1.1 Self-assembly

Self-assembly is a process in which ordered structures are formed spontaneously from a disorganized system of components as a result of weak physical interactions. For self-assembly to occur, components must be mobile. The environment around the components will affect the type of interactions between components which in turn drives the components to form self-assembled structures. Interactions that drive self-assembly include ionic, ion-dipole, dipole-dipole interactions, hydrogen bonding, π- π interactions, van der Waals forces, and metal-ligand interactions.[3] Although not considered as an interaction, the hydrophobic effect can play a role in the self-assembly process in aqueous systems. The hydrophobic effect refers to a process where hydrophobic entities associate with each other in polar solvents to avoid the interactions between polar solvent and non-polar molecules.

In the literature, the terms self-assembly and self-organization are often used interchangeably. The final structure formed by self-assembly is at the thermodynamic minimum, whereas self-organization leads to a structure in a steady state but not necessarily at a thermodynamic minimum. Formation of ordered structures from disordered structures leads to a

decrease in entropy. Therefore, for the self-assembly process to be spontaneous, the enthalpy term should be negative so that the free energy of the reaction is negative. Interactions that drive the self-assembly must be sufficient to overcome the entropic penalty in the formation of ordered states.[4] Self-assembly is an enthalpy driven process in general, but under certain situations an entropy driven process is also possible.[5, 6]

An example of an entropically driven self-assembly process occurs in boloamphhiphilic perylene bisimide dyes bearing oligoethylene glycol chains in water.[7] Although π-π interactions between the dye molecules are enthalpic in nature, the major contribution to self-assembly is the gain of entropy due to the hydrophobic effect and the release of water molecules from the hydration shell of hydrophilic oligoethylene glycol chains.

The concept of autonomous self-organization forms the basis of biological systems and self-assembly processes drive the diversity of structure and function observed in biological processes at the cellular level.[8] The formation of DNA, enzymes, proteins are a result of self-assembly. Molecular recognition leading to self-assembly has profound implications in nature. The ease and efficiency by which nature uses self-assembly to build complex architectures with diverse functions has continuously driven inspiration to chemists towards the design of materials with simpler building blocks. Self-assembly is considered as an efficient process for the bottom-up nanofabrication of materials.

1.1.2 Characteristics of self-assembly based systems

Molecular association leading to self-assembly is reversible and allows the components to adjust their structures, i.e. reorganize and self-correct, once the structures are formed, leading to defect free and complex systems. Since the non-covalent interactions that drive self-assembly

are reversible, structures formed by self-assembly are sensitive to the changes in the environment.

In the chemical world, self-assembly is so far the most promising strategy to form stable (i.e. at the thermodynamic minimum) and structurally diverse nanostructures (1-100 nm) from simple components, that can be difficult to synthesize by classic covalent organic synthesis.[9] For example, self-assembly is the driving force in the formation of molecular crystals, [10, 11] colloids,[12] lipid bilayers,[10] phase separated polymers,[13] or monolayers.[10, 14]

Any entity that interferes with the self-assembly process is regarded as a stimuli. Few examples of stimuli include change in pH, light, mechanical stress, changes in redox potential, heat, and the addition of molecules.[15] The dynamic nature of the interactions in a self-assembly allows the structures to adapt and respond to the application of stimuli. Stimuli responsiveness of self-assembled systems is used as a strategy to incorporate function and properties into materials.[16] For example, in a work by Nieuwenhuizen *et al.* cations have been used as a stimulus to turn on the fluorescence in a crown ether bound fluorophore.[17] Host-guest chemistry between crown ether bonded fluorophores and cations has been used to interrupt the quenching due to photoinduced electron transfer in the fluorophore and turn on the fluorescence. It was found that the host-guest complex formation is different based on the identity of the cation.[17, 18] This approach of using cations as stimuli to promote the self-assembly is used to measure the concentration of ions in the blood.

Self-assembled materials have been actively investigated for applications in drug delivery (active or passive),[19] and tissue engineering.[20] For example, Uludağ *et al.* demonstrated the use of a supramolecular carrier to deliver siRNA to the target site of action.[21] One example for the use of a self-assembly in tissue engineering is the work reported by Kessler *et al.* where

supramolecular materials have been used to regenerate vision by enabling the repair of damaged nerve tissue.[22]

1.2 Gels

The reversible nature of interactions in self-assemblies led to the emergence of materials with diverse properties, such as gels. Gels are defined as colloidal states of matter in which the solid matrix is dispersed in the liquid phase. Gels are viscoelastic materials with liquid like properties, such as the ability to be deformed, and solid like characteristics, such as maintaining a given shape. Gels consist of 3D solid networks and immobilized solvent molecules. Solvent molecules are entrapped inside the solid network through surface tension effects. One way to visually determine if a given material is a gel or not is based on inverting the vial containing the material. If the material does not fall when inverted, then it is considered to be a gel. Gels are useful materials and part of our everyday life. They are found in hair products, tooth paste, cosmetics, adhesives, lubricants and soft lenses.[23]

Gels are classified depending on the origin, type of mobile phase, types of interactions or cross linking that drive the gelation. Gels are divided into categories based on the type of component in the liquid phase of the gel. If the mobile phase is an organic solvent, then the gels are known as organogels. If the mobile phase is water, then the gels are called hydrogels. If one of the mobile phases is air, gels are known as aerogels. If the liquid phase is dried out, then the gels are called xerogels.

Gels are classified as chemical or physical gels based on the interactions that drive the gel formation. Chemical gels are formed as a result of strong covalent interactions. Examples of chemical gels include gels made from polyamide, poly(vinyl alcohol), polyethylene.[24] On the other hand, physical gels or supramolecular gels are formed by weak non-covalent interactions.

Example of physical gels include polymer gels like F127 or gels formed from Low Molecular Weight Gelators (LMWG) (<3000 Da). LMWG are known to form gels in solvents at concentrations as low as < 1 wt%. Examples of LMWG molecules which form supramolecular gels include urea, amides, surfactants, long chain hydrocarbons, peptides, steroids, sugars and fatty acids.[25-31]

1.2.1 Supramolecular gels formed from LMWG

Supramolecular gels are formed when the LMWG is dissolved in a solvent at high temperatures (above gel-sol transition temperature (T_{gs})) followed by slow cooling to room temperature. There are exceptions where gel formation can occur only at high temperatures due to the binding properties of the components in the gel.[30, 31] Other methods, such as sonication, mechanical shaking have also been used for gel preparation.[32, 33] During the gel preparation, self-association of gelator molecules occur to form a matrix that traps solvent mainly by surface tension. The structure of LMWG, and solvent play a major role in the gel formation by facilitating the interactions between gelator molecules and promoting aggregation. The matrix is a result of a hierarchical aggregation process with structures ranging across different length scales from nanometers to micrometers.

The weak physical interactions in supramolecular gels are highly temperature dependent, which in turn make the gels thermally reversible. Thermal responsiveness is a universal characteristic of supramolecular gels and the gel-sol transition occurs at temperatures above the critical gelation temperature for a gel formed at low temperatures. Chemical gels formed by covalent bonds cannot be re-dissolved and are thermally irreversible.[34] This thermal reversibility offers supramolecular gels advantages over chemical gels. For example, the thermal

reversible nature of gels (gel-sol transition) opens up opportunities to trap molecules of interest in the immobilized network and release them, when required.

As a result of weak physical interactions, supramolecular gels have low mechanical strength compared to chemical gels. The reversible nature of interactions in gels can induce interesting mechanical properties, such as thixotropy, and the self-healing of gels. Thixotropy refers to a property in which gel disintegrates into the sol phase on the application of external stress and the gel regains its elastic properties on the removal of stress.[35] Supramolecular gels can self-heal and reform very rapidly after disruption by a shear force.[36] Supramolecular gels are generally stable for long periods of time with the exception of crystallization behavior from the gel structure appearing at longer periods of time.[37]

1.2.2 Gels as functional materials

Chemists explored the functional properties in supramolecular gels using three different approaches: i. tuning molecular structures of the building blocks, ii. using stimuli, iii. introducing additives.[28] Supramolecular gels are rendered sensitive to external stimuli, such as a change in pH,[38] ions, [39] heat[40] or light.[41] For example, incorporating a photo isomerizable unit, such as azobenzene, as a part of the gelator, Shinkai and coworkers induced a reversible gel-sol transition in butanol-cholesterol gels by shining light of different wavelengths on the gel.[42] Irradiation with UV light converted the trans isomer (gelator) into the cis isomer (non-gelator), resulting in the gel-sol transition. Likewise, irradiation with visible light converted the cis isomer (non-gelator) back into the trans isomer (gelator) resulting in the sol-gel transition.

1.3 Applications of supramolecular gels

Supramolecular gels as functional materials have been used for the applications in oil recovery, tissue engineering, optoelectronics, light harvesting, media for crystal growth, drug delivery, and enzymatic reaction media.[43-45] The constrained and compartmentalized nature of the gel provides an advantage for carrying out reactions by bringing the reactants together. The restricted motions in the gel can slow down the kinetics of a reaction compared to reactions carried out in the solution phase.[46] The mechanical characteristics of supramolecular hydrogels resembles tissue components, which makes the gels ideal candidates for tissue engineering applications.

Organogelators, such as alanine derivatives,[47] have been investigated for potential applications in oil spill recovery.[48] In an oil-water mixture, the solid gelator partitioned specifically into the oil phase. Self-assembly of gelators in the oil phase triggered the gelation and thereby the separation of oil from oil-water mixtures.

Shinkai *et al.* designed a naphthalene bisimide gelator for sensing different positional isomers of dihydroxynaphthalene, which are environmental pollutants present in the water and soil.[49] Different isomers formed charge transfer complexes with different colors. This color change is absent in a similar non-gelling matrix, indicating that the gel matrix is crucial for the observed color change.

Biodegradability and biocompatibility are two important requirements for applications *in vivo.* Supramolecular gels formed from components, such as nucleobases, bile salts, carbohydrates, and peptides are found to be biocompatible and biodegradable, and are therefore targeted towards the applications in biology.[50-53] Stimuli responsiveness of supramolecular gels is used as an approach to deliver drugs to the target site, where the stimuli, such as a change in

pH at the target site, leads to the breakdown of the gel structure and release of the drug. This targeted approach to drug delivery can minimize the dosage of drugs required and reduce any side effects. van Esch *et al.* developed a drug delivery system based on a hydrogel-drug conjugate.[54] In the drug delivery system, drug mimics are attached to a cyclohexane trisamide gelling scaffold via an α-chymotrypsin labile linker. In the gel form, the linker is protected from the enzyme inside the cell. However, at higher temperatures, the gel-sol transition occurs and the enzyme has access to the linker, which results in cleavage of the linker and release of the drug.

Chauhan *et al.* developed a gelator based on the α, β-dehydrophenylalanine residue, which formed a hydrogel at neutral pH in acetate buffer.[55] The gel is used as a model drug delivery system to deliver biologically relevant molecules, such as vitamins, antibiotics, and insulin. The presence of ionizable groups, such as amines and carboxylic acids in the gelator provided control on the self-assembly process with a change in pH and salt concentration. As the salt concentration was increased, stronger gels are formed which resulted in the slow release of molecules.

Xu *et al.* used the concept of gelation as a visual test to screen the inhibitors of a phosphatase enzyme.[56] In the absence of inhibitors, the enzyme cleaved the phosphate group from precursor Fmoc-tyrosine phosphate converting it into a hydrophobic form, which formed a gel in water. In the presence of inhibitors, these inhibitors are bound to the active site on the enzyme preventing the phosphate hydrolysis of the precursor and therefore no gelation occurred. This visual inspection of the gel-sol transition is used to further determine the minimum inhibition concentration IC_{50} of the inhibitor.

1.4 NaDC gels

Bile salts are amphiphilic molecules with a hydrophobic convex face and a hydrophilic concave face. Examples of bile salts include sodium deoxycholate (NaDC), sodium taurocholate (NaTC), sodium deoxy taurocholate (NaTDC), sodium cholate (NaCh). The hydrophilic part contributes to the hydrogen bonding and stabilization of water molecules, whereas the hydrophobic part promotes the aggregation. Bile salts self-assemble in water to form nanofiber or helical aggregates.[57, 58] In a model proposed by Small and coworkers, two types of aggregates are found in bile salts.[59] Primary aggregates are formed with 2 to 10 monomers and secondary aggregates are formed as the concentration of bile salt is raised. Primary aggregates are hydrophobic and secondary aggregates are hydrophilic. Bile salt aggregates have different binding properties for the binding of guests. For example, guests bound to the primary aggregates are well protected from anions in the aqueous phase compared to guests located in secondary aggregates.[60-63]

Aggregation properties for bile salts are responsible for functions, such as solubilization of cholesterol, absorption of dietary fats and fat-soluble vitamins and removal of hydrolysis products, such as fatty acids.[64] Bile salts are also known to be adaptable hosts. Therefore, guests with different polarities and sizes can be included in different environments within the aggregates. For example, bile salts are used as hosts for water-insoluble guests, such as photochromic compounds.[65]

There is a clear distinction between the aggregation properties of bile salts and surfactants. Typical surfactants, such as sodium dodecyl sulfate (SDS), have a polar head and hydrophobic chain as a tail. However, bile salts have an amphiphilic structure with a rigid steroid backbone containing hydroxyl and carboxylic acid groups at the polar face, and methyl groups at the non-polar face. The amphiphilic structure on the steroidal backbone of bile salts, rather than clear cut polarity difference between head group and hydrophobic chain in typical surfactants,

make bile salts more complex than the typical surfactants. Unlike regular surfactants like SDS, lack of clear separation between hydrophilic and hydrophobic parts in bile salts, contribute to their distinct aggregation properties. Studies showed that bile salt aggregates have the potential to form gels and the aggregation number increases to very large values near gelation.[57, 58]

NaDC (Chart 1.1) is a bile salt that forms a hydrogel at pH close to neutrality,[66] i.e. around the pK_a of 6.6 for NaDC. At high pH values, the gel does not form and at low pH values, NaDC precipitates.[67] Rodríguez Prieto *et al.* observed an unusual excimer formation of pyrene during the gelation of NaDC.[68] They proposed that gel formation is primarily a result of entanglements between aggregates. In recent work from our group, it was observed that the NaDC gel was made of aggregates out of which 40% are in the aqueous phase and 60% in the gel structure.[69] NaDC is known to form thixotropic gels.[70]

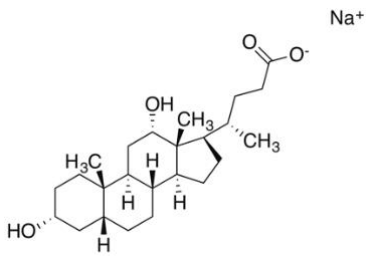

Chart 1.1 Chemical structure of NaDC.

Chemical stimuli, such as the addition of salts and amino acids, were shown to change the properties of NaDC gels. Xu *et al.* demonstrated that the addition of two amino acids L-lysine and L-arginine to NaDC/NaCl gels resulted in a change in phase behavior (i.e. gel-sol transition) at room temperature.[71] The addition of halide salts to the gel was observed to compress the thickness of the electric double layer and reduce electrostatic repulsion between the polar heads of NaDC. As a result, NaDC molecules come closer to each other, which in turn favors the intermolecular hydrogen bonding between NaDC molecules. Enhanced interactions in

the gel network led to an increase in the mechanical strength of the gels.[71] Rodríguez Núñez *et al.* showed that at constant pH and temperature, the storage modulus of the NaDC gel increases by a factor of 100 with an increase in the ionic strength from 0 to 0.6 M NaCl.[72] On the other hand, amino acids were shown to break the hydrogen bonds and weaken the formation of gels leading to a decrease in the mechanical strength of these gels. The gel-sol phase transition in the presence of amino acids have been used to facilitate the release of the dye methylene blue from the entrapped gel network into the sol.[71]

Possible interactions for the NaDC gel formation at neutral pH include the electrostatic interactions between deoxycholate anion (DC^-) and Na^+ in buffer, hydrogen bonding between DC^- and deoxycholic acid (DCA), carboxylate of DC^- and the hydroxyl group of DC^-.[73] Several models suggested hydrogen bonding as the main driving force for NaDC gel formation.[74, 75] The gel-sol transition was shown to be a result of the destruction of hydrogen bonds at high temperatures.[76, 77] These models are further supported by work from Rodríguez Núñez *et al.* where the authors showed that the decrease in the storage modulus at higher temperatures is a result of the weakening of hydrogen bonds.[72] In addition to the temperature, the mechanical strength of NaDC gels is observed to be affected by pH and ionic strength.[72]

1.5 Additives in supramolecular gels

Additives are chemicals added to the gelator to change the properties of the gels. For example, a non-gelling additive can have a significant effect on the gel structure despite not directly affecting the gel formation.[78] Additives are used in three different ways in gels: i. to improve the properties of gels, ii. additive addition leading to the formation of the gel that otherwise cannot be formed without the additive, iii. to modify the self-assembly process.[79-83]

Additives have been used to improve properties, such as the gel's mechanical strength, stability, rigidity and to introduce new functionalities in gels. Shirai *et al.* showed that the addition of polymer additives improved the mechanical strength of gels formed by valine derivatives.[84] In a work by Banerjee *et al.* graphene has been used to improve the rigidity in gels.[85] Additives have been used to modify the self-assembly process i.e. either to facilitate the gel formation[78, 83, 86] or inhibit the gel formation.[87, 88] Xu *et al.* reported a study where the addition of vancomycin to the (Fmoc)-substituted D-alanine gelator led to the transformation of the gel to a sol.[88] The additive vancomycin was shown to interact with the gelating sites of the dimer that are crucial for the self-assembly.[88] In a work by McNeil *et al.* the additive poly(acrylic acid) has been shown to affect the nucleation and growth process in the pyridine based gel resulting in thinner fibers.[78]

In NaDC gels, additives have been used to improve properties, such as the mechanical strength. The effect of salts, metal cations or amino acids on the properties of NaDC gels have been investigated in detail. [58, 89] One such work was reported by Xu *et al.* where a lanthanide salt (europium nitrate) was used to improve the mechanical strength of NaDC gels.[90] Yuan *et al.* found that the addition of graphene oxide (GO) increased the mechanical strength in NaDC gels by providing more binding sites for hydrogen bonding to form in the gel network.[91] Hao *et al.* studied the gel formation mechanisms in NaDC gels in the presence of metal cations.[73] In this work, the authors investigated the differences in the gel formation mechanism by observing changes in morphology, mechanical strength, structure, and the critical gelation concentrations (CGC) under various experimental conditions.

Warner *et al.* investigated NaDC/TRIS hydrogels as templates to develop organic nanoparticles "NanoGUMBOS" (Group of Uniform Materials Based on Organic Salts).[92] TRIS

is used as a modifier to induce the gelation at physiological pH of NaDC gels, which is above the pK_a of NaDC. Warner *et al.* investigated the new properties in these NaDC gels as a function of concentrations of TRIS and pH.[93] Changes in pH and concentrations of TRIS were used to fine-tune the size of NanoGUMBOS, thereby offering a platform for the size-controlled synthesis of these nanoparticles. A small change in the hydrogel conditions was observed to have a drastic effect on the size of nanoparticles (8 nm to 300 nm). Fluorescence anisotropy and microscopy experiments showed that varying the pH and TRIS concentrations changed the structural rigidity and crystallinity in the gels, which led to a change in the gel's mechanical properties and the sol-gel transition temperatures. These changes in gels ultimately affected the size distributions of nanoparticles.

Liu *et al.* investigated the effects of two different polymers, the linear polymer poly(2-(2-methoxyethoxy)ethyl methacrylate-co-oligo-(ethylene glycol) methacrylate) ($P(MEO_2MA_{90}$-co-$OEGMA_{10})$) and the star-shaped polymer poly(2-(dimethylamino)ethyl methacrylate-b-2-(2-methoxyethoxy)ethyl methacrylate) (CDPDPM) on the properties of NaDC/Asp gels.[94] These polymers were added as additives to interact and strengthen the network structure. The oxygen containing functional groups on the polymers provide the binding sites for hydrogen bonding, with CDPDPM providing more binding sites than OEGMA10. Cryo-SEM images showed that the addition of polymers led to denser structures in the gels. The mechanical strength of the NaDC gels increased by 60-fold upon the addition of CDPDPM, and by 2-fold upon the addition of OEGMA10.

1.5.1 Cucurbit[*n*]uril chemistry

Macrocycles with additional receptor sites for guests have been incorporated into gels as additives. These macrocycles act as hosts and bind to guest molecules very selectively through

reversible host-guest interactions. The presence of host cavities for the inclusion of guests and the availability of a library of macrocycles with distinct properties, such as structure, biocompatibility and solubility allows for the introduction of novel functionalities into gels.[95] There are various ways in which macrocycles can affect gel formation. Macrocycles offer a rigid scaffold to direct the binding sites into a position which facilitates gel formation.[96] Macrocycles can be directly involved in the formation of gel fibers through host-guest interactions. Macrocycles can be appended to a gelator molecule as a functional group without direct involvement in gel formation. Macrocycles can be used to enrich the stimuli responsiveness in supramolecular gels.

Cavitands are macrocycles with an intrinsic guest binding cavity.[95] Cucurbit[*n*]urils (CB[*n*]s) belong to the family of cavitands and possess a hydrophilic portal and a hydrophobic cavity. CB[*n*]s are made of glycoluril units and are formed from the condensation reaction between urea and formaldehyde. Varying the number of glycoluril units (*n*) in the macrocycle changes the diameter of the cavity. CB[*n*]s are known for the formation of host-guest complexes with high equilibrium constants compared to other macrocyclic compounds.[97] For example, one of the strongest host-guest complexes known is formed between CB[7] and diamantine diammonium ion with a binding constant of $7.2 \times 10^{17}\ M^{-1}$ in D_2O.[98]

The host-guest chemistry of CB[*n*]s has been used to facilitate the gel formation between polymer strands. For example, Tan *et al.* demonstrated the gel formation between polymer strands, where guest molecules with a higher affinity to CB[*n*] are attached to one polymer strand and the CB[*n*] is attached to another polymer strand.[99] Formation of the host-guest complex between these two polymer strands brings the strands close together to establish crosslinks, which in turn promotes the gel formation.

Wang *et al.* discovered that 1-aminium 4-methylbenzenesulphonate (BAMB) crystallizes as large block-like aggregates.[100] In the presence of CB[6] (Chart 1.2), NMR spectroscopy confirmed the formation of a CB[6]-BAMB pseudo rotaxane. The formation of pseudo rotaxane was observed to disrupt the crystallization process and facilitate the gel formation.

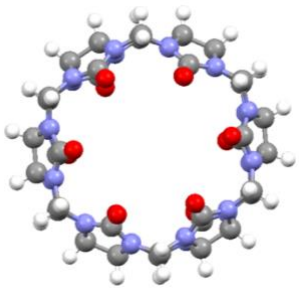

Chart 1.2 Chemical structure of CB[6].

Kim and coworkers found that CB[7] forms a gel in dilute mineral acids in the pH range of 0 to 2.[101] The guest binding properties of CB[7] introduced stimuli responsiveness in the gel. For example, the gel-sol transition occurred on the addition of alkali metal ions to the gel.

Due to its biocompatibility, CB[*n*] based gels have been explored as interesting platforms for therapeutic applications. In a work reported by Scherman *et al.* CB[8] based hydrogels have been investigated for the sustained release of a protein.[102] In another study, Kim *et al.* exploited the host-guest interactions between CB[6] and polyamine conjugated hyaluronic acids to form a supramolecular gel.[103] The gel has been used as a scaffold to entrap NIH3T3 cells for cellular engineering applications.

In earlier work from our group, the effect of CB[6] as an additive on the properties of NaDC gels has been investigated using rheology experiments.[69] Stress sweep experiments were performed to determine the critical stress, a point above which gel breakdown occurs. In a stress-

sweep experiment, the storage and viscous moduli of the gels are monitored as a function of shear stress. The critical stress is used as a parameter to understand the effect of CB[6] on the mechanical strength of NaDC gels. The critical stress was found to be higher for NaDC-CB[6] (40 Pa) compared to NaDC gels alone (16 Pa), indicating that the addition of CB[6] led to stronger gels. Besides the changes for the critical stress, the addition of CB[6] increased the storage and loss moduli of the NaDC gel and increased the gel-sol transition temperature. The formation of stronger gels with CB[6] is attributed to the availability of additional sites for hydrogen bonding (carbonyl groups and amine groups) with CB[6] addition.

Our group investigated the effect of CB[6] in NaDC gels at the molecular level by using steady-state and time-resolved fluorescence experiments as a function of temperature.[69] Results from fluorescence studies showed that the relocation of pyrene from water to the NaDC aggregates occurred during heating of the gel followed by the release of pyrene from aggregates to water during cooling. The relocation of pyrene from aggregates to water during cooling occurred at higher temperatures in the presence of CB[6]. Since weak physical interactions are temperature dependent, relocation of the pyrene during heating is a result of the breaking of hydrogen bonds. This result confirms that CB[6] facilitates the gel formation by offering an extra handle for hydrogen bonds that assists the gel formation. These studies show that CB[6] has an effect on NaDC gels both at the molecular level and at the macroscopic level.

1.6 Existing approaches to explain the function in supramolecular gels

Gelation is discovered through a trial and error approach and by serendipity.[104] Despite the lack of understanding on the self-assembly process, gels have been used as functional materials in high tech applications.[105] However, rational design in gels is still a challenge due to

the lack of understanding of the mechanism for gel formation.[104] The reversible and dynamic nature of supramolecular gels makes it difficult to characterize these gels.

Gel characterization requires information across different length scales, i.e. molecular, microscopic and macroscopic levels. The type of assembly formed at the molecular level can be different from the microscopic level, therefore using a single technique to study the structure is not as informative as it might be assumed. For example, in a two component gel system, it is difficult to characterize the assembly type using a single technique like rheology as both self-sorted and co-assembled gels (Scheme 1.1) have higher mechanical strength compared to gels formed from single components.[106]

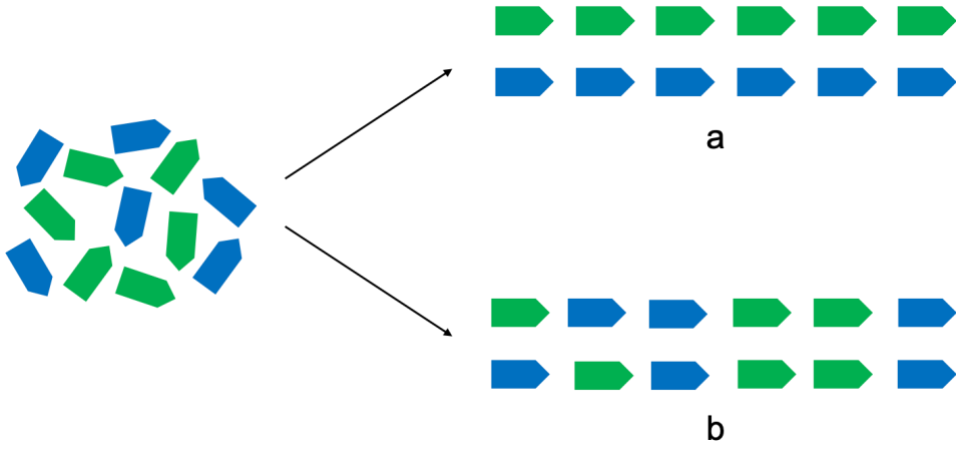

Scheme 1.1 Schematic representation of self-sorted (a) and co-assembled (b) gels.

At the molecular level, techniques such as NMR, UV-Vis absorption, infrared, circular dichroism and fluorescence spectroscopy are used to study molecular packing, follow the gelation process and identify the type of interactions responsible for the gel formation at the molecular level.[107] NMR is used to monitor how much of the gelator has assembled i.e. the relative amount of a gelator that is immobilized in the gel network compared to the liquid phase.[108] UV-Vis spectroscopy is used to determine the aggregation states of gelators, for

example whether the aggregates are H-aggregates or J-aggregates. At the microscopic level, techniques such as microscopy, small angle scattering techniques (SAXS, SANS, WAXS), dynamic light scattering, single crystal diffraction are used to probe the morphology, and the size and shape of aggregates in the gel network.[107] SAXS is used to acquire key parameters for the aggregates, such as its molecular weight, radius of gyration, average particle size, surface to volume ratio.[109] Techniques such as rheology and the determination of gel-sol transition temperatures are used to characterize gels at the macroscopic level.[107] Rheology is used to analyze the mechanical and, self-healing properties or determine the crosslinking density of the gel.

Thermal studies, such as Isothermal titration calorimetry (ITC) and differential scanning calorimetry (DSC) are used to obtain information on the thermodynamics of gel formation. ITC is used to measure the binding affinity (K_a), enthalpy changes (ΔH) and binding stoichiometries (n) of interacting molecules. From those parameters, the Gibbs free energy (ΔG) and entropy (ΔS) are determined using the standard equation. DSC measures the amount of heat absorbed or released during the gel-sol transition. The enthalpy of the gel-sol transition is calculated by integrating the peak corresponding to the transition in the DSC curve. DSC is commonly used to determine the thermal stability of gels.[30]

Although supramolecular gels have been utilized in niche applications and tools to characterize them at the various length scales are known, fundamental insights on the mechanism of gel formation and changes in the gel network on the application of stimuli are very limited. To gain insights on factors that lead to gel formation, understanding of dynamics is essential.[93] Such knowledge is required to be able to design and control new properties in gels.

Introduction of the understanding of dynamics in gels will move gelation from a sporadic phenomenon to a more controllable and functional process. However, existing methods used to characterize the structure of gels are not sufficient to provide information on the dynamics of molecules in the gel. Techniques such as laser flash photolysis, stopped flow and methods such as quenching studies have been used to identify the properties of guests bound to primary and secondary binding sites in bile salt solutions.[110] In a recent work by Khimyak *et al.* dynamics was studied using NMR to understand the gel formation mechanism.[111] In this thesis, I will address the fluorescence techniques used to study the dynamics of bile salt gels.

1.7 Techniques

Fluorescence is described as a process in which molecules absorb light and reemit light at a longer wavelength. Fluorescence techniques are widely used to study supramolecular gels due to the high sensitivity of this technique. For example, low concentrations of fluorophore (μM) can be used to track changes in the gel without affecting the structure of the gel. Fluorophores can be attached to the gel via physical interactions or through chemical crosslinking. Fluorescence emission is sensitive to polarity and the viscosity of the environment in which the fluorophores reside. Fluorescence measurements provide information on a wide range of molecular processes, interactions, rotational diffusion of molecules, binding interactions and conformational changes.

1.7.1 Steady-state fluorescence

Fluorescence spectroscopy is used for analyzing organic compounds with applications in biochemical, medical and chemical research fields.[112] In a steady-state experiment, the fluorophore is excited from the ground state to one of the vibrational levels in the excited state

using light. The excited molecule loses its vibrational energy as a result of collisions with other molecules and reaches its lowest vibrational state in the singlet excited state. The molecule then transitions to one of the vibrational levels in the ground state by the emission of a photon. This process is visualized using the Jablonski diagram.[113] In a typical set up, the emission from the sample is collected at a 90° arrangement to the excitation beam. Emission spectra are obtained by collecting the wavelength distribution of the fluorescence intensities. The intensity and shape of the spectra provides information about the relative amounts of emissive species in the gel structure and the entrapped solvent, type of environment surrounding the fluorophore and the state of species (for example, cis and trans isomers).

Rhodamine 6G and pyrene were chosen as fluorescence probes in the current work. Rhodamine 6G has an absorption maximum at 530 nm and emission maximum at 565 nm. The dye is highly photostable and has a fluorescence quantum yield of 0.95. Pyrene has five distinguished bands in its emission spectrum and the ratio of I/III bands is an indicator of the polarity of the environment in which pyrene is located. For example, the I/III ratio of pyrene in polar solvents ranges between 1.6 and 1.9, whereas in non-polar solvents, the I/III ratio ranges between 0.5 and 0.6.[114] In the current work, emission spectra are collected and analyzed to determine the amount of dye released from the gel into the surrounding medium from the NaDC gel at a given time.

1.7.2 Fluorescence microscopy

Microscopy is widely used to study morphology, shape and size of aggregates in supramolecular gels. Information obtained from microscopy sheds insights about the gelation mechanisms.[115] Resolution and contrast are two characteristic features in microscopy. Electron microscopy techniques such as TEM, SEM provide high resolution images typically in the order

of nanometers. Electron microscopy requires samples to be imaged under vacuum, as the gas atmosphere attenuates the electron beams. Therefore, samples which produce significant amount of vapor must be dried or frozen. Drying procedures can lead to aggregation and structural changes that introduce artifacts for the images of the gel. Therefore, morphology of features in the dried state may not directly correspond to the morphologies in the hydrated state. For example, Adams *et al.* reported that fibers of dipeptide-based gels are much thicker in the dry state compared to fibers in the hydrated state.[116]

There has been considerable interest in using fluorescence microscopy to study supramolecular gels due to the high contrast than optical microscopy, and the ability to image gels in the hydrated state. Fluorescence microscopy yields a lateral and axial resolution of 200 and 500 nm, respectively for a 63x lens (numerical aperture 1.4) and a 488 nm laser. Dyes can be attached to gels either by physical interactions or chemical crosslinking. One advantage of using fluorescent dyes is their specificity towards targets like proteins, lipids, or ions. Fluorescence microscopy can be used to obtain quantitative information, for example, areas with different signal intensity indicate relative amounts of dye in different regions. Also, optical sectioning, i.e. the ability to acquire in focus images, from selected depths in the sample on the fluorescence microscope, allows for the 3D reconstruction of images. Confocal Laser Scanning Microscope (CLSM) works based on the principle of fluorescence.

In a CLSM microscope[117] (Scheme 1.2), light from a laser source is filtered through excitation filters. Filtered light is reflected by the dichroic mirror and is focused on the sample by the objective lens. Once the sample is excited, emitted fluorescence travels back through the same objective lens and passes through the dichroic mirror. The emitted light then passes through the emission filter, which blocks any scattered excitation light, and allows the emitted

light to hit the detector. Fluorescence is emitted along the entire illuminated cone of the sample, not just at the focus. Therefore, the out of focus light reaching the detector produces blurring and hazing in the images. A pinhole is used to eliminate the out of focus light coming from the sample. The pinhole ensures that light reaching the detector comes only from the confocal point in the sample where the excitation light is focused. The technique is called confocal microscopy because the pinhole and sample are on the same focal planes. Images are collected point by point and reconstructed using a computer. In the current work, the effect of additives on NaDC gels is investigated using confocal microscopy by labelling the NaDC gel with dyes, such as Rhodamine 6G.

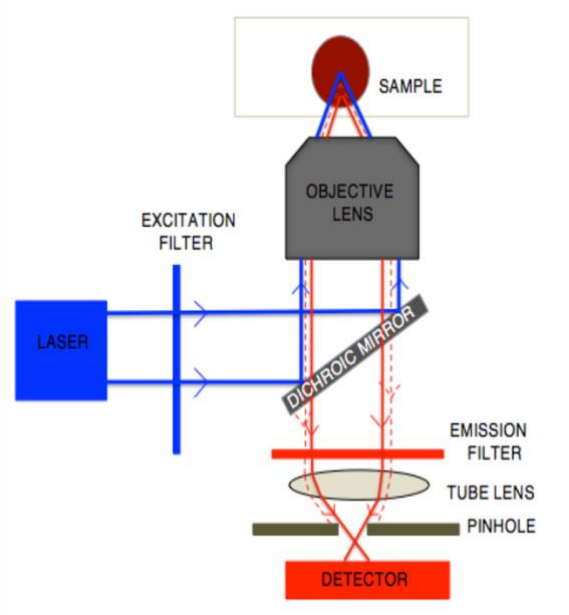

Scheme 1.2 Schematic representation of a CLSM.

1.7.3 Dynamic light scattering

Dynamic light scattering (DLS), also known as photon correlation spectroscopy (PCS) or quasi-elastic light scattering, is a technique to study diffusion of colloidal particles in a dispersed phase.[118] DLS measures the Brownian motion of colloidal particles (typically in the

submicron range) in the dispersed phase. Brownian motion occurs due to collisions of colloidal particles with solvent molecules in the dispersed phase. Brownian motion of particles is recorded by measuring the intensity fluctuations of scattered light from the sample as a function of time. The frequency and the intensity of scattered light is used to determine the translational diffusion coefficient of the colloidal particles. For example, larger particles diffuse slowly resulting in similar positions at different time points, whereas smaller particles diffuse faster and move to different positions at different time points. The hydrodynamic diameter of particles is calculated from the diffusion coefficient using the Stokes-Einstein equation. The Stokes-Einstein equation relates the particle size to the viscosity of the medium and diffusion coefficient. The Stokes-Einstein equation assumes that particles are spheres, therefore the hydrodynamic diameter obtained from DLS corresponds to the diameter of a sphere that has the same translation diffusion coefficient as the particle.

In a typical DLS setup (Scheme 1.3a), the sample is excited using a laser source. Light passed through the sample cell and scatters at all angles. The scattered light from the sample is measured by the detectors. The detector positions are either at 90º or 173º, and the detector position is chosen depending on the concentration of the sample under investigation. The attenuator is used to adjust the intensity of the laser source to ensure that the scattered light intensity falls within the detector range. The scattered light from the detector is processed by a correlator. The correlator measures the degree of similarity between signals collected at successive time intervals (Scheme 1.3b). These time intervals are in the range of ns to µs. The correlator then constructs a correlogram which provides information about the sample (Scheme 1.3c). The time at which correlation starts to decay indicates the mean size of the sample, and the steepness of the decay line reflects the polydispersity of the sample. A steeper decay indicates

that the sample is monodisperse, while a noisy baseline in the correlogram is an indication of aggregation. The information from the correlator is processed in a computer where the size information is derived (Scheme 1.3d). In this thesis, the focus of DLS studies is on the qualitative analysis of the correlation function rather than the determination of the size distribution, as the former reveals information about the gels that cannot be obtained from the size distribution curves.

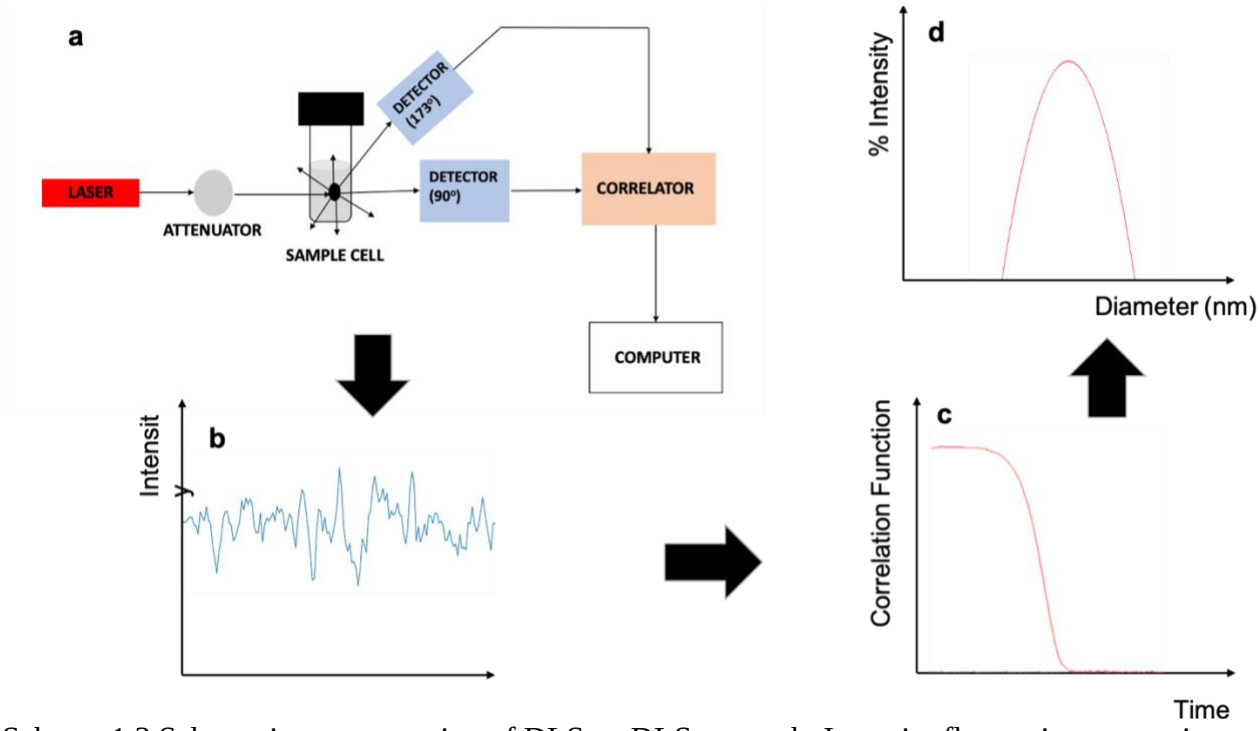

Scheme 1.3 Schematic representation of DLS. a. DLS set up, b. Intensity fluctuations capturing Brownian motion as a function of time, c. DLS correlogram d. Size distribution profile.

1.8 Objectives

The objective of this thesis is to design a pathway to gain a fundamental understanding on how multiple components in a supramolecular gel contribute to distinct properties of the gel. I envision this pathway as an attempt to move away from the existing trial and error approach in the development of functional gels. This understanding is important to achieve control on the

properties of gels for potential applications in materials science. To achieve this goal, correlations are made between structure, dynamics and function in a two-component gel system, i.e. NaDC-CB[6] gel.

In Chapter 2, I address the length-scale problem by obtaining information for NaDC-CB[6] gels at the microscopic level using dynamic light scattering and fluorescence microscopy as a function of CB[6] concentration. These studies are designed to shine light on the changes in aggregate size and morphology, kinetics of gel formation and thermo-reversible properties of NaDC-CB[6] gels as a function of CB[6] concentration. In Chapter 3, the effect of CB[6] on NaDC gels is investigated from a functional point of view. The release properties of dyes of different hydrophobicities from the NaDC-CB[6] into the surrounding medium are investigated. In Chapter 4, colocalization studies are performed to investigate the location of dyes of different hybrophocities in NaDC-CB[6] gels. Through dynamics studies performed using fluorescence recovery after photobleaching (FRAP), I aim to capture the role of an additive CB[6] in NaDC gels that cannot be explained from the structural information described in Chapter 2.

Overall, the conclusions developed in this thesis highlight that function cannot be solely explained by structural studies and understanding of dynamics is essential. The techniques and methods developed in this thesis can act as a core knowledge to study in the future drug delivery systems, such as multi component supramolecular gels of interest. The highlighted pathway in this thesis creates an opportunity for the rational design of drug delivery systems.

Chapter 2 Structural characterization of NaDC gels in the presence of CB[6]

2.1 Introduction

Introduction of multiple components, such as additives, to low molecular weight gelators (LMWG) broadens the access to a wide range of properties that are otherwise not possible with just the LMWG. The multiple components in gels create an additional level of control for the self-assembly process, which makes the tailoring of properties possible. Although the use of multiple components gives opportunity to prepare materials with distinct properties, the degree of information that these systems provide is huge.[119] The properties of multicomponent gels are not only a result of the primary assembly, but also a result of how structures interact in different ways over different length scales. The length scales are defined at three levels: molecular, microscopic and macroscopic levels (Scheme 2.1).[120] There is no simple link between microscopic, macroscopic and molecular length scales.[37] In order to decode multicomponent gel systems for the design or control of their properties it is important to understand how the properties are affected at all length scales. Therefore, determining the structure at just one length scale is not sufficient to understand the nature of these systems in order to build a predictive framework to rationally design functional gels. For example, computational approaches in the area of supramolecular gels helps to identify if a given library of gelators can form gels,[121] but these studies do not tell us why some gelators actually form gels and others cannot. In order to understand the phenomenon of gel formation, chemists require techniques and tools that capture the complexity that arises over different length scales. The techniques used for studies at different length scales do not necessarily complement each other in all cases, which makes it essential to obtain information across the length scales.[120]

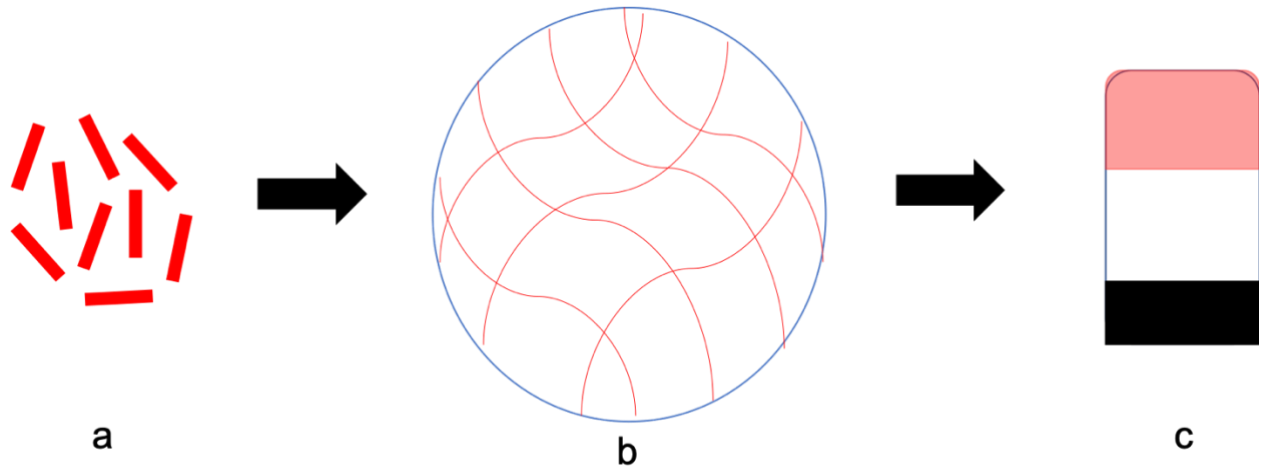

Scheme 2.1 Schematic representation of length scales in supramolecular gels. a,b,c represents molecular, microscopic and macroscopic length scales, respectively.

The multi component gel of interest in this thesis is the NaDC-CB[6] gel, where NaDC is the LMWG and CB[6] is the additive. For NaDC-CB[6] gels, earlier studies performed in the group involved techniques like steady-state and time-resolved fluorescence, and rheology measurements.[69] Fluorescence-based techniques provided insights on the effect of additives in gels at the molecular level, whereas rheology measurements provided insights on the macroscopic properties, such as the mechanical strength of the material. However, studies at the microscopic length scale are crucial to understand how the additive and gelator are aligned spatially in the gel. The locations where guest molecules like drugs reside in these gels is also of importance to optimize these materials for drug delivery applications.

Studies at the microscopic length scale have been reported for NaDC gels in the presence of salts and amino acids.[71] However, the reported studies were performed using electron microscopy techniques. Morphologies observed in electron microscopy techniques, like transmission electron microscopy (TEM) and scanning electron microscopy (SEM), are dependent on the method of sample preparation, which for these two techniques require drying

of the sample. As a result, information obtained may not necessarily correspond to the gel in the hydrated state. Drying itself will introduce artefacts and cause considerable distortion or aggregation in the samples.[116] Therefore, standard electron microscopy techniques may not give an image of the real morphologies of the gels in the hydrated state.[107]

Confocal laser scanning microscopy (CLSM) provides an advantage over electron microscopy techniques for its ability to carry out studies with the hydrated gel. Studies of the gel in the hydrated state shed insights on both the structure and dynamics of the gel. CLSM gives high resolution images with depth selectivity and enhanced contrast compared to other optical microscopy techniques.[122, 123] A unique characteristic of CLSM is its ability to generate 3D reconstructions of topologically complex objects without destroying the sample. CLSM offers a limit of resolution of ~ 200 nm, with a 63x lens and a 488 nm laser. CLSM studies on the NaDC-CB[6] gels of interest can provide insights on morphologies of the gel by capturing the components in the gels that do not diffuse. The freely diffusing components in the gel appear as background noise in the image and therefore are not visible with this technique.

Information on diffusing components in the gel at the microscopic level can be obtained using a technique called dynamic light scattering (DLS). DLS is a technique commonly used to determine the diffusion behavior of macromolecules in solution and to measure the size of particles in the sub-micron range.[124] Unlike CLSM where a specific area in the gel tagged with dye is investigated, in DLS a small volume of gel is studied. DLS has been used to monitor the process of gel formation by providing information on size, shape, aggregation number and polydispersity of aggregates over time and temperature.[107, 125, 126] For example, the relationship between scattered light intensity and the hydrodynamic diameter obtained from DLS has been used to show if the aggregates in the sample are disk like or spherical like. In summary, DLS and

CLSM are complementary techniques yielding information about the aggregates in the mobile and immobile phases of the gel, respectively.

2.1.1 Objectives

The objective of this chapter is to obtain structural information on NaDC-CB[6] gels at the microscopic level using DLS and CLSM. Since LMWG have concentration dependent assembly,[120] the studies are carried out at different additive concentrations. Structural information of aggregates in solution, sol and gel states are obtained to shed light on the mechanism of the gel formation. Temperature based studies on DLS and CLSM are carried out to reflect on the effect of CB[6] on the thermo-reversibility of NaDC gels. Time dependent studies are carried out to study the effect of CB[6] on the kinetics of gel formation at the microscopic level. For CLSM studies, gels are tagged with a hydrophilic rhodamine 6G dye (Chart 2.1).

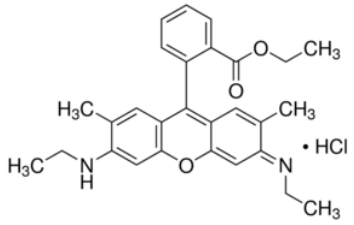

Chart 2.1 Chemical structure of rhodamine 6G.

2.2 Experimental

2.2.1 Materials

NaDC (Fluka, > 98%), NaH_2PO_4 (Anachemia, > 98%), Na_2HPO_4 (Anachemia, > 98%), methanol (Fisher grade), rhodamine 6G (Sigma Aldrich, 99%), N-(4-aminophenyl)imidazole (API, Sigma Aldrich, 98%), 1,6-diaminohexane (DAH, Sigma Aldrich), hydrochloric acid (HCl, BDH 36.5-38%), and deionized water (Barnstead NANOpure deionizing systems, 17.8 MΩ cm) were used

as received. Coverslip (24 × 60 mm, 0.16-0.19 mm thickness), Press-To-Seal Silicone isolator (Round well, 9 mm diameter, 0.8 mm depth), adhesive on both sides, Grace Biolabs), HybriWell™ Sealing System (21.6 mm × 21.6 mm × 0.25 mm), 110 µL approximate volume, 25.5 mm × 30 mm OD, Fluor "Friendly" Adhesive Chamber, Grace Biolabs) were used for microscopy experiments. Filters (0.45 and 0.2 µm nylon) and glass syringes (10, 50 mL) were used for the filtrations. Hellma cells (10 mm × 10 mm) were used for the DLS measurements.

The DAH salt was recrystallized by adding acetone (15 mL) to a 11 mmol DAH solution dissolved in 1.85 mL concentrated HCl (38%), followed by vacuum filtration to obtain white crystals. The sample CB[6]-SG-1 (purity 84%) was used in this study was prepared in-house. CB[6] was synthesized and purified based on the standard protocols in the group.[69] The CB[6] concentration was determined by titrating the stock solutions with recrystallized DAH. In this titration, DAH^{2+} displaces API^{+} bound with CB[6] leading to a decrease in the steady-state fluorescence intensity of API^{+}.

2.2.2 DLS studies for structural characterization

Phosphate buffer stock solution (0.5 M) at pH 6.5 was prepared by mixing appropriate volumes of NaH_2PO_4 (0.5 M) and Na_2HPO_4 (0.5 M) stock solutions. NaDC stock solutions (0.2 M) were prepared in deionized water. The NaDC stock solution was heated at 60 °C for 15 min to dissolve the NaDC solid. NaCl stock solutions (0.9 M) were prepared with filtered water.

All the syringes were washed with methanol and water 7 times each. This was followed by washing of the glassware with methanol and water 7 times each using syringes equipped with 0.2 µm filters. All the stock solutions were prepared using filtered water.

For NaDC solutions, 375 µL of the NaDC stock solution and 875 µL of deionized water was added into a 3-dram sample vial. The solution was heated at 60 °C for 15 min. While this

solution was hot, 250 µL of the NaCl stock solution was added, followed by heating of this mixture at 60 °C for 15 min. For NaDC-CB[6] solutions, a given amount of CB[6] was dissolved in 875 µL of deionized water and 250 µL of the NaCl stock solution. The addition of NaCl led to the solubilization of CB[6] at room temperature. This solution was heated for 15 min at 60 °C. While the solution was hot, 375 µL of the NaDC solution was added, followed by heating at 60 °C for 15 min.

For NaDC gels, 375 µL of the NaDC stock solution and 975 µL of deionized water was added into a 3-dram sample vial. The solution was heated at 60 °C for 15 min. While this solution was hot, 150 µL of phosphate buffer was added, followed by heating of this mixture at 60 °C for 15 min. For NaDC-CB[6] gels, a given amount of CB[6] was dissolved in 975 µL of deionized water and 150 µL phosphate buffer. The addition of phosphate buffer led to the solubilization of CB[6] at room temperature. This solution was heated for 15 min at 60 °C. While the solution was hot, 375 µL of the NaDC solution was added, followed by heating at 60 °C for 15 min. No final filtrations were performed on the samples before DLS measurements.

The final concentrations of NaDC and phosphate buffer in all the samples were the same at 50 mM. The final concentrations of CB[6] in the samples were 0, 2.5, 5.0, 7.5 mM. All samples have a baseline Na^+ cation concentration of 200 mM. The samples (solutions and gels) were left at room temperature for 20 h (resting period) before carrying out any measurements. Studies on sols were carried out by subjecting the gels (after 20 h resting period) to heating for 15 min at 60 °C.

A Malvern Zeta-sizer nanoseries DLS instrument was used for particle size measurements. An excitation wavelength of 633 nm and a scattering angle of 173° were used for the measurements. For each data set, a total number of 5 runs were performed. A fluorescence

filter (633 nm, narrow band) was used. The data were analyzed using a general-purpose fitting routine. All the measurements were performed using a heating block. The total runs performed for a given sample were averaged using the ZS explorer software (version 2.0.0.98) and averages of correlograms are reported in this chapter.

2.2.3 CLSM studies for structural characterization

Rhodamine 6G (1 mM) stock solutions were prepared in methanol. NaDC and phosphate buffer stock solutions were prepared in the same way as described in the previous section.

For NaDC gels, 750 µL of the NaDC stock solution and 1944 µL of deionized water was added into a 3-dram sample vial. The solution was heated at 60 °C for 15 min. While this solution was hot, 6 µL of the dye stock solution and 300 µL phosphate buffer were added, followed by heating of this mixture at 60 °C for 15 min. For NaDC-CB[6] gels, a given amount of CB[6] was dissolved in 1944 µL of deionized water and 300 µL phosphate buffer. The addition of phosphate buffer led to the solubilization of CB[6] at room temperature. This solution was heated for 15 min at 60 °C. While the solution was hot, 6 µL of the dye stock solution and 750 µL of the NaDC solution were added, followed by heating at 60 °C for 15 min.

For NaDC solutions, 750 µL of the NaDC stock solution and 2244 µL of deionized water was added into a 3-dram sample vial. The solution was heated at 60 °C for 15 min. While this solution was hot, 6 µL of the dye stock solution were added followed by heating of this mixture at 60 °C for 15 min. For NaDC-CB[6] solutions, a given amount of CB[6] was dissolved in 2244 µL of deionized water. This solution was heated for 15 min at 60 °C. While the solution was hot, 6 µL of the dye stock solution and 750 µL of the NaDC solution were added, followed by heating at 60 °C for 15 min.

The final concentration of NaDC in the gel samples was 50 mM. The final concentration of phosphate buffer in the gel samples was 50 mM. The final concentrations of CB[6] in the gel samples were 0, 2.5, 5.0, 7.5 mM. The final concentration of rhodamine 6G in the gel samples was 2 μM.

Coverslips and gaskets were rinsed with water and methanol before use. Approximately 100 μL of sol was transferred into the gasket immediately after sample preparation. The gasket was sealed by placing a glass coverslip on top of the open side of the gasket. The gasket was left at room temperature for 20 h (resting period) before carrying out any measurements. The resting period of 20 h was identified after imaging gels at different time points over a 20 h time frame (Figure 2.1). As shown in Figure 2.1, with increasing time, an increase in the number of features in the sample was observed. However, after 8 h the sample reached its equilibrium with no appearance of new features. For convenience of the user, the 20 h time period was chosen as the resting period and it was kept consistent for the experiments described in this chapter, unless otherwise noted.

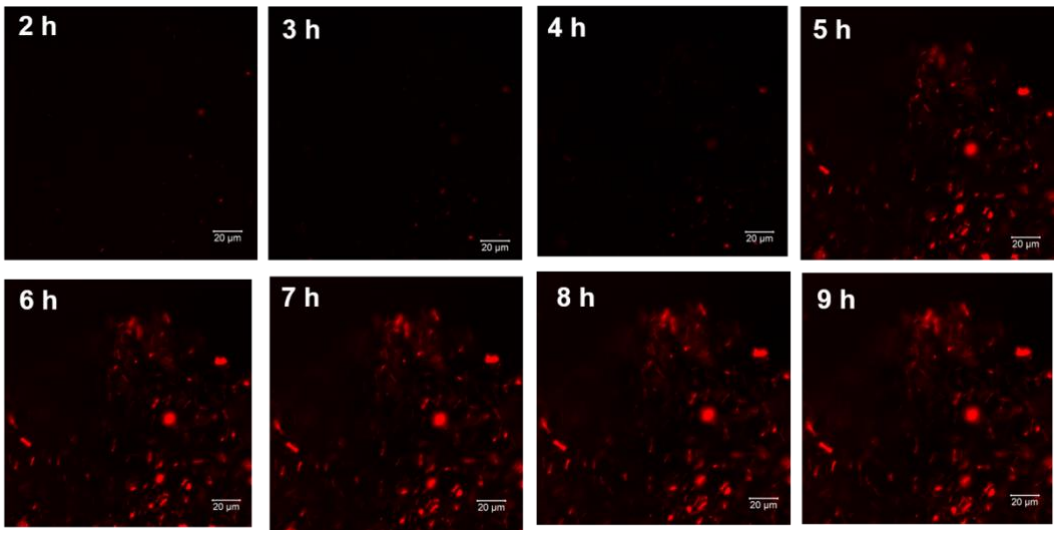

Figure 2.1 Confocal images of the NaDC gel (50 mM) tagged with rhodamine 6G (2 μM) at different time points during the resting period. Scale bar 20 μm.

After 20 h, images of the samples were collected using an inverted CLSM microscope (Zeiss LSM 880) equipped with a 514 nm Argon laser and the following objectives: 20× Plan-NeoFluar long working distance (LWD) with numerical aperture (NA) 0.4, 63× oil immersion lens with NA 1.4. The laser intensity was set at 20% and the excitation filter MBS 458/514 nm was used. The pinhole diameter was set to 1 Airy Unit (AU). AU is defined as the diameter of the central maximum peak in the diffraction pattern of a focused beam. The range for the detection of the emission with a GaAsP detector was set to 530-650 nm. The detector gain was set at the range 600-800 V. The equipment was controlled using the software Zen Black from Zeiss. Images were acquired with optimal pixel size chosen by the software, and 12 bits of pixel depth. Images were collected over an area of 110.5 × 110.5 μm^2 with an optimal frame size of 352 × 352 pixels. Images were taken in a volume at the center of the gasket and at a certain depth (~50 μm from the edge of coverslip) as the edge of gasket showed dye accumulation in the presence of the dye (Figure 2.2a) and auto-fluorescence in the absence of the dye (Figure 2.2b).

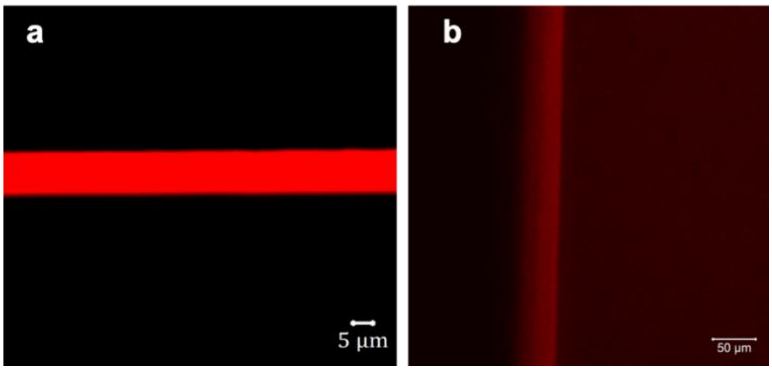

Figure 2.2 Confocal image of the gasket edges, a. with rhodamine 6G (2 μM), b. without rhodamine 6G.

2.2.4 Vial inversion tests

Inversion tests were used to monitor gel-sol transition temperatures. The temperatures at which the gel in an inverted vial falls under gravity is defined as gel-sol transition temperature.

Gel samples were prepared in the same way as described in the previous DLS section. After 20 h, inverted vials (inner diameter 1.5 cm) with the gel samples were kept at 25, 45, 65 °C for 10 min at each temperature in a heating bath and the temperature at which the gel fell under gravity was noted.

2.2.5 CLSM thermo-reversibility studies

Samples were prepared in the same way as described in the previous CLSM section. All measurements were performed on the Linkam heating stage. The sample was heated to set temperatures between 25 and 85 ºC at a rate of 5 ºC/min followed by cooling at the same rate. Scans were collected at 20 ºC intervals (25, 45, 65, 85 ºC). Images at different temperatures were collected for the same area of the gel. After the stage reaches a particular temperature, a 5 min equilibration time was left before collecting the images. To avoid any surface effects at the coverslip, images were collected at a particular depth in the sample (~100 µm). The region of interest was chosen in the scanned area and changes in the region of interest were monitored across the temperatures. The images for the region of interest at each temperature was processed using the ImageJ analysis software.

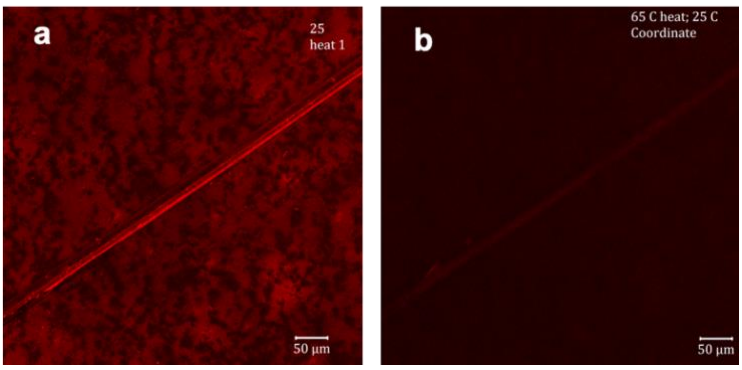

Figure 2.3 Confocal image of a scratch on the top of the coverslip before (a) and after the heating cycle (b). (x,y,z) coordinates for images a and b are the same indicating that both images cover the same area in the gasket.

The gel structures were observed to move out of focus during the heating stage experiments (Figure 2.3) because of the movement of the stage on the microscope (~100 µm along z direction depending on the temperature). This movement interfered with the results. The stage movement was accounted for by scratching the surface of the cover slip with a diamond cutter. At each temperature after the equilibration time of 5 min, the coordinates of the heating stage were adjusted such that the scratch was in focus (Figure 2.4). The image at each temperature was collected at a known depth from the scratch inside of the sample. Refocusing the scratch at each temperature ensured that the image was collected in the same area as for the previous temperature.

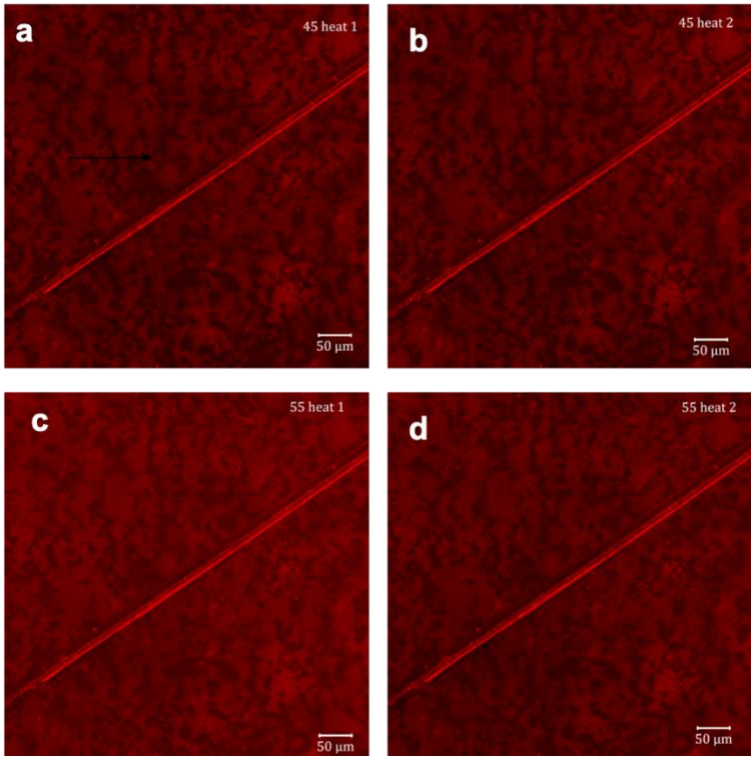

Figure 2.4 Confocal image of the scratch on the top of the coverslip at 45 ºC (a,b) and 55 ºC (c,d). Coordinates for images a, b, c, d were adjusted after considering the stage movement during the heating.

2.2.6 DLS thermo-reversibility studies

Samples were prepared in the same way as described in the previous DLS section. DLS experiments were performed using the same settings as described in the DLS section above. Data were collected at temperatures of 20, 35, 50 and, 65 °C. After the instrument reached a given temperature, the samples were equilibrated for 5 min before the results were collected. The changes in viscosity as a function of temperature were not accounted for in this study as the focus is on the qualitative analysis of the correlation function and not on the determination of the hydrodynamic diameter for which the viscosity changes matter.

2.2.7 CLSM kinetics studies

Samples were prepared in the same way as described in the previous CLSM section. Samples were transferred into gaskets immediately after sample preparation and while hot. The samples were equilibrated for 5 min before the results were collected. A chosen area was imaged at 5 min intervals for a period of 30 min.

2.2.8 DLS kinetics studies

Samples were prepared in the same way as described in the previous DLS section. The samples were equilibrated for 5 min before the results were collected. DLS scans were run at 5 min intervals for a period of 30 min.

2.3 Results

2.3.1 DLS structural characterization studies

Earlier work on the characterization of NaDC solutions showed that NaDC self-assembles into two types of aggregates (i.e. primary and secondary).[59] In a certain pH range these aggregates assemble further to form a gel.[72] Previous studies in the group showed that the

NaDC gel consists of aggregates which are distributed in the aqueous phase and the gel structures in the gel.[69] The objective of the DLS experiment is to determine if the addition of CB[6] has an effect on the size of NaDC aggregates. Studies were performed for solutions, sol and gel states. DLS was used to characterize the aggregates that diffuse in the sample, which corresponds to all aggregates in the solution and sol sample and the aggregates that are free in the aqueous phase of the gel. The immobilized aggregates in the gel are not observable by DLS.

The exponential decay of the correlogram is related to the size of the diffusing particle (Figure 2.5). The correlation time in DLS experiments is a measure of how long a diffusing particle remains in the same detection volume in the sample. Smaller particles move faster and have shorter correlation time, and therefore appear as a faster decay in the correlogram. On the other hand, larger particles move more slowly, resulting in a delay for the decay. The correlation coefficient, defined as the correlation function at time t=0 (i.e. Y-intercept in the correlogram) indicates the ability of aggregates to freely diffuse in the sample. A higher correlation coefficient indicates freely diffusing aggregates which is a characteristic of solutions. A lower correlation coefficient is an indicates aggregates are no longer able to diffuse freely in the sample, a characteristic of gels. The two parameters I used from the DLS studies reported are the shape of the decay and the correlation coefficient.

DLS results in NaDC-CB[6] solutions are summarized in Figure 2.5. The decay was delayed with the addition of CB[6] when compared to the correlograms for the NaDC solution. These results indicate that aggregates in NaDC-CB[6] solutions are larger compared to the NaDC aggregates in solution in the absence of CB[6]. Therefore, the additive CB[6] increases the size of aggregates in the solution, suggesting that CB[6] is associated with the NaDC aggregates.

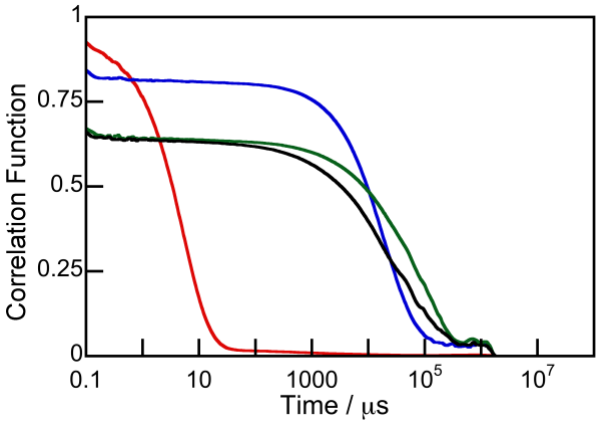

Figure 2.5 Correlograms for NaDC-CB[6] solutions at CB[6]/NaDC ratios of 0 (red), 0.05 (blue), 0.1 (green), 0.15 (black) at 25 ºC. Concentration of NaDC in all the samples is 50 mM.

A sol is formed by heating the gel above its gel-sol transition temperature. In a sol state, the sample is mobile and flows. Sol and solution are different samples in terms of chemical compositions. The sol contains buffer whereas the solution does not contain buffer. The sol is formed initially during sample preparation and once the sol is cooled to room temperature the gel is formed. Therefore, the sol is a critical intermediate step in the gel formation. DLS experiments with sols were performed by heating the pre-formed gel at 60 °C for 15 min. The heating conditions are chosen such that I was able to visually observe the transformation of the gel into the sol.

DLS results for the NaDC-CB[6] sols are summarized in Figure 2.6. The decays were delayed in the presence of CB[6] when compared to the sol that does not contain CB[6]. This delay indicates that the aggregates in the sol are larger in the presence of CB[6] compared to the aggregates in the NaDC sol that does not contain CB[6]. The changes in the correlation coefficient (Y-intercept in the correlogram) for the samples with CB[6] suggest that aggregates are no longer able to diffuse freely when CB[6] is present. A lower correlation coefficient in Figure 2.6 compared to Figure 2.5 for CB[6] samples could indicate that microscopically gel

containing CB[6] has not completely transformed into sol in the 15 min heating time. However, because the time of sol formation was kept constant across all the samples, the size arguments are still relevant.

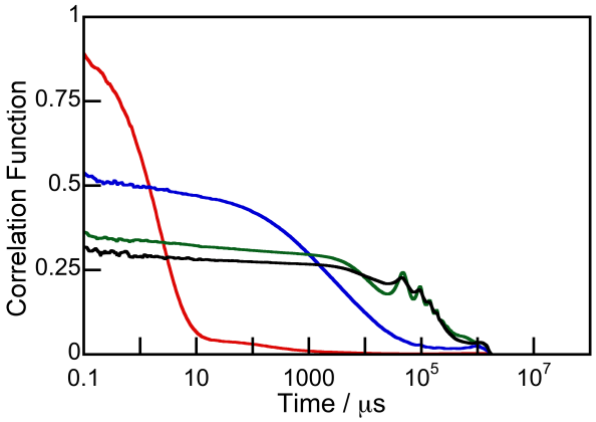

Figure 2.6 Correlograms for NaDC-CB[6] sol at CB[6]/NaDC ratios of 0 (red), 0.05 (blue), 0.1 (green), 0.15 (black) taken at 60 ºC. Concentration of NaDC in all the samples is 50 mM.

For gels, the correlation coefficients reveal information about aggregates that are immobile in a sample. More gelator is incorporated in the immobile phase for samples of equal gelator concentration that have a lower correlation coefficient. DLS results in NaDC-CB[6] gels (Figure 2.7) showed a decrease in the correlation coefficient of the samples with CB[6]. The low correlation coefficient suggests that some aggregates in the gel are immobile. These immobile aggregates likely correspond to aggregates in the gel structure. The decrease in the correlation coefficient with increase in CB[6] concentrations suggests that more aggregates are becoming a part of the gel structure with the addition of CB[6] to the gel. Also, the observed delays in the decay for gels with CB[6] is consistent with studies in sols and solutions (Figures 2.5, 2.6).

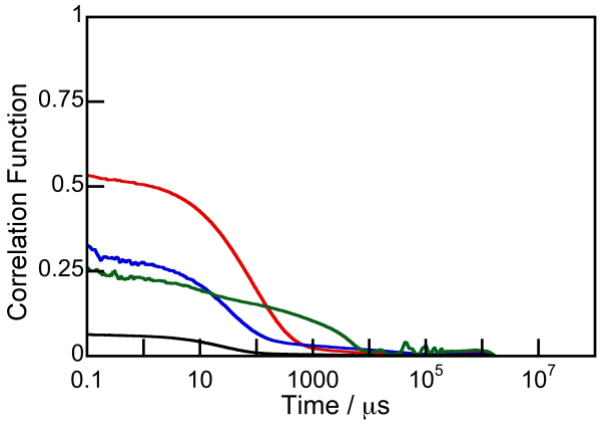

Figure 2.7 Correlograms for NaDC-CB[6] gels with different CB[6]/NaDC ratios of 0 (red), 0.05 (blue), 0.1 (green), 0.15 (black) taken at 25 ºC. Concentration of NaDC in all the samples is 50 mM.

In summary, DLS results showed that the CB[6] effect on the size of NaDC aggregates begins in the solution phase before the addition of buffer and translates into the sol and gel structures. Also, studies in gels suggest that the distribution of aggregates between the aqueous phase and the gel structure was affected with the addition of CB[6], with more aggregates becoming a part of the gel structure.

2.3.2 CLSM structural characterization studies

The purpose of this experiment is to identify the effect of CB[6] on NaDC gels at the microscopic level using CLSM, with a focus on the morphologies and the size of the features observed in the CLSM images. The microscopy experiments reveal different information compared to the DLS experiments. DLS experiments gave information about aggregates diffusing in the aqueous phase of the gel. On the other hand, CLSM experiments provide information on the aggregates in the gel structure which are immobile (Figure 2.1). My hypothesis is that aggregates in the aqueous phase of the gel diffuse fast and appear as background noise in the image. The hypothesis was confirmed by carrying out CLSM studies in NaDC solutions with different CB[6] concentrations, where aggregates of NaDC are dispersed in

the aqueous medium. Results in Figure 2.8 agree with the proposed hypothesis that freely diffusing aggregates are apparent on the microscope and appear as background noise. These results indicate that the aggregates seen in the aqueous phase of the gel in DLS experiments cannot be seen on the CLSM images.

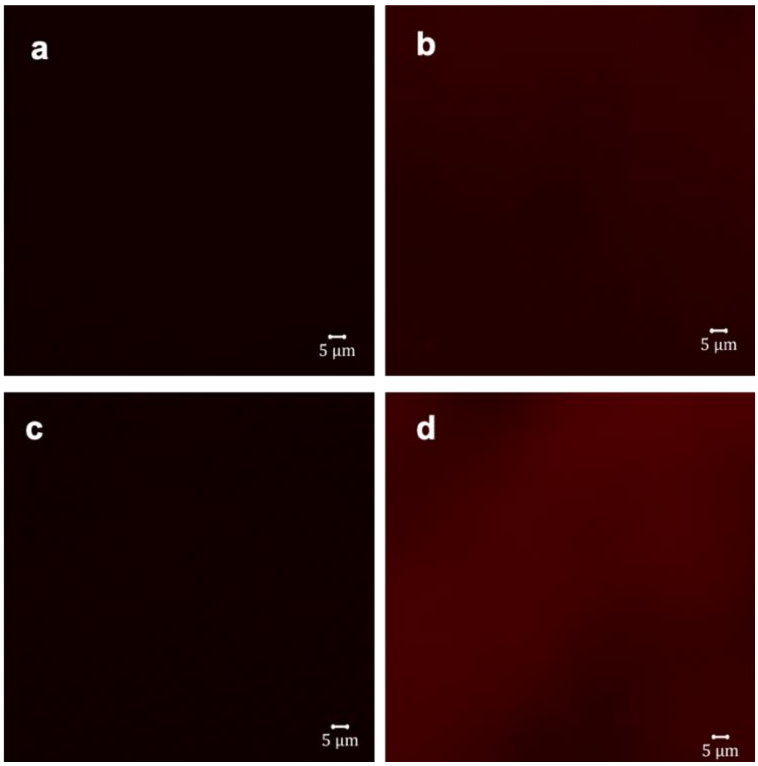

Figure 2.8 Confocal images for NaDC-CB[6] solutions tagged with rhodamine 6G (2 µM) at CB[6]/NaDC ratios of 0 (a), 0.05 (b), 0.1 (c), 0.15 (d). Images were taken after 20 h resting at room temperature. Concentration of NaDC in all the samples is 50 mM.

CLSM experiments in the gel showed that in the absence of CB[6], the NaDC gel was composed of spherical aggregates with an average size of around 3 µm (Figure 2.9 a) (see appendix for size determination analysis). These aggregates are referred to as gel structures throughout this thesis. At a 0.05 CB[6]/NaDC ratio, an increase in the number of gel structures was observed compared to the NaDC gel without CB[6] (Figure 2.9 b), with an average size of 5 µm for the gel structures. At a CB[6]/NaDC ratio of 0.1, cylindrical gel structures were observed

with an average length of about 10 μm (Figure 2.9 c). Finally at a 0.15 CB[6]/NaDC ratio, fibers of with an average length around 100 μm were observed (Figure 2.9 d). The observed morphology and size differences between gels with different CB[6]/NaDC ratios suggest that CB[6] incorporates more NaDC aggregates from the aqueous phase into the gel structure in NaDC-CB[6] gels.

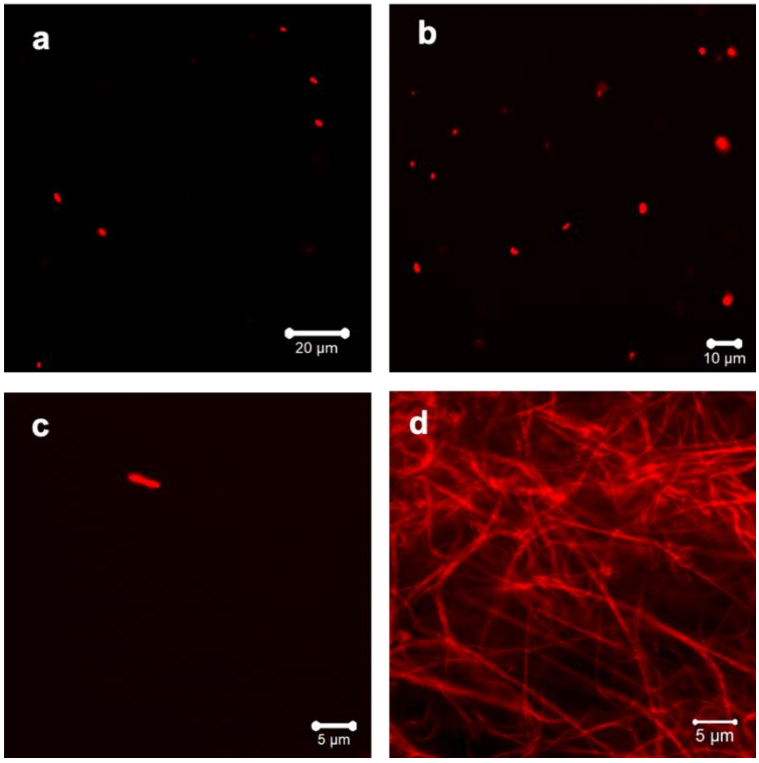

Figure 2.9 Confocal images for NaDC-CB[6] gels tagged with rhodamine 6G (2 μM) at CB[6]/NaDC ratios of 0 (a), 0.05 (b), 0.1 (c), 0.15 (d). Images were taken after a 20 h resting period at room temperature. Concentration of NaDC in all the samples is 50 mM.

2.3.3 CLSM thermo-reversibility studies

The purpose of this experiment is to see the effect of CB[6] on the gel-sol and sol-gel transitions by changing the temperature and collecting CLSM images. Results in the Figure 2.8 and 2.9 show that aggregates in the gel structure and the aqueous phase of gels can be easily differentiated in CLSM experiments with the former appearing as a gel structure and the latter

appearing as background noise. The points of interest for the gel-sol transition are the disappearance of the gel structures in the images. My hypothesis is that the temperature where the gel-sol transition occurs is dependent on the amount of CB[6] in the gel.

The gel samples after the resting period were subjected to temperatures of 25, 45, 65 and 85 °C. The choice of this temperature range was determined using vial inversion tests. Inversion tests results showed that the NaDC gel fell at 45 °C, whereas the NaDC-CB[6] gel with a 0.15 CB[6]/NaDC ratio fell at 65 °C.

Results using the heating stage showed that for the gel with a 0.15 CB[6]/NaDC ratio (Figure 2.10), the finer gel structures disappeared at 65 °C. The gel structures at 25 °C in Figure 2.10 are different from the gel structures in Figure 2.9d. This difference is due to the resolution for the image when using the 20× LWD lens for the studies shown in Figure 2.10 (Table A1 in the Appendix) as the use of this lens was required for the measurements using the heating stage. The black spots in the images are bubbles formed as a result of heating the sample. During cooling, hysteresis was observed, where no sharp features are seen in the image at 25 °C. This hysteresis indicates that sol-gel and gel-sol transitions at the microscopic level occur at different temperatures.

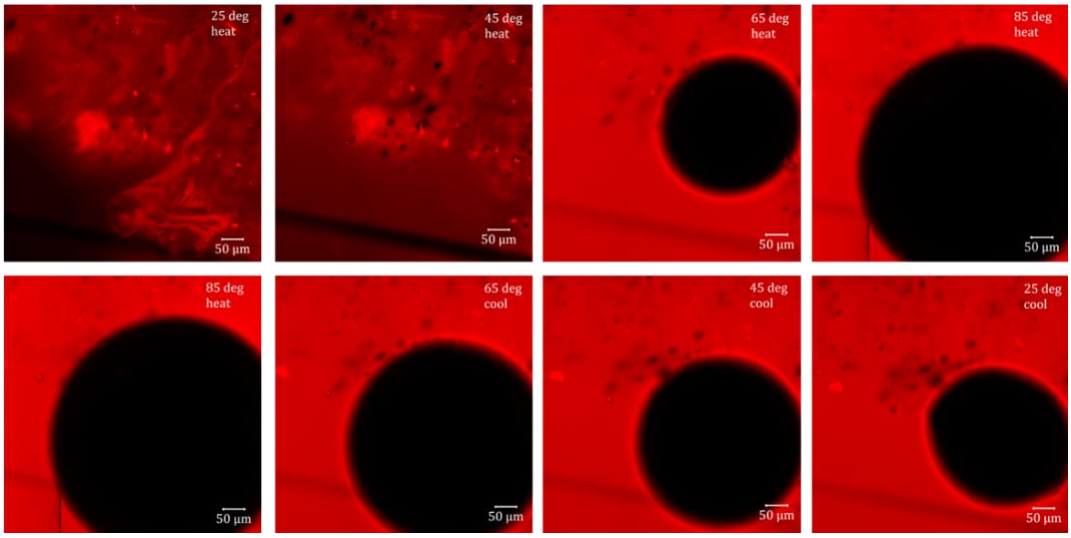

Figure 2.10 Confocal images for the NaDC-CB[6] (0.15 CB[6]/NaDC) gel tagged with rhodamine 6G (2 µM) at different temperatures (25, 45, 65 and 85 ºC) using the heating stage. Top and bottom panels correspond to heating (increasing temperatures left to right) and cooling cycles (decreasing temperatures left to right), respectively.

For NaDC gels (Figure 2.11), the spherical gel structures highlighted in red disappeared at 45 °C, which corresponds to a lower temperature compared to the NaDC-CB[6] gel (Figure 2.10). Also, hysteresis was observed during cooling. In summary, the CLSM results on the heating stage showed that the temperature for the gel-sol transitions differed with the addition of CB[6] to NaDC gels.

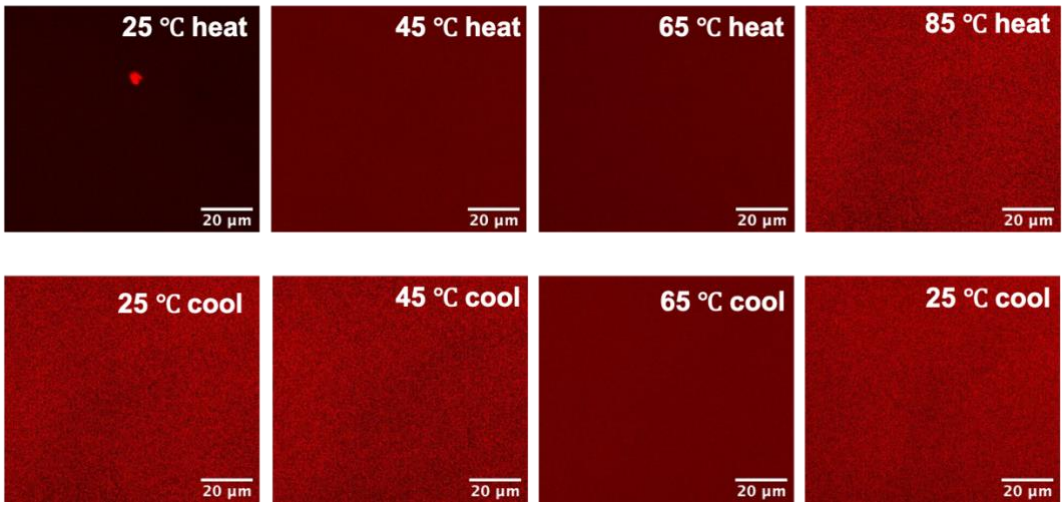

Figure 2.11 Confocal images of NaDC gel tagged with rhodamine 6G (2 µM) at temperatures (25, 45, 65 and 85 ºC) on the heating stage. Top and bottom panels correspond to heating (increasing temperatures left to right) and cooling cycles (decreasing temperatures left to right), respectively. The concentration of NaDC is 50 mM.

2.3.4 DLS thermo-reversibility studies

The effect of CB[6] on the size of the NaDC aggregates was investigated using temperature dependent DLS studies. For NaDC gels, the increase in temperature showed a higher correlation coefficient and a faster decay (Figure 2.12). The increase in the correlation coefficient suggests an increase in the number of freely diffusing aggregates in the sol thereby indicating that the gel was transformed into the sol. The faster decay indicates that the aggregates that are freely diffusing in the aqueous phase are smaller aggregates at the higher temperatures. The increase in the correlation coefficient is significant between the temperature of 35 and 50 °C, indicating that the gel-sol transition occurred in this temperature range. As seen in Figure 2.12, hysteresis was observed between the heating and cooling cycles. For example, at 25 °C (red trace in Figure 2.12), the decay is faster in the cooling cycle compared to the heating cycle, which indicates that size of the aggregates at 25°C before heating and after cooling are different. Before heating, the sample is a gel at 25 °C, but after cooling the sample is still a sol at 25 °C.

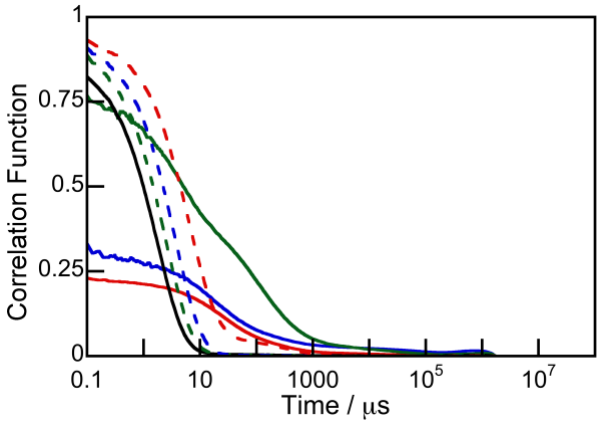

Figure 2.12 DLS correlograms for NaDC gels at 20 (red), 35 (blue), 50 (green) and 65 ºC (black). Solid lines and dashed lines correspond to the heating and cooling cycles, respectively. The concentration of NaDC in this samples is 50 mM.

For NaDC-CB[6] gels, similar to the NaDC gel, an increase in the correlation coefficient and a faster decay were observed with the increase in temperature (Figure 2.13). However, unlike the NaDC gel, the increase in the correlation coefficient is significant between the temperatures of 50 and 65 °C, indicating that the gel-sol transition occurred in this temperature range. This result agrees with the temperature studies carried out on the CLSM, where at ca. 65 °C the gel structures disappeared in the image (Figure 2.10).

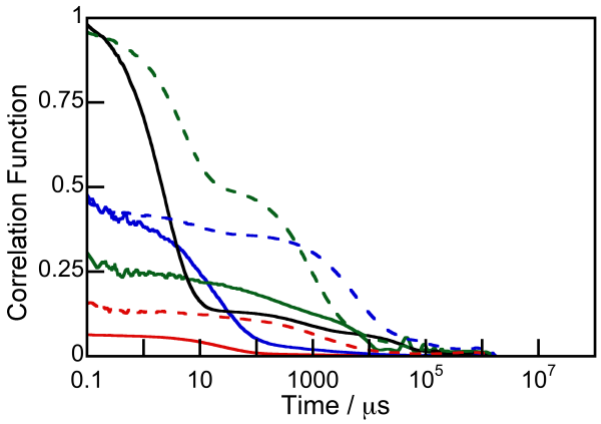

Figure 2.13 DLS correlograms for the NaDC-CB[6] gel (0.15 CB[6]/NaDC ratio) at 20 (red), 35 (blue), 50 (green) and 65 ºC (black). Solid lines and dashed lines correspond to heating and cooling cycles, respectively. The concentration of NaDC in this samples is 50 mM.

2.3.5 CLSM kinetics studies

Gel formation was investigated using kinetics experiments, where images for the sol were tracked for a period of 30 min at 5 min intervals. The images for 0 min in Figure 2.14 and 2.15 exclude the equilibration time of 5 min after which images were collected. The kinetics were studied using CLSM and DLS experiments to obtain complementary information.

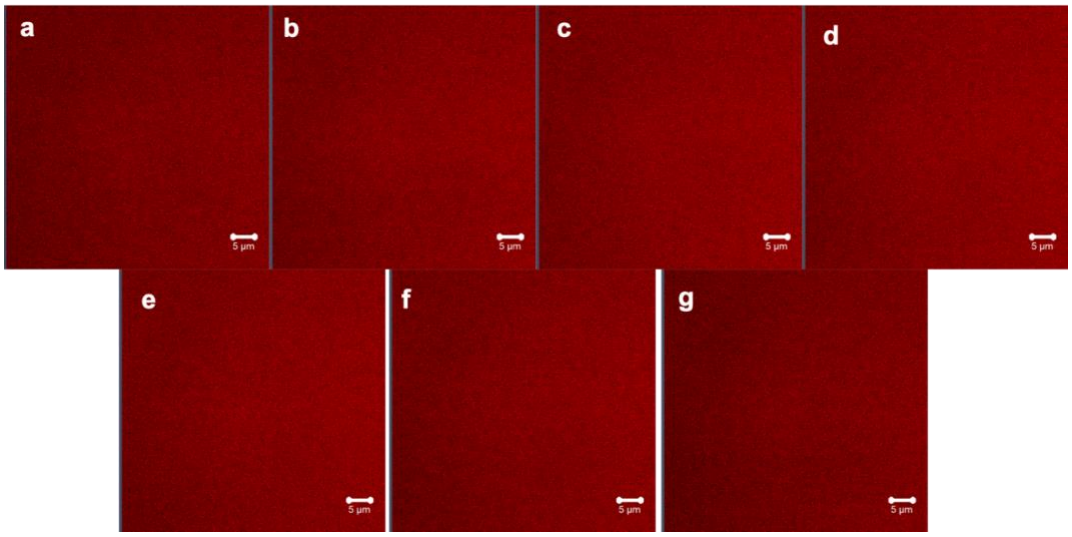

Figure 2.14 Confocal images for the NaDC gel tagged with rhodamine 6G (2 μM) collected at time points of 0 (a), 5 (b), 10 (c), 15 (d), 20 (e), 25 (f) and 30 min (g) during gel formation. The concentration of NaDC in this samples is 50 mM. Images were collected at room temperature.

The hallmarks of interest in the CLSM experiments are the appearance of gel structures in the image as the sol transitions into the gel. Although the imaged area is kept constant across the time points (Figure 2.14), scans were taken for different areas during the 30 min interval to determine if the imaged area in Figure 2.14 represents the gel sample as a whole. During the 30 min interval, CLSM images for NaDC gel showed the absence of gel structures (Figure 2.14), whereas for the NaDC-CB[6] gel, gel structures appear within equilibration 5 min time frame (Figure 2.15).

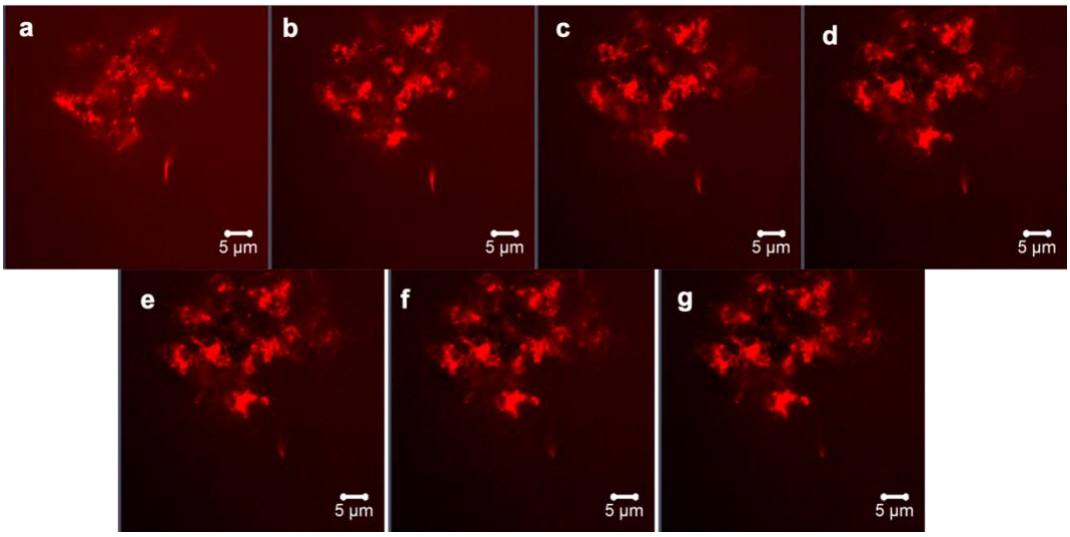

Figure 2.15 Confocal images for the NaDC-CB[6] gel (0.15 CB[6]/NaDC ratio) tagged with rhodamine 6G (2 µM) collected at time points of 0 (a), 5 (b), 10 (c), 15 (d), 20 (e), 25 (f), 30 min (g) during gel formation. Concentration of NaDC in all the samples is 50 mM. Images were collected at room temperature.

2.3.6 DLS kinetics studies

Kinetic experiments conducted by DLS are shown in Figure 2.16. These experiments were carried out using 5 min intervals similar to the CLSM experiments and data were collected for a period of 30 min. For NaDC gels (Figure 2.16a), the decays remained fast over time indicating that the sol-gel transition has not occurred within 30 min. A growth on the right end of x-axis in Figure 2.16a was observed with time, however this change is not significant to reach any conclusions. For NaDC-CB[6] samples (Figures 2.16b-d), the decrease in the correlation coefficient was observed with time. The correlation curves do not follow a clear trend with time because the sample with NaDC-CB[6] is changing so fast that correlation functions from repeat runs did not overlap with each other leading to scattered averages. The decrease in the correlation coefficient as time progresses is an indication of gel formation as the number of freely diffusing species, are now incorporated into the immobile phase of the gel. In summary,

complementary information from CLSM and DLS kinetics experiments showed that CB[6] speeds up the time for gel formation in NaDC gels at the microscopic level

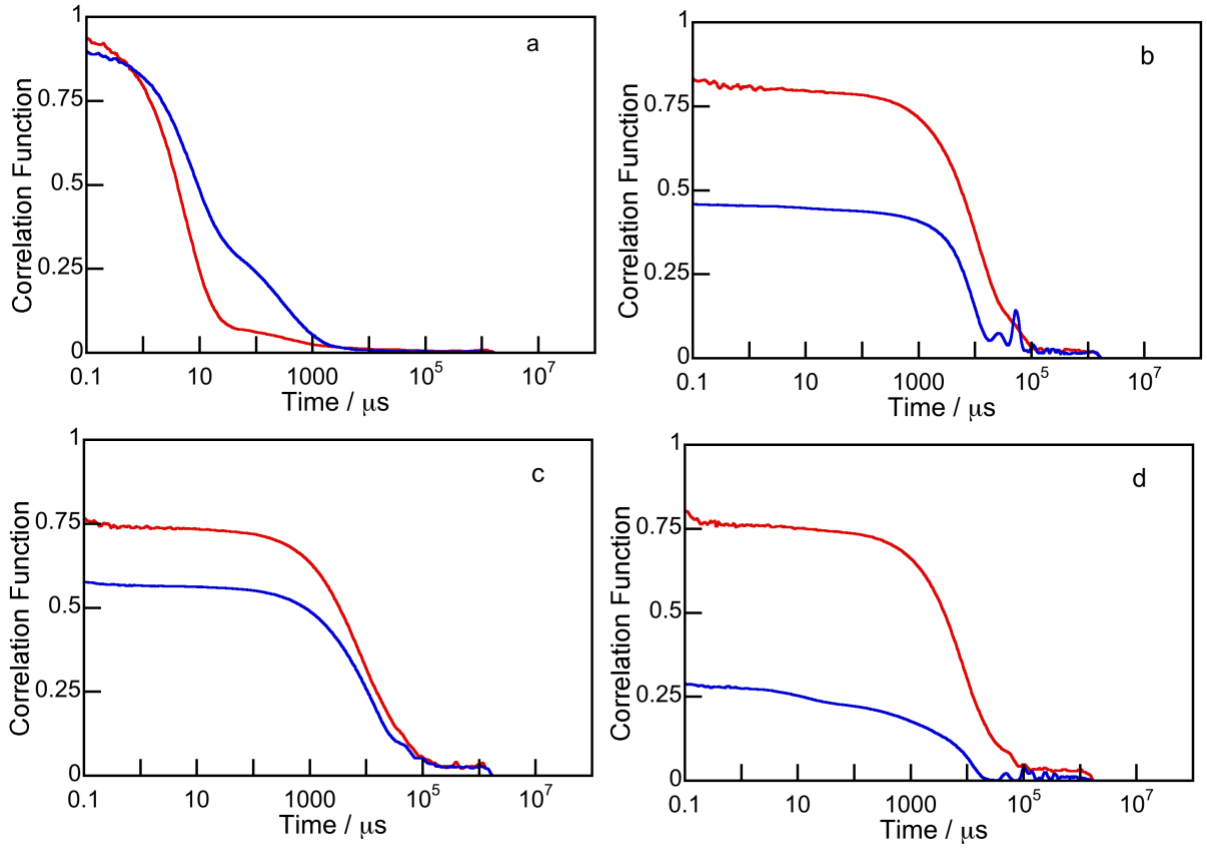

Figure 2.16 DLS correlograms for NaDC-CB[6] gels at CB[6]/NaDC ratios of 0 (a), 0.05 (b), 0.1 (c), 0.15 (d). Traces in each plot are collected at time points of 0 (red solid line), 30 min (blue solid line). Concentration of NaDC in all the samples is 50 mM. Images were collected at 25 ºC.

2.4 Discussion

The effect of CB[6] on the structure, thermo-reversibility and formation kinetics of the NaDC gel was investigated in detail in this chapter. Both DLS and CLSM were chosen as complementary techniques, with the former revealing information on the aggregates that are freely diffusing in the aqueous phase and the latter on aggregates that are a part of the immobile gel structure. The purpose of this discussion is to compare and contrast the information obtained

from the two techniques and to obtain mechanistic insights on the effect of CB[6] on the NaDC gels.

DLS is frequently used to determine the size of particles from a size distribution analysis, but in the case of gels an analysis of the initial amplitude and a qualitative analysis of the decay provides more relevant information. Size distribution profiles reports on the sizes of aggregates assuming a spherical shape and the reported sizes correspond to the hydrodynamic diameter of aggregates. Information such as the correlation coefficient and the decay, which provide a wealth of information, are lost in the size distribution analysis. For example, size distribution profiles in DLS fail to capture information of the concentration of diffusing particles, while this effect is apparent as changes in the correlation coefficient. The use of correlograms to study gels is supported by several reports in the literature.[127-129] For example, the correlation function returning to zero at longer times indicates that a gel is formed.[129] A depression in the correlation coefficient of correlogram is also a sign of gel formation.[130] Correlograms have also been used to monitor the kinetics of gel formation.[129] Therefore, to strengthen my arguments that correlograms without size distribution profiles are still reliable, a test study was performed. In this test study, the size distribution profiles from my data were compared to the existing literature. Size distribution profiles showed that NaDC solutions are composed of aggregates with sizes around 1 nm and 500 nm (Figure A5). The result is consistent with literature studies where aggregates of sizes around 1-2 nm and 150-270 nm have been reported for NaDC solutions.[131] The smaller and larger aggregates formed can be ascribed to primary and secondary aggregates described in the aggregation model developed by Chapman and coworkers.[59]

The mechanism of gel formation was developed based on DLS studies for NaDC in the sol, solution, and gel states. For NaDC, the decays of correlograms in the sol state and in solution

were similar (Figure 2.5, Figure 2.6), suggesting that the structure of the aggregates in these samples were similar. In the NaDC sol, electrostatic interactions between cations in the buffer and the carboxylate (COO^-) groups of aggregates reduces the electrostatic repulsion between the COO^- groups of aggregates. The reduction in electrostatic repulsion brings aggregates closer thereby promoting hydrogen bonding between aggregates, i.e. between OH and COO^- groups.[72, 74, 132] The enhanced hydrogen bonding could possibly result in entanglements between aggregates that contributes to the gel structure. Entanglements between aggregates is supported by DLS studies, where NaDC gels showed extended decays in the correlograms (Figure 2.7) compared to the correlograms for the NaDC sol (Figure 2.6). My model suggesting the role of cations in the NaDC gel formation is consistent with previous findings that showed an increase in mechanical strength of NaDC gels in the presence of NaCl and NaBr.[71] Binding of cations to the CB[6] portal makes CB[6] a mediator that facilitates electrostatic interactions between the COO^- and Na^+ ions. The addition of CB[6] promotes new hydrogen bonding interactions between OH and COO^- groups of NaDC and the carbonyls of CB[6], thereby strengthening the gel. Decrease in the correlation coefficient with the addition of CB[6] (Figure 2.7) also suggest that more NaDC aggregates are incorporated into the gel structure at higher CB[6] concentrations.

Despite its poor resolution compared to electron microscopy techniques, CLSM is chosen to study the structural characterization in NaDC gels. Earlier reports of structural characterization in NaDC gels were performed using electron microscopy techniques,[71] where samples are freeze dried before imaging. Therefore, to avoid drying artefacts, it is necessary to image gels in a hydrated state. My choice of a hydrophilic dye, such as rhodamine 6G is based on the distribution of dye in the gel. Rhodamine 6G due to its positive charge is soluble in water

and can interact with the aggregates in the aqueous phase and the gel structure. This dye can also interact with CB[6] portals as positively charged species, such as cations are known to bind to the portals of CB[6].[133] However, given the concentration of cations in the gel, binding of rhodamine 6G to CB[6] instead of the binding of cations is highly unlikely. Also, the size of rhodamine 6G is too big to fit into the CB[6] cavity. The distribution of rhodamine 6G in water, aggregates in the aqueous phase of the gel and gel structures makes this dye a good choice over hydrophobic dyes like pyrene.

The formation of fibers (Figure 2.9 d) at higher concentrations of CB[6] suggests that CB[6] favors entanglements between aggregates during the gel formation. Overall, DLS and CLSM studies in solutions, sols, and gels reflect a nucleation-elongation mechanism where aggregates in solution reach a critical size. The critical size is dependent on the amount of CB[6] in the solutions(Figure 2.5). The nucleation is followed by elongation leading to gel structures of different morphologies. A similar observation of nucleation-elongation mechanism was reported for calcium cholate gels.[134]

The observed changes in morphology (Figure 2.9) of NaDC gels at different CB[6] concentrations support my hypothesis from DLS studies that CB[6] incorporates more aggregates from the aqueous phase into the gel structure. A further CLSM study with a focus on the location of CB[6] in the gel is suggested to confirm the hypothesis. The techniques discussed in this chapter are qualitative and do not provide information of the fraction of the aggregates located in the aqueous phase and gel structure. Further research should be undertaken to quantify the effect of CB[6] on the distribution of aggregates between aqueous phase and gel structure.

Thermo-reversibility studies suggest that the effect of CB[6] in NaDC gels goes beyond changes in morphology and that the additive plays an active role in the gel-sol and sol-gel

transitions of NaDC gels. Interactions, such as hydrogen bonding, are known to weaken with increasing temperatures. Breakdown of the gel, i.e. disappearance of gel structures, at higher temperatures indicates that hydrogen bonding is the driving force for gel formation. This conclusion agrees with the proposed model for gel formation and the literature.[72] DLS and CLSM studies combined provided insights into the breakdown mechanism of the gel. At higher temperatures, gel structures breakdown into aggregates (Figure 2.10, Figure 2.11) which further breakdown into smaller aggregates (Figure 2.12, Figure 2.13). It is interesting to note that both phenomena occur in the same temperature range. It was observed that the temperatures at which breakdown occurs differs with the addition of CB[6] (Figure 2.10, Figure 2.13). The extra handle of hydrogen bonding interactions between CB[6] and the aggregates could have made the gel less susceptible to breakdown at lower temperatures unlike the breakdown observed for the NaDC gel.

Thermo-reversibility studies were reported for NaDC/NaCl gels using DLS, micro-viscosity and micro polarity measurements.[135] However, the additive in the reported study, i.e. NaCl, interacts with aggregates differently than the additive CB[6] in my study. The reported study describes NaDC as a gel made of higher order aggregates. The study defines aggregates as one system and did not differentiate between aggregates in the aqueous phase and the gel structure, thereby limiting the scope of the results. Overall, arguments developed in the reported study[135] cannot be translated to my study as the gels in both the studies are chemically different.

Kinetics of gel formation has been studied using techniques, such as NMR[136] and fluorescence.[134] Spectral variations such as reduced peak intensities, line broadening and chemical shift changes serve as an indication of the degree of incorporation of free molecules into the rigid component of gels. Once the molecules are incorporated into the rigid gel structure,

they become invisible to solution-state NMR experiments.[136] However, use of NMR is limited to track the kinetics of slow gelation processes.[120] In another study, gelation kinetics of calcium cholate gels was monitored using fluorescence measurements.[134] Cholate gels were tagged with 8-anilinonapthalene-1-sulfonic acid (ANS) dye and the gel formation is defined as a point when emission peak intensity remained unchanged with time.

Techniques, such as steady-state fluorescence, used to track the gelation process for NaDC are limited in terms of length scale. For example, fluorescence properties of pyrene are used to track the gelation process of NaDC.[68] The formation of the gel is defined as a point when the fluorescence emission intensities for both the pyrene monomer and excimer remain constant with time. However, the study focuses on the molecular length scale, i.e. hydrophobic regions, where the dye is localized and do not necessarily reflect the properties of the gel as a whole. Simple visual tests, like vial inversion tests,[120] that study the gel as a whole could be helpful to gain some insights on the kinetics of NaDC and NaDC-CB[6] gel formation. The advantage of using of CLSM (Figure 2.14, Figure 2.15) and DLS (Figure 2.16) to track the kinetics in this thesis is that both techniques reveal information at the microscopic level, while the DLS studies a small volume of the gel, CLSM focuses on the area where the dye is localized in the gel. Also, the results showed that DLS and CLSM techniques were able to capture the kinetics for gel formation more precisely than vial inversion tests. For example, both techniques showed that formation of gel at 0.15 CB[6]/NaDC ratio occurred faster compared to the inversion test.

Besides my understanding though this chapter that CB[6] affects the distribution of aggregates between the aqueous phase and the gel structure, kinetics studies showed that CB[6] speeds up the process of incorporation of aggregates into the gel structure. However, the

explanation for CB[6] promoting the gel formation kinetics remains unknown and will be a question of interest to explore in the future.

2.5 Conclusions

Combination of findings from DLS and CLSM studies provided deeper insights into the effect of additives to a gel while complementing the previous studies in NaDC gels. This is the first CLSM study that investigates NaDC gels in a hydrated state at the microscopic level. The results suggest that the effect of CB[6] as the additive on NaDC gel goes beyond the changes to the gel's structure into kinetics and thermo-reversibility. This study contributes to a new understanding of gel formation and gel breakdown mechanisms, which is an essential knowledge that can be used to control the properties of NaDC gels. Overall, the findings highlight the type of studies that can be feasible with the techniques DLS and CLSM, opening up the possibility to apply these methods for the characterization of multicomponent supramolecular gels.

Chapter 3 Effect of CB[6] on the release of dyes from NaDC-CB[6] gels

3.1 Introduction

Hydrogels have been used to protect, target and deliver drugs in a controllable manner.[137] The use of hydrogels as drug delivery systems are shown to enhance the efficacy, and reduce the toxicity and the required dosage of drugs. Due to the presence of high-water content, hydrogels resemble tissues making them great candidates for biocompatibility. Solubilizing drugs in hydrogels prevents drug aggregation and degradation, which are problems reported when dissolving drugs in organic solvents. Drug-gelator interactions are studied to tune the drug release properties in hydrogels.[138] For example, strategies like covalent conjugation, electrostatic interactions, hydrophobic domains, host-guest interactions in hydrogels have been used to modulate the drug release properties.[73]

Due to the presence of reversible and weak physical interactions, supramolecular gels have been investigated for applications in drug delivery. A supramolecular gelator tagged with a drug or a model dye can form a stable gel under certain conditions but break up in the presence of particular stimulus resulting in targeted and controlled delivery of drugs.[139] For example, Chen and coworkers employed supramolecular gels based on triptycene derived macrotricyclic polyether networks formed via host-guest complexation for encapsulation and controlled release of squarine dyes.[140] Feng and coworkers studied coumarin based gelators for photo-controlled release of dyes from the gels.[141] In another work, Hamachi and coworkers demonstrated stimuli responsiveness of a supramolecular hydrogel based on a phosphate type hydrogelator to temperature, pH, Ca^{2+}, or light.[142] The authors used a combination of stimuli to construct logic gates. The study showed that the supramolecular gels hold and release bioactive substances in response to a combination of logic gates.[142]

Drug or model dye release from hydrogels has been investigated using static and dynamic diffusion methods. In a static diffusion method, the release medium is added on top of the gel. Drug release is monitored by analyzing aliquots retrieved from the top of the gel over time using UV-Vis, HPLC, fluorescence, or NMR measurements.[142] The aliquots of supernatant are replaced by fresh release medium every time after analysis. In such a case, a volume correction is applied for the calculations of the amount of drug release. In a dynamic diffusion method, the gel sample loaded with the drug is placed at the bottom of the vessel containing the release medium. The paddle in the apparatus stirs the system continuously. The release medium is analyzed at different time points using analytical techniques to calculate the amount of drug released. A different apparatus to study dynamic diffusion includes a Franz diffusion cell.[143] In this set up, the gel loaded with the drug is placed in the upper chamber. The lower chamber is filled with the release medium. The upper and lower chambers are separated by a semi permeable membrane. The lower chamber is surrounded by a water jacket to maintain the temperature of the release medium constant. A simple model for a Franz diffusion cell includes the use of a dialysis bag.[144] In this set up, the gel is loaded into a dialysis bag with a certain Molecular Weight Cut Off (MWCO). The MWCO is chosen to allow the release of the drug from the gel with the gel staying intact inside of the dialysis bag. The bag is sealed and placed into a beaker containing the release medium to monitor the release.

3.1.1 Objectives

The objective of the current work is to show the role of additives, i.e. CB[6] on the release of small molecules from the NaDC gel. CB[6] offers the possibility of exploiting well defined interactions in the NaDC gel, which in turn could affect the gel formation and the gel's structure at different length scales. The small molecules chosen for this study should meet two

criteria. These molecules should not form host-guest complexes with CB[6] and the molecules should have different hydrophobicities. Based on these criteria, pyrene and rhodamine 6G are chosen as the small molecules of interest. The two molecules although large enough to not fit into the cavity of CB[6], can be involved in a weak interactions with CB[6]. My expectation is that these small molecules reside in different regions of the gel depending on their hydrophobicities. Rhodamine 6G is mainly located in water and pyrene is expected to be located in the hydrophobic regions of the NaDC aggregates. For the release studies, I chose the static diffusion method to monitor the release, where only one surface of the gel is exposed to the release medium. I have demonstrated that CB[6] has a different role as an additive on the release of small molecules with different hydrophobicities from NaDC gels.

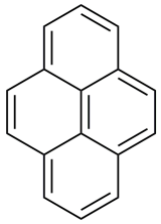

Chart 3.1 Chemical structure of pyrene.

3.2 Experimental

3.2.1 Materials

NaDC (Fluka, > 98%), NaH_2PO_4 (Anachemia, > 98%), Na_2HPO_4 (Anachemia, > 98%), methanol (Fisher grade), rhodamine 6G (Sigma Aldrich, 99%), N-(4-aminophenyl)imidazole (API, Sigma Aldrich, 98%), 1,6-diaminohexane (DAH, Sigma Aldrich), hydrochloric acid (HCl, BDH 36.5-38%), deionized water (Barnstead NANOpure deionizing systems, 17.8 MΩ cm) were used as received. Absorbance cells 10 mm × 10 mm (Hellma), fluorescence cells 10 mm × 10 mm

(Hellma), 8 dram snapped cap glass vials (for spectroscopic measurements), 3 dram snapped cap glass vials (for sample preparations) were used.

DAH salt was recrystallized by adding acetone (15 mL) to 11 mmol DAH solution dissolved in 1.85 mL concentrated HCl, followed by vacuum filtration to obtain white crystals. The sample CB[6]-SG-1 (purity 84%) was used in this study. CB[6] was synthesized and purified based on the standard protocols in the group.[69] The CB[6] concentration was determined by titrating the stock solutions with recrystallized DAH. In this titration, DAH^{2+} displaces API^{+} bound with CB[6] leading to a decrease in the steady-state fluorescence intensity of API^{+}. Pyrene was recrystallized from ethanol twice and the purity of pyrene was established by observing a mono-exponential fluorescence decay in water.[145]

3.2.2 Sample preparation

Rhodamine 6G (3.5 mM) and pyrene (1 mM) stock solutions were prepared in methanol. Phosphate buffer stock solutions (0.5 M) at pH 6.5 were prepared by mixing appropriate volumes of NaH_2PO_4 (0.5 M) and Na_2HPO_4 (0.5 M) stock solutions. NaDC stock solutions (0.2 M) were prepared in deionized water. The NaDC stock solutions were heated at 60 °C for 15 min to dissolve the NaDC solid.

For NaDC gels, 750 µL of the NaDC stock solution and 1942 µL of deionized water was added into an 8-dram sample vial. The solution was heated at 60 °C for 15 min. While this solution was hot, 8 µL of dye stock and 300 µL phosphate buffer were added followed by heating of this mixture at 60 °C for 15 min. For NaDC-CB[6] gels, CB[6] solid was dissolved in 1942 µL volumes of deionized water and 300 µL phosphate buffer. The addition of phosphate buffer led to the solubilization of CB[6] at room temperature. This solution was heated for 15 min at 60 °C. While the solution was hot, 8 µL of dye stock and 750 µL NaDC solution were

added followed by heating at 60 °C for 15 min. The sample vial was wrapped with an aluminum foil and left undisturbed for 20 h at room temperature in a water bath to allow for the formation of gels. The 20 h time period in which gels were left undisturbed is referred to below as the "resting period". To maintain similar resting conditions for the gelation processes for samples with different concentrations of CB[6], all the gel samples with NaDC and CB[6] were prepared simultaneously.

The final concentrations of NaDC and phosphate buffer in the gel samples were 50 mM. The final concentrations of CB[6] in the gel samples were 2.5, 5.0, or 7.5 mM. All gels have a concentration of Na^+ ions of 200 mM. The final concentration of pyrene in the gel samples was 5 μM. Release experiments with rhodamine 6G were performed with 10 μM and 1 mM concentration of the dye in the gel samples.

3.2.3 Equipment

Absorption spectra were collected on a CARY 100 spectrometer between 200-650 nm using a step size of 1 nm and integration time 0.1 s. Steady-state fluorescence spectra were collected using a PTI QM40 spectrophotometer. The excitation and emission monochromator bandwidths were set to 2 nm. The step size was set to 0.5 nm and the integration time was set to 0.25 s. For pyrene studies, the samples were excited at 331 nm and the emission spectra were collected between 350-550 nm. For rhodamine 6G studies, the samples were excited at 480 nm and the emission spectra were collected between 490-700 nm. For the mechanism of dye release studies, emission spectra of the release medium and controls were excited at 330 nm and the emission spectra were collected between 350-600 nm.

3.2.4 Dye release studies

After the 20 h resting period, 15 mL of phosphate buffer (50 mM) was added on top of

the gel (3 mL) as the surrounding medium (Scheme 3.1). At regular time intervals, 3 mL of surrounding media was taken from the top of the gels and the surrounding medium was analyzed using fluorescence (10 µM rhodamine 6G and 5 µM pyrene) or absorbance (1 mM rhodamine 6G) measurements. After the measurement, the surrounding medium was added back into the sample vial taking care to minimize any volume loss. Data was collected every hour for an average period of 6 h.

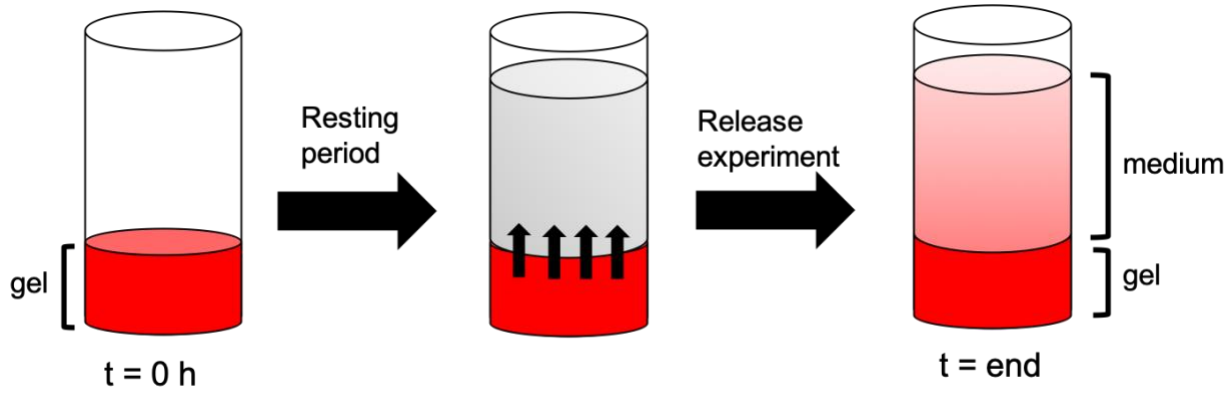

Scheme 3.1 Schematic representation of release studies setup.

A calibration curve was constructed with the known concentrations of the dye in 50 mM phosphate buffer on the same day. The concentration of the dye in the surrounding medium at a given time during the release was obtained by using the calibration curve. The percentage of dye released into the surrounding medium (DR%) at a given time was obtained using equations 3.1 and 3.2.

$$n_{\mathrm{t}} = \left(\frac{I - c}{m}\right) \times V$$

Eq. 3.1

$$\mathrm{DR}(\%) = \left(\frac{n_{\mathrm{t}}}{n_{\mathrm{i}}}\right) \times 100$$

Eq. 3.2

The parameter *I* corresponds to the integrated area of the fluorescence spectrum between 360 and 420 nm for studies with 5 µM pyrene and the integrated area between 530-580 nm for studies with 10 µM rhodamine 6G. For the studies using 1 mM rhodamine 6G, *I* corresponds to the absorbance value at the absorption maximum of 526 nm. The parameters *m* and *c* correspond to the slope and intercept of the calibration curve, respectively obtained on the same day as the release experiments were performed. *V* is the volume of the surrounding medium (15 mL), while n_t is the number of moles of the dye in the surrounding medium at a given time and n_i is the initial number of moles of the dye in the gel before the resting period. The value of n_i was obtained from absorbance measurements.

3.2.5 Mass balance

The mass balance is a measure to determine if any loss of dye occurred during the release studies. The mass balance before and after the release experiments was determined by absorbance measurements. These measurements were performed for samples in the sol phase to eliminate interference from light scattering by the gel. The initial absorbance was determined right after sample preparation and before the resting period of 20 h for gel formation. After the release experiment was completed, the surrounding medium and the gel were heated together at 60 °C for 15 min to form a homogeneous sol and the absorbance of this sol sample was determined.

The percentage of mass balance (*MB*%) for the dyes in the gels was calculated using equation 3.3.

$$MB(\%) = \left(\frac{A_{\text{end}}}{A_{\text{initial}}}\right) \times DF \times 100$$

Eq. 3.3

The parameter A_{end} is the absorbance of the sol after the release experiments was completed, $A_{initial}$ is the absorbance of the sol before the resting period (t = 0 h in the Scheme 3.1). *DF* is the dilution factor, which corresponds to the ratio between sample volume for the release studies (i.e. sum of the volumes for the gel and surrounding medium), and the volume for the gel sample at t = 0 h. The *DF* was 6 for all the release studies.

3.2.6 Loading efficiency

The loading efficiency is a measure to determine if any loss of dye occurred while the gel was formed. An absorption spectrum of the sol at 60 °C was collected before the resting period (t = 0 h in the Scheme 3.1) to determine the initial concentration of the dye in the sol. After the 20 h resting period, the gel was heated at 60 °C for 15 min and the absorption spectrum of the sol was collected to determine the concentration of the dye in the sol at 20 h.
The loading efficiency (*LE*%) for the dyes in the gel was calculated using equation 3.4.

$$LE(\%) = \left(\frac{A_{\mathrm{t=20h}}}{A_{\mathrm{t=0h}}}\right) \times 100$$

Eq. 3.4

The parameter $A_{t=20h}$ is the absorbance of the sol after 20 h resting period and $A_{t=0h}$ is the absorbance of the sol before the resting period.

3.2.7 Baseline correction for scattering in the absorption spectra in gels

Gels were shown to scatter light. The purpose of the baseline correction is to remove the effects of scattering from the raw absorbance data (see details in the results section below). The wavelength range for baseline correction is chosen such that the dye does not absorb in the range and the range is close to the wavelength where the dye has a maximum in the absorption spectra,

but for which a solution with no scattering the dye does not absorb. For pyrene, the wavelength range between 360-380 nm was chosen, whereas for rhodamine 6G, the wavelength range between 400-420 nm was chosen.

The following steps were followed in the case of pyrene, and the same method was used for rhodamine 6G:

1. For the sample at 0 h (red) and end of study (blue), the wavelength range between 360-380 nm was chosen to determine the baseline.
2. Absorbance values and wavelength in the range 360-380 nm were fit to a linear relationship (Figure 3.1) and the slope (m) and intercept (c) were determined.

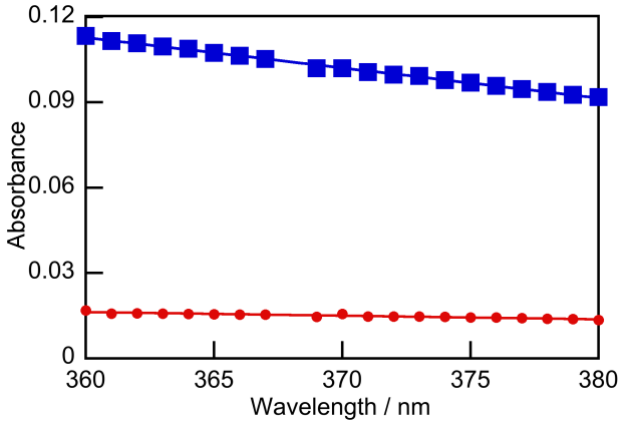

Figure 3.1 Absorption spectra for pyrene (5 µM) in NaDC gels (50 mM) at CB[6]/NaDC ratio of 0.15 plotted in the wavelength range of 360-380 nm.

3. Each wavelength point across the spectrum (250 to 600 nm) was substituted in equation 3.5 (obtained from the data shown in Figure 3.1) to determine the contribution of scattering to the absorbance at that wavelength. The calculated absorbance was labeled as baseline (BSL) (dashed line shown in Figure 3.2)

$$A_{\mathrm{BSL}} = (m \times \lambda) + c$$

Eq. 3.5

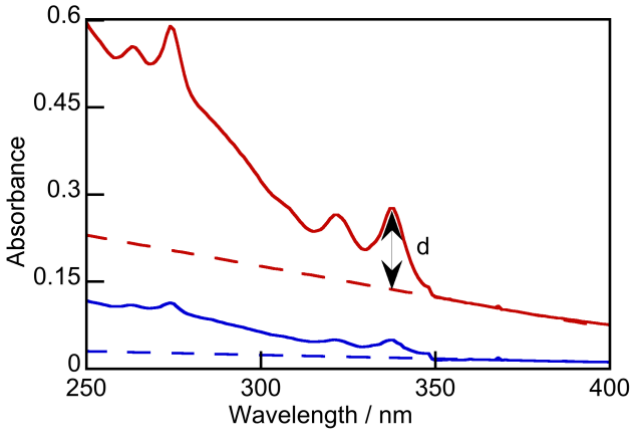

Figure 3.2 Absorption spectra for pyrene (5 μM) in NaDC gels (50 mM) at CB[6]/NaDC ratio of 0.15. Solid lines represent the experimental data, dashed lines represent the baselines, difference 'd' corresponds to the baseline-corrected absorbance at 337 nm.

4. The baseline corrected absorbance (A_{corr}) at a particular wavelength (equation 3.6) was obtained by subtracting the initial spectrum from the BSL spectrum in Figure 3.2

$$A_{\text{corr}} = A_{\text{initial}} - A_{\text{BSL}}$$

Eq. 3.6

5. Steps 2-4 were repeated for spectra collected at 20 h. Corrected absorbance values at 337 nm are used to calculate MB% and LE%.

The baseline correction treatment was an approximation. For example, absorption of pyrene approaches zero at 300-310 nm for a pyrene solution in water. However, the baseline correction of the spectrum does not approach zero at 300-310 nm for the data under consideration. However, at 337 nm, a substantial amount of scattering was subtracted from the spectrum while calculating MB% and LE%.

3.2.8 Mechanism of dye release

The gel samples with CB[6]/NaDC ratios of 0 and 0.15 were prepared with rhodamine 6G (10 μM) and pyrene (5 μM) to investigate the dye release mechanism. After the 20 h resting period, 15 mL of phosphate buffer (50 mM) was added on to the top of the gel as the surrounding medium. The sample was left undisturbed for an average period of 6 h. During this time period, the dye can diffuse into the surrounding medium from the gel. At the end of 6 h, the polarity of

the surrounding medium was analyzed by adding pyrene (2 μM) to 3 mL of release medium. Four controls for this study include 50 mM NaDC solution, 7.5 mM CB[6] solution, 50 mM phosphate buffer, 0.15 CB[6]/NaDC solution. All the control solutions were prepared with pyrene (2 μM).

The blank (50 mM phosphate buffer) is subtracted from the emission spectra of the samples. The intensity of the I and III bands (based on the maxima of bands) for the pyrene emission in the corrected spectra were used to determine the I/III ratio.

3.3 Results

3.3.1 Release experiments of rhodamine 6G (10 μM) in NaDC-CB[6] gels

The purpose of this study was to investigate the effect of CB[6] on the release of rhodamine 6G from NaDC gels. Rhodamine 6G is a positively charged dye which emits fluorescence in the range of 530-600 nm. For this study, gels at CB[6]/NaDC ratios of 0, 0.05, 0.1, 0.15 were loaded with rhodamine 6G. Release medium was added to the top of the gel after 20 h of gel preparation. With time, rhodamine 6G diffuses into the release medium and the dye release was monitored by collecting emission scans of the release medium at a given time. As seen in the Figure 3.3, Figure B1, Figure B2, fluorescence intensities of the release medium at a given time were unaffected by the presence of CB[6].

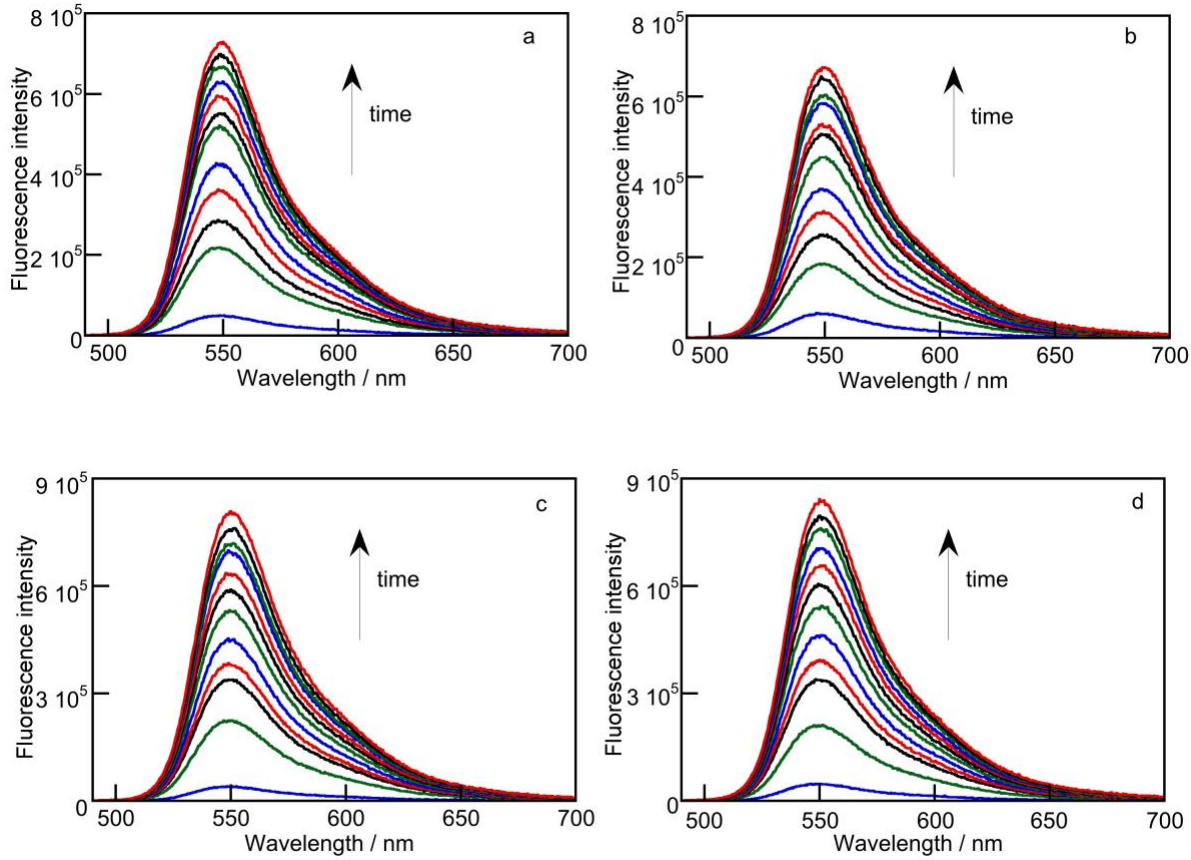

Figure 3.3 Emission spectra of the surrounding medium collected at different time points during the release of rhodamine 6G (10 μM) from NaDC gels (50 mM) with different CB[6]/NaDC ratios: 0 (a), 0.05 (b), 0.1 (c), 0.15 (d). Time interval 0-400 min.

The amount of rhodamine 6G released at a given time was quantified by comparing the fluorescence intensity with intensities of known concentrations of rhodamine 6G in the medium. To achieve this, a calibration curve was constructed with known concentrations of rhodamine 6G in the release medium (Figure 3.4, Figure B3, Figure B4).

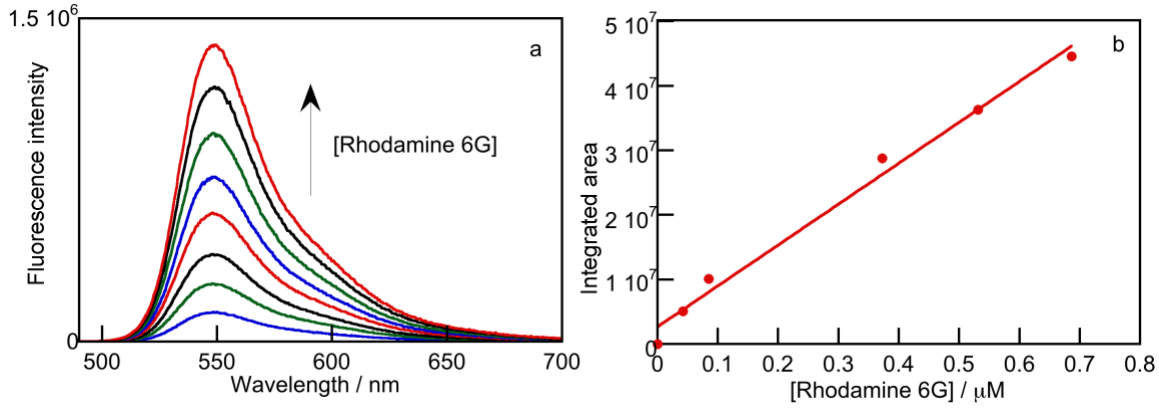

Figure 3.4 a. Emission spectra of known concentrations of rhodamine 6G in phosphate buffer collected for the calibration curve. b. Calibration curve.

The percentage of dye released into the surrounding medium at a given time was determined by comparing the number of moles of dye in the medium at a given time with the initial number of moles of the dye in the gel. Percentage of dye released into the surrounding medium was plotted as a function of time (Figure 3.5, Figure B5). A gradual release of the dye was observed with time. As seen in Figure 3.5 and Figure B5, release of rhodamine 6G was unaffected by the presence of CB[6] in the gel. The time period to reach half the maximum release ($T_{1/2}$) was 100 min for all the gels irrespective of the CB[6] concentration.

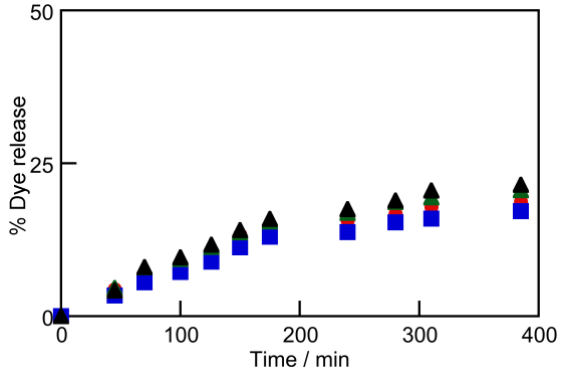

Figure 3.5 Release profile for rhodamine 6G (10 μM) from NaDC gels (50 mM) with different CB[6]/NaDC ratios: 0 (red), 0.05 (blue), 0.1 (green), 0.15 (black).

3.3.2 Release experiments of rhodamine 6G (1 mM) in NaDC-CB[6] gels

Release studies were also performed at a higher concentration of rhodamine 6G (1 mM) to understand if at the higher concentrations of rhodamine 6G, release can be affected by the presence of CB[6]. My hypothesis is that at higher concentrations of rhodamine 6G, dye molecules compete with cations in buffer to interact with CB[6], which in turn may affect the release pattern. Gels with CB[6]/NaDC ratios of 0, 0.05, 0.1, 0.15 were loaded with 1 mM rhodamine 6G. At 1 mM rhodamine 6G, the dye concentration in the gel is high and fluorescence intensities fall out of the linear range for the calibration curve. Therefore, instead of measuring fluorescence, the release study was done by measuring absorbance of the dye into the release medium at a given time. Absorbance was tracked over a time period of 550 min. As seen in Figure 3.6 and Figure B6, the absorbance at 526 nm for rhodamine 6G at the end of the release experiment is consistent for gels at CB[6]/NaDC ratios of 0, 0.05, 0.1. However, for gels with 0.15 CB[6]/NaDC ratio, the absorbance at 526 nm for rhodamine 6G at the end of the experiment is almost three-fold higher compared to gels at lower CB[6]/NaDC ratios.

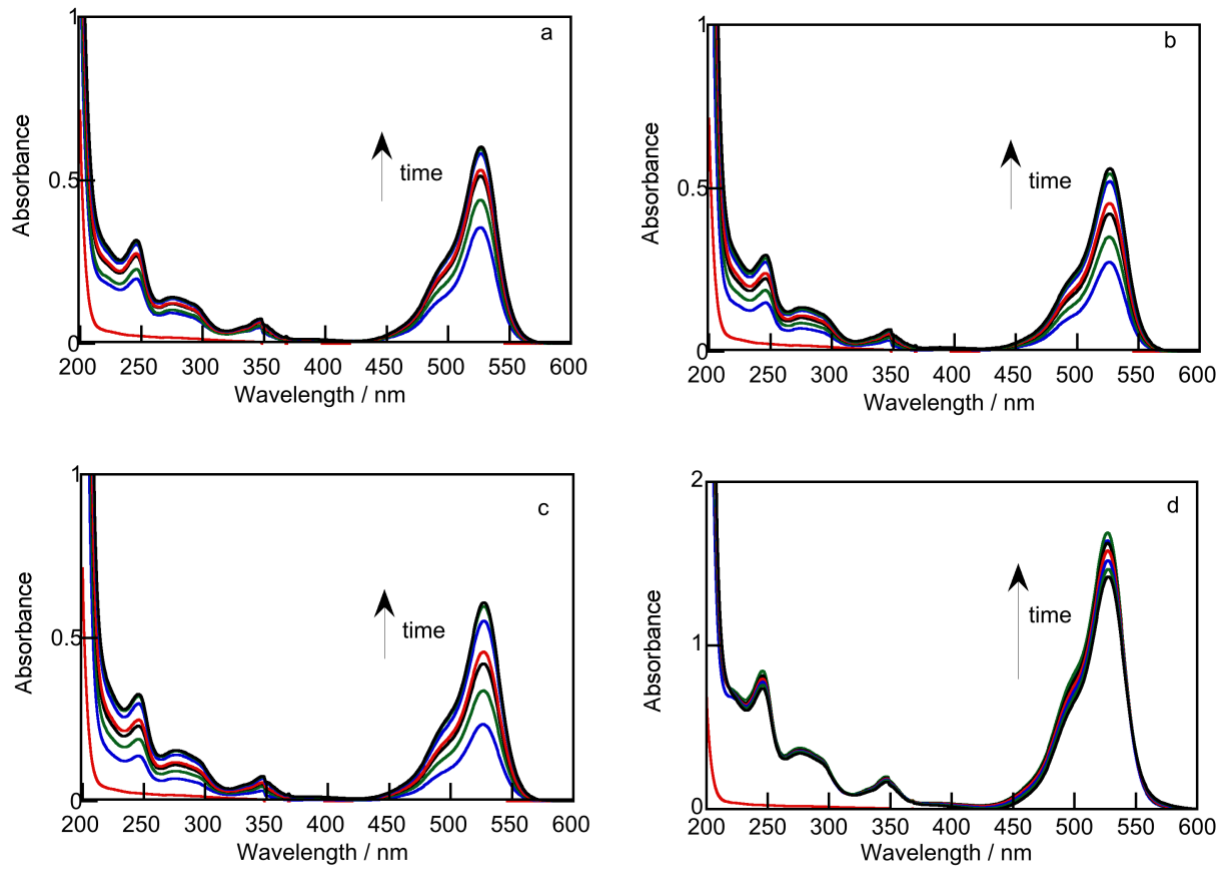

Figure 3.6 Absorption spectra of the surrounding medium collected at different time points during the release of rhodamine 6G (1 mM) from NaDC gels (50 mM) with different CB[6]/NaDC ratios: 0 (a), 0.05 (b), 0.1 (c), 0.15 (d). Time interval 0-550 min.

A calibration curve with known concentrations of rhodamine 6G was constructed to quantify the amount of dye released into the surrounding medium from the gel at a given time. Absorbance values at 526 nm were plotted as a function of the dye concentration to determine the calibration curve, which in this case is linear (Figure 3.7).

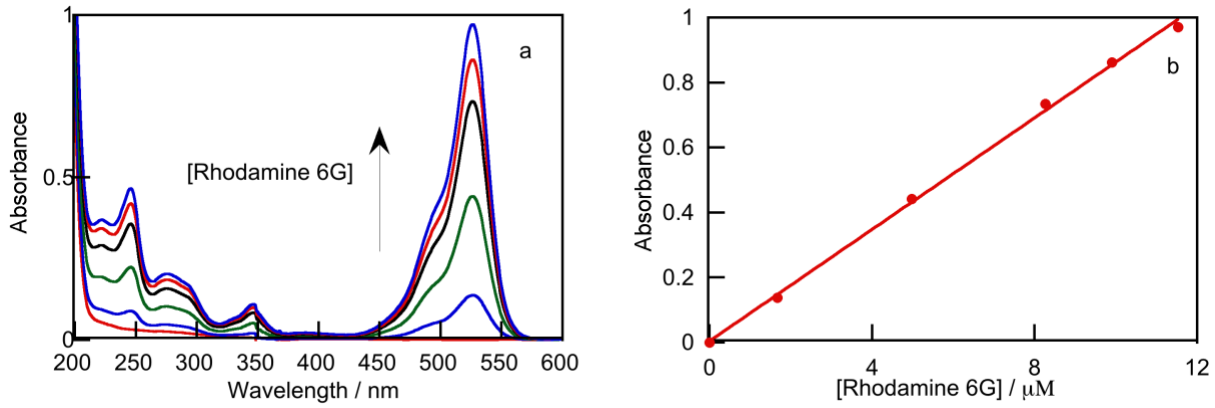

Figure 3.7 a. Absorption spectra of known concentrations of rhodamine 6G in phosphate buffer collected for the calibration curve. b. Calibration curve.

The percentage of dye released was determined by comparing the moles of dye in the surrounding medium at a given time with the initial number of moles of the dye in the gel. The percentage of dye released was plotted as a function of time. As seen in Figure 3.8 and Figure B7, the release pattern of the dye is similar for gels at CB[6]/NaDC ratios of 0, 0.05, 0.1.

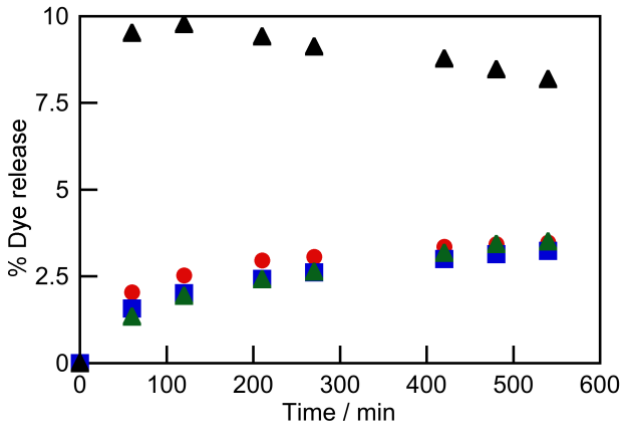

Figure 3.8 Release profile for rhodamine 6G (1 mM) from NaDC gels (50 mM) with different CB[6]/NaDC ratios: 0 (red), 0.05 (blue), 0.1 (green), 0.15 (black).

However for gels at CB[6]/NaDC ratios of 0.15, a burst release pattern was observed where the percentage release reached a maximum value before the first reading collected at 60

min. After an initial rise, the gradual fall of the amount of dye released for 0.15 CB[6]/NaDC gel suggests that either the aggregation of the dye or that other absorption artefacts may be occurring in the surrounding medium.

Results with the hydrophilic dye rhodamine 6G showed that at the lower concentration of rhodamine 6G, release was unaffected by the presence of CB[6]. However at higher concentrations of rhodamine 6G, dye release was found to be affected only at the highest CB[6]/NaDC ratio studied.

3.3.3 Release experiments of pyrene (5 μM) in NaDC-CB[6] gels

Primary aggregates of NaDC have hydrophobic sites which can interact with hydrophobic guest molecules.[146] I chose pyrene as a hydrophobic dye to perform release studies and to understand how CB[6] affects the release of a dye which is known to interact with the hydrophobic regions of the gel. Gels with CB[6]/NaDC ratios of 0, 0.05, 0.1, 0.15 loaded with 5 μM pyrene were used for the release experiments. Emission spectra of pyrene in the release medium were collected at different time intervals (Figure 3.9, Figure B8). As seen in Figure 3.9 and Figure B8, fluorescence intensities of pyrene in the release medium at a given time varied with the concentration of CB[6] in the gel, unlike the constant release of rhodamine 6G at the lowest rhodamine 6G concentration studied. At a given time, fluorescence intensities of the release medium were lower for the gels at highest CB[6]/NaDC ratios.

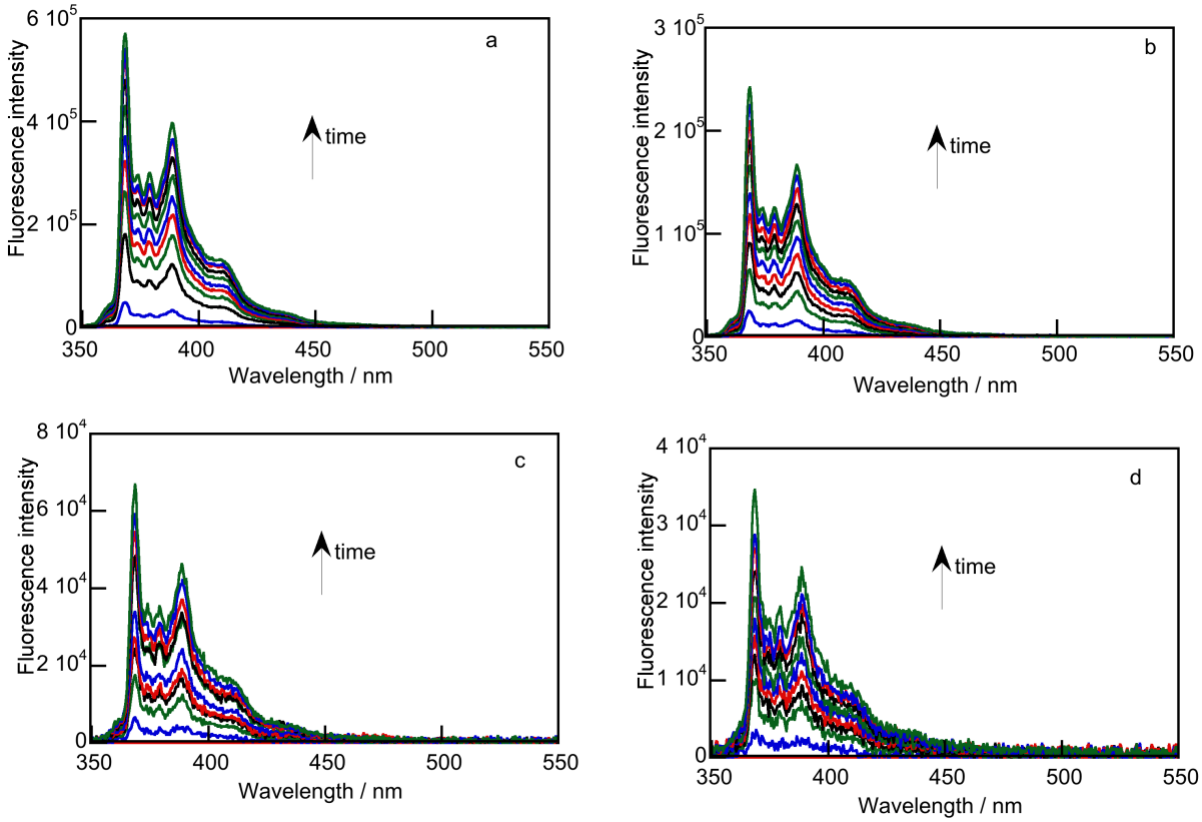

Figure 3.9 Emission spectra of the surrounding medium collected at different time points during the release of pyrene (5 μM) dye from NaDC gels (50 mM) with different CB[6]/NaDC ratios: 0 (a), 0.05 (b), 0.1 (c), 0.15 (d). Time interval 0-360 min.

The number of moles of pyrene in the medium at a given time was calculated by comparing intensities at a given time with a known calibration curve of pyrene in phosphate buffer (Figure 3.10, Figure B9). The percentage of dye released into the surrounding medium at a given time was determined using equation 3.2 and the data obtained were plotted as a function of time (Figure 3.11, Figure B10).

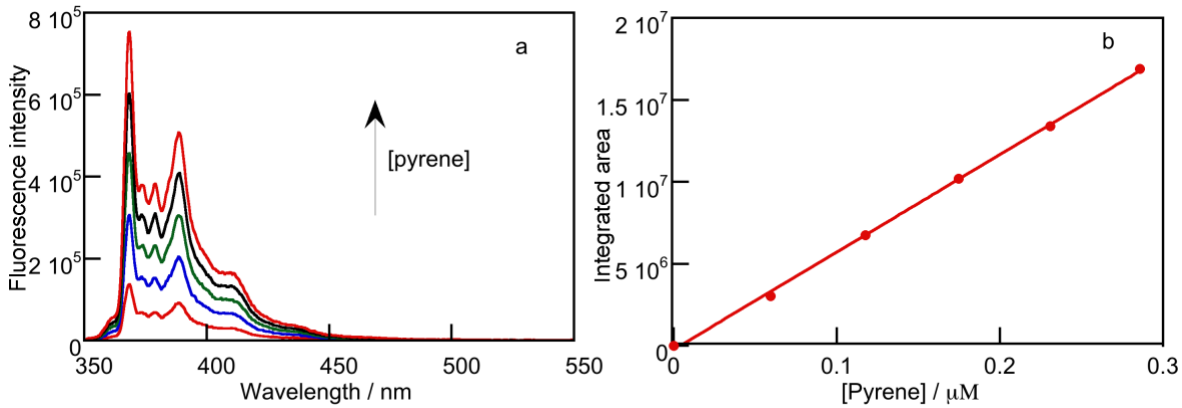

Figure 3.10 a. Emission spectra of known concentrations of pyrene in phosphate buffer collected for the calibration curve. b. Calibration curve.

As shown in Figure 3.11 and Figure B10, the amount of dye released from the gel into the surrounding medium decreased with the increase in the CB[6]/NaDC ratio in the gel. However, the relationship between the percent of dye released with the CB[6]/NaDC ratio is not linear. Gels with a CB[6]/NaDC ratio of 0.05 reported a 10% dye release at the end of the experiment. Gels with a CB[6]/NaDC ratio of 0.1 reported a 3% dye release at the end of the experiment. The time period to reach half the maximum release ($T_{1/2}$) was found to be around 95 min for the gels irrespective of the CB[6] concentration. The release results with pyrene (5 μM) and rhodamine 6G (10 μM) indicate that CB[6] affects the release kinetics differently for each of these dyes. These differences can be due to the different locations for the dyes in the gels due to their different hydrophobicities.

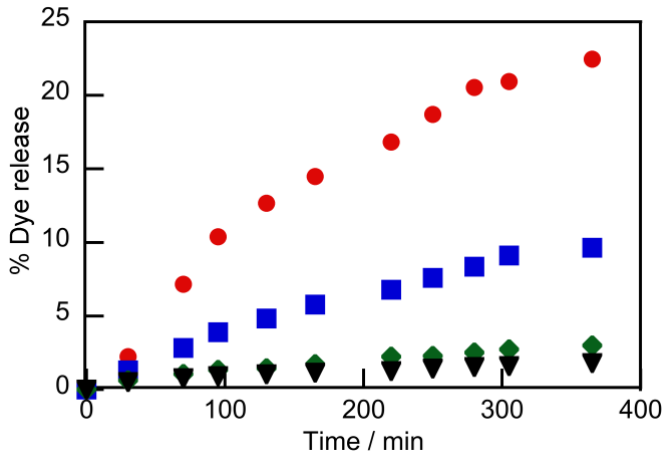

Figure 3.11 Release profile for pyrene (5 µM) from NaDC gels (50 mM) with different CB[6]/NaDC ratios: 0 (red), 0.05 (blue), 0.1 (green), 0.15 (black).

3.3.4 Loading efficiency of the dyes in NaDC-CB[6] gels

Release experiments require a 20 h resting period for gels before the addition of the surrounding release medium. Due to this long resting period and the long time periods for the release studies, dye precipitation from the gel could have occurred which would interfere with the quantification of the release results. Previous evidence suggested that dyes, such as pyrene or rhodamine 6G are likely to deposit on glass surfaces or precipitate when the solution is left in glass containers for certain periods of time.[147] Therefore, it is required to rule out artefacts, such as the dye precipitation to validate the release results.

Artefacts during the resting period of gels for 20 h between the gel preparation and release studies is ruled out by performing loading experiments. In this control experiment, the amount of dye in the gel was measured by collecting the absorption spectra before the resting period at 0 h and after resting period at 20 h. The loading efficiency was determined using equation 3.4. To minimize scattering from the gels, the gels were converted into the sol phase by

heating at 60 °C for 15 min before taking measurements. Loading experiments were performed for gels with rhodamine 6G and pyrene and the results are shown in Table 3.1.

Table 3.1 LE(%) of dyes in NaDC-CB[6] gels at CB[6]/NaDC ratios of 0, 0.05, 0.1, 0.15. Dyes under study are rhodamine 6G and pyrene. Errors correspond to data from two individual experiments.

NaDC:CB[6] ratio	LE%				
	Rhodamine 6G / 10 µM		Rhodamine 6G / 1 mM	Pyrene / 5 µM	
	without baseline corrections	with baseline corrections	without baseline corrections	without baseline corrections	with baseline corrections
0	101±1	101±1	110±20	102±4	100.±1
0.05	101±1	101±1	110.±1	101±3	97±1
0.1	101±1	101±1	107±8	101±1	98±1
0.15	103±6	102±8	110±20	100±10	140±30

At higher concentrations of CB[6], I observed scattering from the sol sample which appears as a continuous increase in the absorbance as the wavelength is decreased (Figures B11, B12, B13, B17). Since Rayleigh scattering is inversely proportional to the fourth power of the wavelength, scattering is more prominent in the spectra of dyes which absorb at shorter wavelengths. Baseline corrections were performed for the raw data and the results are shown in Table 3.1. The results for the loading experiments indicate that no dye precipitation occurred during the resting period.

3.3.5 Mass Balance of the dyes in NaDC-CB[6] gels

Artefacts during the release study, which takes 7 h, were ruled out by performing mass balance (MB) studies. My hypothesis is that a MB close to 100% indicates the absence of dye precipitation during the release study. In this control experiment, the amount of dye in the gel was measured by collecting the absorption spectra of sol samples before the resting period at 0 h. At the end of the release study, the absorption spectrum of the sol sample was collected. The MB was determined using equation 3.3. Mass balance experiments were performed for gels with rhodamine 6G and pyrene and the results are shown in Table 3.2.

Scattering from the sol samples (Figures B14, B15, B16) was subtracted using baseline corrections and the results for the calculated MB values were shown in Table 3.2. Results from mass balance experiments indicate that dye precipitation during the release study did not occur.

Table 3.2 MB(%) for dyes in NaDC-CB[6] gels at CB[6]/NaDC ratios of 0, 0.05, 0.1, 0.15. Dyes under study are rhodamine 6G and pyrene. Errors correspond to data from two individual experiments.

NaDC:CB[6] ratio	MB%				
	Rhodamine 6G / 10 µM		Rhodamine 6G / 1 mM	Pyrene / 5 µM	
	without baseline corrections	with baseline corrections	without baseline corrections	without baseline corrections	with baseline corrections
0	93±2	99±2	120±10	110.±2	112±8
0.05	97±3	101±3	80±20	115±5	113±3
0.1	96±1	100.±1	90.±4	132±6	126±1
0.15	101±9	110±10	90±10	90±20	127±4

3.3.6 Release mechanism of the dyes in NaDC-CB[6] gels

Pyrene was chosen for the release studies because it has unique photophysical properties. The emission spectrum of pyrene has 5 vibronic bands, where the ratio of the vibronic bands I (at the peak close to 368 nm in the emission spectra) and III (at the peak close to 378 nm in the emission spectra) is sensitive to the polarity of the environment around pyrene.[114] The I/III ratio of pyrene in phosphate buffer was 1.93±0.01, and in NaDC solutions this ratio was 0.77±0.01. The observed I/III ratio for pyrene is the weighted average of I/III ratios for pyrene located in different environments within the gel. For example, the I/III ratio of pyrene in the NaDC-CB[6] solution (1.28±0.06) was between the I/III ratio in NaDC (0.77±0.01) and the I/III ratio in CB[6] solution (1.92±0.03).

The purpose of this study was to identify if the release of the dye corresponds to the release of the free dye or release of dye along with NaDC aggregates. The release medium at the end of the release study was analyzed to obtain the information on the mechanism of dye release. Pyrene (2 μM) was added to the release medium and the I/III ratios were obtained to investigate the polarity of the environment around pyrene. My hypothesis is that if NaDC aggregates diffused along with the dye into the surrounding medium, I would expect a lower I/III ratio. The I/III ratios for various release mediums are reported in Table 3.3. The results for the I/III ratios show that the polarity of the environment around pyrene in the release medium was unchanged across different media and this value is close to the I/III ratio in phosphate buffer. This result indicates that release of pyrene from the gel into the surrounding medium corresponds to the diffusion of free dye from the gel into the medium.

Table 3.3 Pyrene I/III ratios in different release mediums.

Release medium	I/III ratio
Rhodamine 6G/NaDC gel	1.95±0.02
Rhodamine 6G/NaDC-CB[6] gel	1.90±0.01
Pyrene/NaDC gel	1.93±0.01
Pyrene/NaDC-CB[6] gel	1.88±0.01

3.4 Discussion

Fluorescence correlation spectroscopy (FCS) experiments performed in the group showed that the NaDC gel is made of aggregates out of which some of the aggregates are in the aqueous phase of the gel while other aggregates are in the gel structure.[69] The hydrophobic effect and hydrogen bonding play a major role in the formation of bile salt aggregates.[148] Rhodamine 6G is a positively charged molecule that can interact with the negatively charged carboxylate groups on NaDC. Because of its hydrophilic nature, I expect rhodamine 6G to be located in the aqueous phase of the gel. However, a fraction of rhodamine 6G molecules can interact with the negatively charged carboxylate groups on the surface of the NaDC aggregates. Since rhodamine 6G in the aqueous phase is in equilibrium with the dye in the gel's structure, the addition of the surrounding medium displaces the equilibrium between free and bound rhodamine 6G in the gel and the release rate is the time it takes to establish the new equilibrium.

For NaDC-CB[6] gels, the hydrogen bonds formed between hydroxyl groups of NaDC and the carbonyls of CB[6] or/and electrostatic interactions between the carboxylate moiety of deoxycholate and Na^+ ions bound to the portal of CB[6] are possible interactions involved in the formation of the gel. The microscopy studies (chapter 2) suggested that CB[6] incorporates more

NaDC aggregates into the gel structure from the aqueous phase by providing an extra handle for hydrogen bonding and electrostatic interactions between the NaDC aggregates. As a result, there will be fewer NaDC aggregates free to diffuse in the aqueous phase. Positively charged molecules binding to the outer portals of CB[n]'s are well reported in the literature.[133] Besides the interaction of rhodamine 6G with NaDC, a competition between Na^+ cations in the buffer and rhodamine 6G for the binding to the portals of CB[6] is possible. Given the large excess of Na^+ cations compared to rhodamine 6G in the gel, the binding of rhodamine 6G with CB[6] is unlikely. My findings suggest that the diffusion of rhodamine 6G from the gel into the medium was unaffected by the presence of CB[6], which excludes the possibility of CB[6] binding to rhodamine 6G. The similar dye release pattern for NaDC and NaDC-CB[6] gels (Figure 3.5) indicate that the dye release corresponds to free rhodamine 6G in the aqueous phase of the gel. These results show that the time it takes for rhodamine 6G to reestablish the equilibrium between the gel's structure and the entrapped aqueous phase is not affected by the addition of CB[6].

At the higher concentration of rhodamine 6G, the number of positively charged rhodamine 6G molecules interacting with NaDC aggregates increases. The added interactions in the gel at the higher rhodamine 6G concentration may have strengthened the gel which led to a slowdown of the diffusion of free rhodamine 6G molecules from the aqueous phase into the surrounding medium. This slow-down was reflected in the dye release studies, where the percentage of dye released was lower for the gel with 1 mM rhodamine 6G (Figure 3.8) compared to the gel with 10 μM rhodamine 6G (Figure 3.5). Although studies[149] showed that rhodamine 6G forms a dimer at 1 mM, the release was expected to occur for the monomer (λ_{max}, 526 nm) as the formation of dimer (489 nm) was ruled out based on the absorption spectra. The addition of CB[6], as per my hypothesis, led to a higher fraction of NaDC

aggregates to be immobilized in the gel structure compared to the aqueous phase. The inclusion of rhodamine 6G bound NaDC aggregates from the aqueous phase into the gel structure leads to enhanced hydrogen bonding interactions between NaDC/rhodamine 6G. Higher concentrations of rhodamine 6G in the gel increase the likelihood of rhodamine 6G interactions with the portals of CB[6] compared to Na^+ cations binding with CB[6]. The new interactions between NaDC/rhodamine 6G and CB[6]/rhodamine 6G break the existing interactions between NaDC aggregates and increases separation between the aggregates. The increased separation between aggregates at higher CB[6]/NaDC ratios result in faster release of rhodamine 6G from the NaDC-CB[6] gel as shown in Figure 3.8. A similar phenomenon was observed in a release study of methylene blue, which is a cationic dye, from NaDC/NaCl gels in the presence of amino acids.[71] It was observed that L-lysine (L-Lys) disrupts hydrogen bonding between NaDC molecules and the formation of new hydrogen bonding between NaDC and L-Lys (or between L-Lys and L-Lys) influences the strength and ordering of the intermolecular interactions between NaDC, NaCl, and water resulting in faster release of methylene blue. The concentration ratio between L-Lys and NaDC is 1:1, whereas the concentration ratio in my case of rhodamine 6G to NaDC ratio is 0.02:1. Therefore, the role of dye interactions with NaDC aggregates was ignored in the amino acids/NaDC/NaCl study due to the predominance of other molecules in the system. A gel breaking up as a result of new interactions through hydrogen bonding in the amino acids/NaDC/NaCl work agrees with my understanding of release studies (Figure 3.8), where the new interactions between amino acids and gel aggregates increases the separation between aggregates leading to more aggregates becoming part of the aqueous phase, which resulted in the faster release of methylene blue. A similar study of drug-NaDC interactions destroying the gel structure was observed by Snowden and coworkers.[150] In this study, addition of drugs into gels

showed a spectral shift of a broad peak in the infra-red spectra, indicating the destruction of hydrogen bonding between NaDC aggregates and the formation of new hydrogen bonding interactions between NaDC and the drug molecule.

NaDC aggregates have sites that bind hydrophobic guest molecules.[146] Pyrene is a hydrophobic dye primarily located in the hydrophobic regions of the aggregates. The I/III ratios of pyrene in 50 mM NaDC gel was 0.77 ± 0.01, which indicates that pyrene molecules are located in a hydrophobic environment in the NaDC gel. Time resolved fluorescence measurements for pyrene in NaDC gels were fit to two lifetimes corresponding to pyrene in water and pyrene bound to NaDC aggregates. The I/III ratios and lifetime measurements suggest that pyrene is bound to hydrophobic regions of NaDC aggregates.[69] Based on my hypothesis from chapter 2, I expect that pyrene partitions between NaDC aggregates in the aqueous phase and the gel structure. Based on the release data, the 22% of pyrene released correspond to the maximum amount of pyrene that can be released based on its solubility in water (0.7 uM).

CB[6] was chosen over the other members of the CB[*n*] family, which have larger cavity sizes, to ensure that the inclusion of pyrene into the CB[6] cavity was not possible. However reports suggest that pyrene can weakly interact with CB[6] ($K = (3.1 \pm 0.9) \times 10^2\ M^{-1}$ in 50% w/v of formic acid at 15 °C).[151] Due to pyrene's hydrophobic nature and weak interaction of this dye with CB[6], I expect a partitioning to occur for pyrene between aggregates in the aqueous phase of the gel, aggregates in gel structure and with CB[6] in the gel.

Addition of CB[6] leads to the incorporation of pyrene bound to NaDC aggregates into the gel structure. As more pyrene molecules become a part of the gel structure at higher concentrations of CB[6], the number of pyrene molecules freely diffusing in the aqueous phase of the gel was decreased. Since, it takes more time for pyrene to travel through the aggregates in

the gel structure, the amount of pyrene released from the gel was decreased. However, the effect of CB[6] on the release kinetics with the CB[6] concentration in not linear, indicating that the incorporation of aggregates into the gel structure reaches a limit above a specific concentration of CB[6].

In a work on NaDC-TRIS gels, it was shown that increasing the TRIS buffer concentrations led to an increase in hydrogen bonding interactions in the gel, which was reported to increase the size of the water pockets in the gel.[92] These larger water pockets at higher TRIS concentrations led to faster release of large molecules, such as bovine serum albumin (BSA). In my work, I have no evidence that suggested that hydrogen bonding interactions between NaDC/CB[6] increased the size of water pockets in the gel. However, even if the water pockets are affected by CB[6], it had no impact on the release of a small molecule, such as pyrene.

Dual release kinetics in NaDC/TRIS gels were reported for the rhodamine B and fluorescein dyes.[152] In this work, dyes are encapsulated in core-shell NaDC/TRIS gels, where the core and shell are formed by varying the TRIS/NaDC concentration ratio. This study is a proof of concept for combinatorial drug release from NaDC/TRIS gels, where the dyes rhodamine B and fluorescein that are encapsulated respectively in the core and shell, have different release rates due to microstructural differences between core and shell. In the NaDC/TRIS study, dyes are loaded into different regions, such as the core/shell of the hydrogels during the sample preparation to tune the release kinetics. Unlike the NaDC/TRIS study, CB[6] addition in the work changed the localization of dyes in the gel between the aqueous phase and the gel structure. In the absence of CB[6], although evidence suggested that location of pyrene and rhodamine 6G are different in NaDC gels, the release kinetics are similar (red traces in Figure 3.5 and 3.11). However, in the NaDC/TRIS study, the location of rhodamine B and fluorescein contributed to

distinct release profiles. The core/shell morphology reported in NaDC/TRIS gels cannot be applied to my work because the preparation of NaDC gels and buffers used are different between the two studies. Although the two studies were focused on achieving tunable release rates by changing the microenvironment around the dyes, the strategy used to achieve this goal differed.

Investigation of the dye release mechanism further validated my observation that the dye released corresponds to the dye in the aqueous phase. The similar I/III ratios of pyrene in the release medium and the phosphate buffer control experiment indicates that the dye released into the surrounding medium corresponds to free dye. The I/III ratio of the surrounding medium in the pyrene release study show that pyrene released corresponds to diffusion of free pyrene from aggregates in the aqueous phase.

3.5 Conclusion

While there were reports on changing the microenvironment around dyes and loading these dyes into preferential regions of interest of the gel to tune the release kinetics, this is the first study that reports on the role of an additive in changing the distribution of dyes in different regions in the gel, thereby affecting the release properties. The study highlights the multiple interactions between additive and gelator; between dyes and gelator are the key factors to tune the release kinetics of small molecules from the gel. Although the results highlight that the release kinetics changes as a function of additive concentration, it is evident that the concentration of additive is not directly proportional to the percent of dye release. In order to establish a generic understanding of the release mechanism, it is important that the release kinetics be studied for dyes with different properties to ensure that the effect of additive introduction to the gels is investigated instead of properties related to the effect of a specific dye. This study points out that to understand how all components in a gel interact with each other is

integral in controlling the properties of a gel. This chemistry creates an opportunity to achieve control in the rational design of drug delivery systems.

Chapter 4 Role of CB[6] on the distribution and dynamics of small molecules in NaDC gels

4.1 Introduction

The release studies in chapter 3 suggest that the hydrophilic and hydrophobic dyes are located in different regions of the gel. The hypotheses developed based on the DLS and microscopy results in chapter 2 suggest that CB[6] plays an active role in the incorporation of NaDC aggregates from the aqueous phase into the gel structure. The hypotheses generated in chapter 2 and chapter 3 are tested in this chapter through colocalization studies using CLSM.

Colocalization studies are used to determine if two dyes are localized within a certain volume in a given image. Colocalization occurs when dyes bind to targets that lie in close proximity within the gel structure. For example, consider a sample tagged with two dyes A and B. Dyes A and B are represented by red and green emission channels. In a given area, images are collected in each emission channels. The images representing each channel are digitally combined to give a merged image. In a merged image, colocalization of dyes A and B is represented by the pixels with various shades of orange and yellow (formed by the fusion of green and red colors). The merged image helps us identify the regions in the sample where the dyes A and B are colocalized.

The intensity values of each pixel in the two channels representing dyes A (x-axis), B (y-axis) are plotted against each other to generate a scatter plot (Figure 4.1). The scatter plot correlates the relationship between two sets of data to determine if colocalization occurs. Scatter plots are divided into 4 quadrants depending on the thresholds set for the red and green emission channels. The lower left quadrant 4 in the scatter plot represents pixels that have low intensity levels in both the channels. Quadrant 1 represents pixels with high green and low red intensities. Quadrant 2 represents pixels that have low green and high red intensities. Pixels distributed in

quadrant 1, 2 and 4 indicate a lack of colocalization (Figure 4.1 c-e). Quadrant 3 represents pixels with high intensity levels in both green and red emission channels. These pixels are considered to be colocalized (Figure 4.1 a-b). Besides qualitative indication of colocalization, scatter plots can be used to identify populations in distinct regions of the sample.

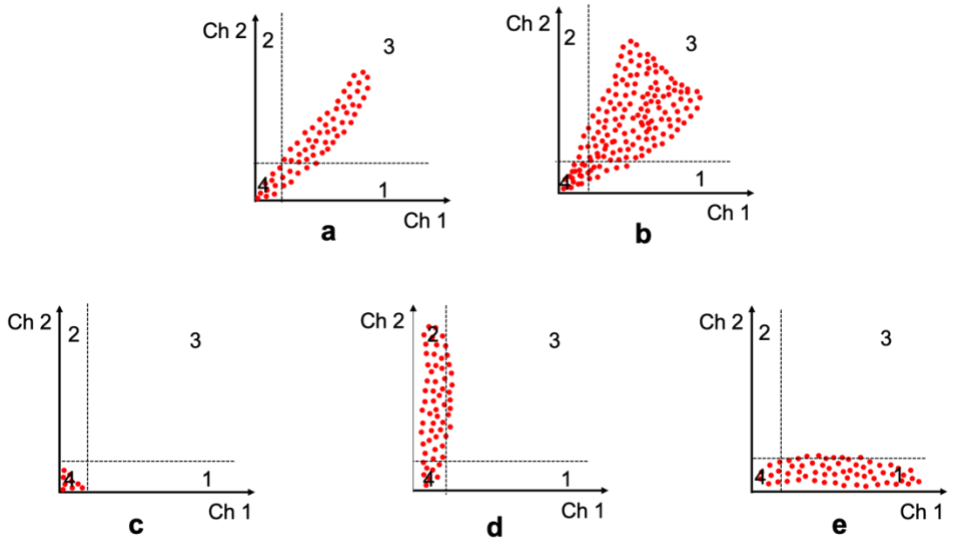

Figure 4.1 Scatter plots for the analysis of the microscopy images using two dyes A and B in a sample showing the presence of colocalization (a,b) and the absence of colocalization (c-e). 1-4 represents the different quadrants.

Colocalization studies are highly dependent on the resolution of the microscope. The resolution of any super resolution fluorescence microscope is not sufficient to identify the binding of two dye molecules through a comparison of their distributions in a given area in the image. Therefore, two dyes colocalized in the same structure does not mean that an interaction between these dyes occurs at the molecular level. Such a study of molecular association would require techniques like fluorescence resonance energy transfer (FRET) or electron microscopy.

In multicomponent gels, colocalization studies have been used to distinguish between self-sorting or co-assembly. In a work by Hamachi et al. two dyes that bind specifically to the peptide or the amphiphilic phosphate gelators enabled the visualization of the type of self-

assembly using confocal microscopy.[153] The results from colocalization studies show that each gelator entangles into separate fibers in the gels confirming the self-sorting mechanism. A similar study of visualizing self-sorting of supramolecular fibers using colocalization studies has been performed for functional protein gels.[154]

In this Chapter, colocalization studies are performed in a two-component gel system made of the gelator NaDC and additive CB[6]. Studies tagging different components in the gels with dyes to study the assembly process have been reported in the literature.[155] Selection of dyes for these studies relied on their structural similarity with the gelators, the labelling of gelators with the dye via chemical bonds, or dyes containing gelators with self-assembled motifs.[153, 154] In contrast, selection of dyes in the current colocalization studies relies on the properties of NaDC and CB[6] as hosts to form supramolecular host-guest complexes.

For the first set of colocalization experiments, gels are tagged with rhodamine 6G (hydrophilic dye) and nile red (hydrophobic dye) (Chart 4.1). While Rhodamine 6G is expected to mainly be located in the aqueous phase of the gel, Nile red ($pK_a \sim 4$) is expected to mainly be localized in the hydrophobic regions of the NaDC aggregates located both in the aqueous phase and the gel structure. For the second set of colocalization experiments, gels are tagged with trans-4-[4-(dimethylamino)styryl]-1-methylpyridinium iodide (DSMI) and berberine (Chart 4.1). Berberine is known to interact with NaDC aggregates.[156] DSMI on the other hand, binds inside the CB[6] cavity.[157]

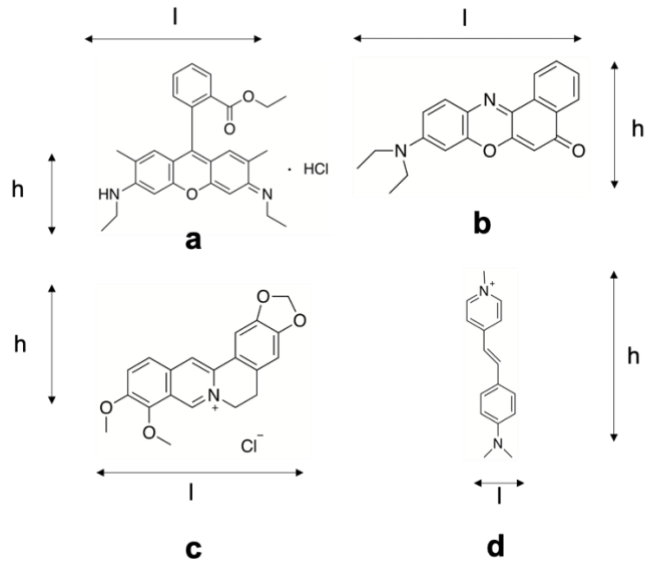

	l	h
a	14.4	5.5
b	13.9	5.6
c	14.4	5.5
d	4.8	14.2

Chart 4.1 Chemical structures of a. rhodamine 6G, b. nile red. c. berberine, d. trans-4-[4-(dimethylamino)styryl]-1-methylpyridinium iodide (DSMI). The Table shows the length and height dimensions of dyes in Å estimated using Chem Draw.

In chapter 3, it was observed that CB[6] has an effect on the release of a hydrophobic dye from NaDC gels. However, the release studies reflect the mobility of a hydrophobic dye at a macroscopic length scale from the gel into the release medium that was placed on top of the gel (Figure 4.2). Studies in chapter 2 showed that the length scale matters when dealing with multicomponent supramolecular gels and each length scale gives information which may or may not reflect the information obtained on a different length scale. In this chapter, the effect of CB[6] on the mobility of a hydrophobic dye within NaDC gels was studied at a microscopic length scale (Figure 4.2).

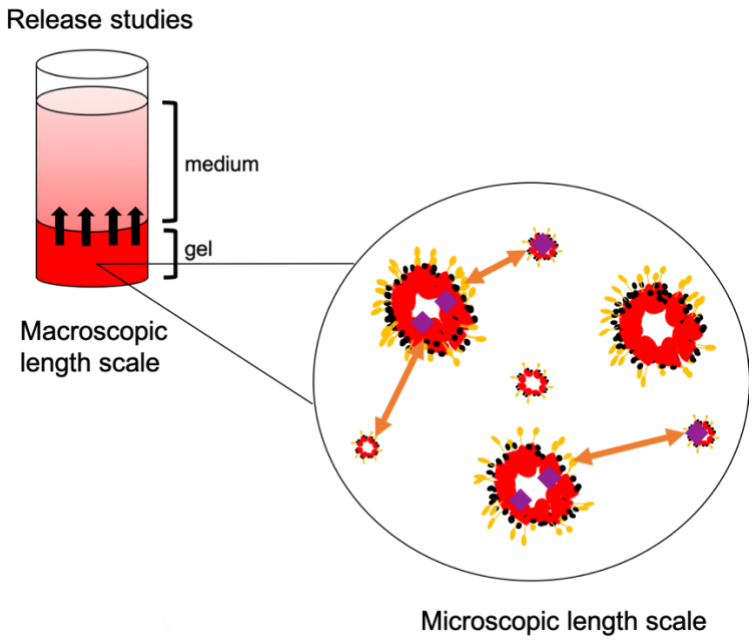

Figure 4.2 Cartoon representing length scale differences in diffusion of small molecules from the gel.

Mobility of small molecules in gels at a microscopic length scale can be studied using techniques, such as fluorescence recovery after photobleaching (FRAP), fluorescence correlation spectroscopy (FCS), single particle tracking (SPT), nuclear magnetic resonance diffusometry (NMRd). FRAP relies on local irreversible bleaching of a small area in the sample containing fluorescent dyes with high intensity laser irradiation, followed by studying the recovery of fluorescence as a result of diffusion of non-bleached dye molecules from surrounding areas into the bleached area (Figure 4.3).[158] Diffusion coefficients obtained from FRAP cover the range from 0.01to 100 $\mu m^2 s^{-1}$.[159] SPT is a technique in which single particle trajectories are tracked in a sample.[160-162] For SPT, a very thin sample is required to prevent losing the particles from the focal plane for which the image is collected. Diffusion coefficients obtained from SPT cover the range from 0.001to 10 $\mu m^2 s^{-1}$.[159] Since SPT is a single molecule technique, it requires higher sensitivity, resolution and signal-to-noise ratio compared to FRAP. FCS measures fluorescence

intensity fluctuations as a result of diffusion of a fluorescent dye in and out of the volume under focus.[163] Diffusion coefficients obtained from FCS cover the range from 0.1 to 100 $\mu m^2 s^{-1}$.[159] In NMRd, a magnetic gradient is applied to a sample, and the relaxation processes of the molecules are analyzed to study the diffusion.[164, 165] Diffusion coefficients obtained from NMRd cover the range from 0.001to 100 $\mu m^2 s^{-1}$.[159]

FRAP has proven to be a valuable technique to characterize diffusion processes in hydrogels.[166] In a work by Hennink *et al.* FRAP was used to show the continuous release of proteins from hydrogels.[167] In a multicomponent gel system, such as agarose-dextran gels, FRAP has been used to show hindered diffusion of proteins and polysaccharides in gels compared to the diffusion in aqueous solutions.[168] In work by Hamachi *et al.* FRAP was used to show the retainment of fluidity of individual fiber components in a self-sorted supramolecular gel system.[153] In this chapter, I chose FRAP as a technique to study the mobility of a hydrophobic dye within NaDC-CB[6] gels.

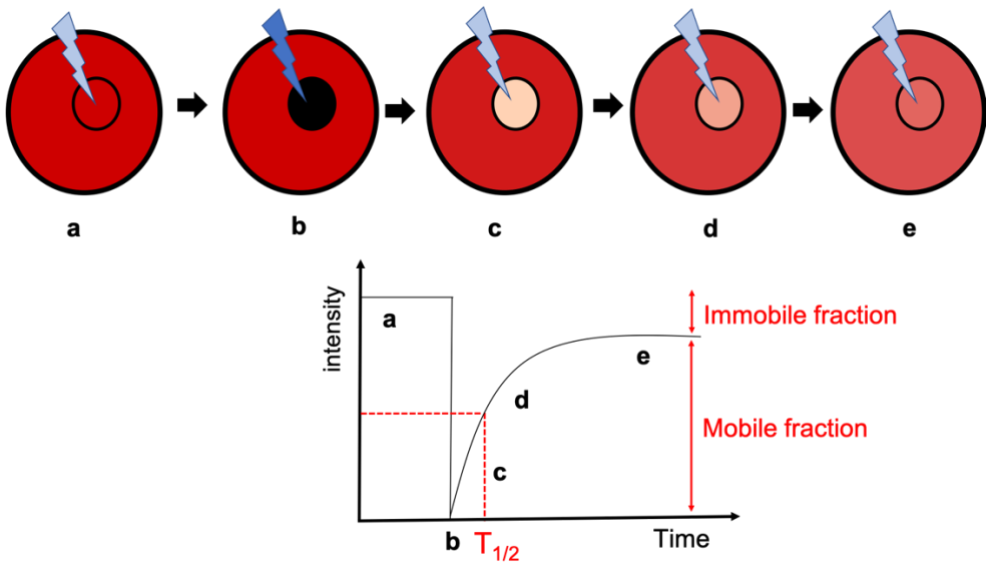

Figure 4.3 Top panel represents the basic FRAP approach. Red panels represent a sample region containing fluorescent molecules. Panels a-e represents the baseline intensity (a), photo-bleaching of a circular area (b), time-dependent recovery of fluorescence intensity within the bleached region (c-e). The arrows reflect the intensity of laser light used during the process. The bottom panel depicts a typical intensity profile obtained during a FRAP experiment.

FRAP experiments record temporal changes in fluorescence intensity in the bleached area of the sample thereby generating a kinetic curve (Figure 4.3). The curve is fit to appropriate models to extract the diffusion coefficient, half-life and mobile fraction in the samples under investigation.[169] The half-life ($T_{1/2}$) is defined as the time it takes for the intensity to reach half of the maximum intensity observed for the recovery (Figure 4.3). The shorter the half-life, the faster the recovery and the higher the diffusion coefficient. The mobile fraction (M_f) is the fraction of recovered fluorescence intensity and gives information about the percentage of freely diffusing dye molecules in the sample (Figure 4.3).

The ideal fluorescent dye for FRAP studies should satisfy two criteria: the dye should have a high quantum yield, i.e. be highly fluorescent, and the dye should be moderately susceptible to photobleaching.[170] The latter is essential to permit bleaching during the bleaching phase and limiting the bleaching during the recovery phase, when the sample is irradiated with

an attenuated laser beam. For the FRAP studies in this chapter, the dye should meet an additional criterion, i.e. the dye should be hydrophobic to ensure its localization inside of the hydrophobic regions of the NaDC aggregates. Based on the above considerations, nile red was chosen as the dye for the FRAP studies described in this chapter.

4.1.1 Objectives

The first objective of the colocalization experiments described in this chapter is to obtain insights on the location of a hydrophilic and a hydrophobic dye in the gel. The second objective of the colocalization experiments is to determine if CB[6] is present in the immobile gel structure. The objective of the FRAP studies is to study how CB[6] affects the mobility of a hydrophobic dye, such as nile red within NaDC gels at a microscopic length scale.

4.2 Experimental

4.2.1 Materials

NaDC (Fluka, > 98%), NaH_2PO_4 (Anachemia, > 98%), Na_2HPO_4 (Anachemia, > 98%), methanol (Fisher grade), rhodamine 6G (Sigma Aldrich, 99%), N-(4-aminophenyl)imidazole (API, Sigma Aldrich, 98%), 1,6-diaminohexane (DAH, Sigma Aldrich), hydrochloric acid (HCl, BDH 36.5-38%), deionized water (Barnstead NANOpure deionizing systems, 17.8 MΩ cm) were used as received. Coverslip (24 × 60 mm, 0.16-0.19 mm thickness), Press-To-Seal Silicone isolator (Round well, 9 mm diameter, 0.8 mm depth), adhesive on both sides, Grace Biolabs), HybriWell™ Sealing System (21.6 mm × 21.6 mm × 0.25 mm), 110 µL approximate volume, 25.5 mm x 30 mm OD, Fluor “Friendly” Adhesive Chamber, Grace Biolabs) were used for microscopy experiments.

The DAH salt was recrystallized by adding acetone (15 mL) to a 11 mmol DAH solution dissolved in 1.85 mL concentrated HCl, followed by vacuum filtration to obtain white

crystals. The sample CB[6]-AA-3 (purity 91%) was used in this study. CB[6] was synthesized and purified based on the standard protocols in the group.[69] The CB[6] concentration was determined by titrating the stock solutions with recrystallized DAH. In this titration, DAH^{2+} displaces API^{+} bound with CB[6] leading to a decrease in the steady-state fluorescence intensity of API^{+}.

4.2.2 Colocalization studies with rhodamine 6G/nile red and rhodamine 6G/berberine

Rhodamine 6G (0.5 mM), berberine (0.5 mM) and nile red (0.5 mM) stock solutions were prepared in methanol. Phosphate buffer stock solutions (0.5 M) at pH 6.5 were prepared by mixing appropriate volumes of NaH_2PO_4 (0.5 M) and Na_2HPO_4 (0.5 M) stock solutions. NaDC stock solutions (0.2 M) were prepared in deionized water. The NaDC stock solution was heated at 60 °C for 15 min to dissolve the NaDC solid. NaCl stock solutions (1 M) were prepared in water.

For NaDC gels, 125 µL of the NaDC stock solution and 321 µL of deionized water was added into a 3-dram sample vial. The solution was heated at 60 °C for 15 min. While this solution was hot, 2 µL of each of the dye stock solutions and 50 µL of the phosphate buffer solution were added, followed by heating of this mixture at 60 °C for 15 min. For NaDC-CB[6] gels, 4.1 mg of CB[6] was dissolved in 321 µL of deionized water and 50 µL of the phosphate buffer. The addition of phosphate buffer led to the solubilization of CB[6] at room temperature. This solution was heated for 15 min at 60 °C. While the solution was hot, 2 µL of each of the dye stocks and 125 µL of the NaDC solution were added, followed by heating at 60 °C for 15 min.

The final concentrations of NaDC and phosphate buffer in the gel samples were the same at 50 mM. The final concentrations of CB[6] in the gel sample was 7.5 mM. The final concentration of dyes in the gel samples was 2 µM each.

For NaDC solutions, 125 µL of the NaDC stock solution and 296 µL of deionized water was added into a 3-dram sample vial. The solution was heated at 60 °C for 15 min. While this solution was hot, 2 µL of each of the dye stock solutions and 75 µL of the NaCl stock solution were added, followed by heating of this mixture at 60 °C for 15 min. For NaDC-CB[6] gels, 4.1 mg of CB[6] was dissolved in 296 µL of deionized water and 75 µL of the NaCl stock solution. The addition of NaCl led to the solubilization of CB[6] at room temperature. This solution was heated for 15 min at 60 °C. While the solution was hot, 2 µL of each of the dye stock solutions and 125 µL of the NaDC solution were added, followed by heating at 60 °C for 15 min.

The final concentrations of NaDC and NaCl in the solutions were 50 mM and 150 mM, respectively. The final concentrations of CB[6] in the solution was 7.5 mM. The final concentration of dyes in the solutions was 2 µM for each dye.

Coverslips and gaskets were rinsed with water and methanol before use. Approximately 100 µL of the sample was transferred into the gasket immediately after sample preparation. The gasket was sealed by placing a glass coverslip on top of the open side of the gasket. The gasket was left at room temperature for 20 h (resting period) before carrying out any measurements.

For samples with nile red and rhodamine 6G, images were collected using an inverted CLSM microscope (Zeiss LSM 880) equipped with a 488 nm Argon laser and a 543 nm He-Ne laser. Images were collected using a 63× oil immersion objective (NA 1.4). Laser intensities were set at 30% and 20% for the 488 nm and 543 nm lasers, respectively. The excitation filter MBS 488/543 nm was used. The pinhole diameter was set to 2 Airy Unit (AU). The range for the emission wavelengths for the channel detecting the rhodamine 6G emission was set to 515-550 nm, while the channel for the detection of nile red was set to 650-730 nm. The detector gains for the rhodamine 6G and nile red channels were set at 800 and 700 V, respectively. The equipment

was controlled using the Zen Black software. Images were acquired with an optimal pixel size chosen by the software, and 12 bits of pixel depth. Images were collected with an optimal frame size of 992 × 992 pixels. To avoid any surface effects at the coverslip, images were collected at a particular depth in the sample (~50 µm).

For samples with berberine and rhodamine 6G, images were collected using an inverted CLSM microscope (Zeiss LSM 880) equipped with a 488 nm Argon laser and a 405 nm diode laser. Images were collected using a 63× oil immersion objective (NA 1.4). Laser intensities were set at 20% for both the lasers. The excitation filters MBS 488 and MBS 405 were used. The purpose of the laser filters is to select specific wavelengths to illuminate the dye of interest. The pinhole diameter was set to 3 Airy Unit (AU). The range of the emission wavelengths for the detection channel was set to 515-550 nm. The detector gain for the channel was set at 800 V. Since both the dyes emit in the same spectral region, the experiment was done in two tracks, where in track 1 the sample was excited with the 405 nm laser and in track 2 the sample was excited with the 488 nm laser. Images were acquired with an optimal pixel size chosen by the software, and 12 bits of pixel depth. Images were collected with an optimal frame size of 732 × 732 pixels. To avoid any surface effects at the coverslip, images were collected at a particular depth in the sample (~50 µm).

4.2.3 Colocalization studies with DSMI and berberine

DSMI (0.5 mM) and berberine (0.5 mM) stock solutions were prepared in methanol. Phosphate buffer stock solutions (0.5 M) at pH 6.5 were prepared by mixing appropriate volumes of NaH_2PO_4 (0.5 M) and Na_2HPO_4 (0.5 M) stock solutions. NaDC stock solutions (0.2 M) were prepared in deionized water. The NaDC stock solution was heated at 60 °C for 15 min to dissolve the NaDC solid. NaCl stock solutions (1 M) were prepared in water.

Gels and solutions were prepared in the same way as described in the previous section with DSMI and berberine added as dyes. The final concentrations of NaDC and phosphate buffer in the gel samples were the same at 50 mM. The final concentrations of NaDC and NaCl in the solutions were 50 mM and 150 mM, respectively. The final concentrations of CB[6], DSMI, berberine in gels and solutions were 7.5 mM, 2 µM and 2 µM, respectively.

Coverslips and gaskets were rinsed with water and methanol before use. Approximately 100 µL of sample was transferred into the gasket immediately after sample preparation. The gasket was sealed by placing a glass coverslip on top of the open side of the gasket. The gasket was left at room temperature for 20 h (resting period) before carrying out any measurements.

Images of the samples were collected using an inverted CLSM microscope (Zeiss LSM 880) equipped with a 488 nm Argon laser and a 405 nm diode laser. A 63× oil immersion objective (NA 1.4) was used. The laser intensity was set at 20% and the excitation filters MBS 488 and MBS 405 were used. The purpose of the use of the laser filters is to select specific wavelengths to illuminate the dye of interest. The pinhole diameter was set to 2 AU. The emission range for the berberine channel detector was set to 515-550 nm and for the DSMI detector this range was set to 580-650 nm. The detector gain for the berberine and DSMI channels were set at 700 and 600 V, respectively. The equipment was controlled using the Zen Black software. Images were acquired with an optimal pixel size chosen by the software, and 12 bits of pixel depth. Images were collected with an optimal frame size of 732 × 732 pixels. To avoid any surface effects at the coverslip, the images were collected at a particular depth in the sample (~50 µm).

4.2.4 FRAP studies

The nile red (0.5 mM) stock solution was prepared in methanol. Phosphate buffer stock solutions (0.5 M) at pH 6.5 were prepared by mixing appropriate volumes of NaH_2PO_4 (0.5 M) and Na_2HPO_4 (0.5 M) stock solutions. NaDC stock solutions (0.2 M) were prepared in deionized water. The NaDC stock solution was heated at 60 °C for 15 min to dissolve the NaDC solid. NaCl stock solutions (1 M) were prepared in water.

Gels and solutions were prepared in the same way as described in the previous section with nile red as the added dye. The final concentrations of NaDC and phosphate buffer in the gel samples were the same at 50 mM. The final concentrations of NaDC and NaCl in the solutions were 50 mM and 150 mM, respectively. The final concentrations of CB[6] and nile red in gels and solutions were 7.5 mM and 2 μM, respectively.

Coverslips and gaskets were rinsed with water and methanol before use. Approximately 100 μL of sol was transferred into the gasket immediately after sample preparation. The gasket was sealed by placing a glass coverslip on top of the open side of the gasket. The gasket was left at room temperature for 20 h (resting period) before carrying out any measurements.

FRAP experiments were conducted on Zeiss LSM 880 microscope equipped with a 543 nm He-Ne laser and a 63× oil immersion objective lens (NA 1.4). Nile red was excited using a 543 nm laser (10% intensity) and the emission was collected in the range of 650-740 nm. The MBS 488/543 nm laser filter was used to select specific wavelengths to illuminate the dye of interest. Images upto 100 scans were collected at a resolution of 512 × 512 pixels over an area of 135 μm^2 continuously. The size of the pinhole was set at 3 AU with a detector gain of 600 V. All experiments were conducted at room temperature and at a depth of 100 μm in the sample from the surface of coverslip to avoid any surface artefacts.

4.3 Results

4.3.1 Colocalization studies with rhodamine 6G/nile red and rhodamine 6G/berberine

The purpose of this colocalization study is to verify the hypothesis that a hydrophilic dye and a hydrophobic dye are located in different regions of the gel. Colocalization experiments were carried out for rhodamine 6G and nile red that correspond to a hydrophilic dye and a hydrophobic dye, respectively. Rhodamine 6G and nile red interact with the gels differently. Despite being mainly in the aqueous phase of the gel, rhodamine 6G due to its positive charge, can interact with the negatively charged carboxylic acid groups on NaDC aggregates leading to a distribution of rhodamine 6G between the aqueous phase and the gel structure. As discussed in chapter 2, rhodamine 6G can weakly interact with the portals of CB[6], however given the excess concentration of sodium cations compared to rhodamine 6G in the samples, the interaction of rhodamine 6G with CB[6] is unlikely. Nile red is weakly fluorescent in water but shows strong fluorescence in hydrophobic environments.[171] Mishra *et al.* showed that nile red resides in the hydrophobic regions of NaDC aggregates.[135] Although CB[6] can accommodate hydrophobic dyes inside its cavity,[172] the size of nile red is too large to fit into the cavity of CB[6].[173] Therefore, nile red does not interact with CB[6] in the gel.

It was evident from the microscopy results in chapter 2 that CLSM provides information on the immobile gel structure, while the aggregates in the aqueous phase appear as a background intensity. The bench mark of interest to show colocalization is the yellow color coding in the merged image formed as a result of the mixing of the green and red emission channels specific to the dyes and the distribution observed in the scatter plots.

Despite providing rich information about the sample, colocalization experiments often result in artefacts that lead to the misinterpretations of the data. For example, strong fluorescence

cross talk of dyes between the emission channels can result in false positives. High levels of cross talk can make images unusable for extracting any quantitative colocalization information.[174] Although nile red and rhodamine 6G have distinct emission profiles with their maxima around 650 and 550 nm respectively, it is important to rule out the possibility of any cross talk for the dyes between the emission channels. Cross talk can be examined by collecting the images of gels with a single dye using the same experimental settings as for the colocalization experiment. For samples with a single dye, features appearing in both the emission channels is an indication of cross talk. Cross talk control experiments for nile red and rhodamine 6G in NaDC-CB[6] gels are shown in Figure 4.4. The results indicate that nile red is specific to the red channel, whereas rhodamine 6G was detected in both channels confirming that cross talk occurred for this dye.

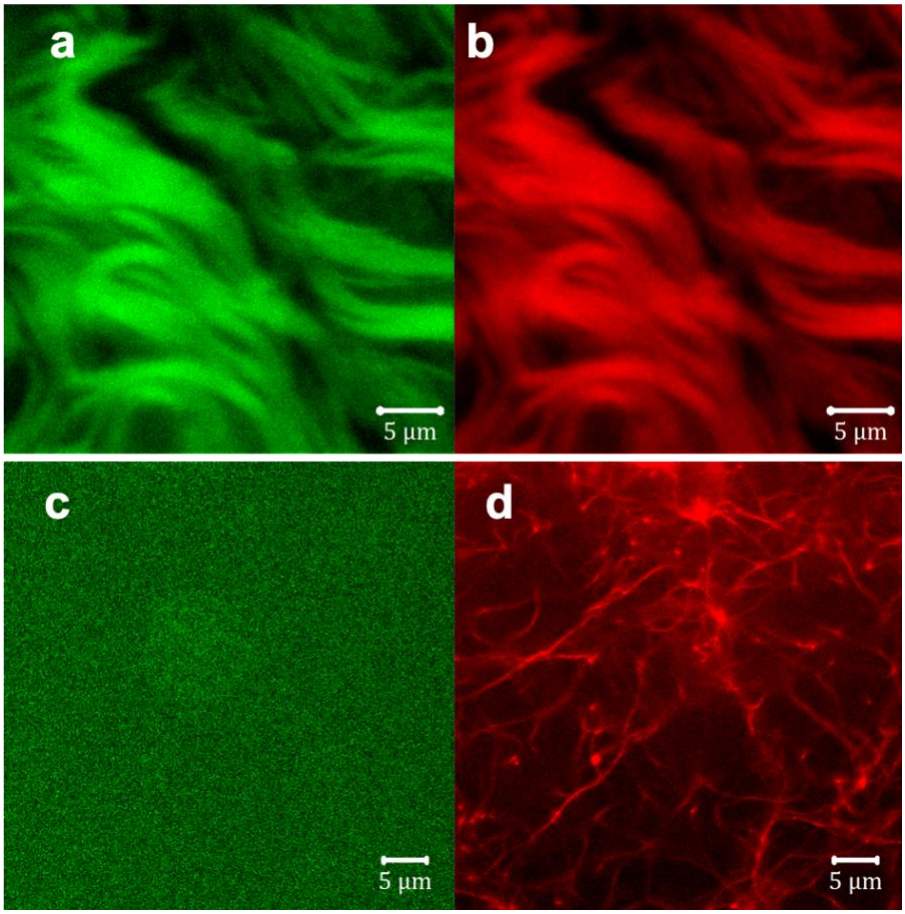

Figure 4.4 Confocal images of NaDC-CB[6] gel (0.15 CB[6]/NaDC ratio) tagged with rhodamine 6G (a,b) and nile red (c,d). Left and right panels represent emission channels that correspond to rhodamine 6G and nile red, respectively.

Due to cross talk between rhodamine 6G and nile red at the given bandwidths of the detection channels, colocalization experiments were attempted with berberine and rhodamine 6G, which correspond to a hydrophobic and a hydrophilic dye, respectively. Since berberine and rhodamine 6G have similar emission maxima, cross talk evaluation was not possible in this case. Therefore, the dyes berberine and rhodamine 6G are excited separately with different lasers and the obtained images were merged to get insights on the colocalization. Colocalization experiments of berberine and rhodamine 6G in solutions act as a positive control. Unlike the compartmentalized nature of gels, solutions are homogeneous, therefore, studies in solutions

should reflect colocalization. The yellowish-green color coding in the merged images shown in Figure 4.5 demonstrates the colocalization of dyes in solutions.

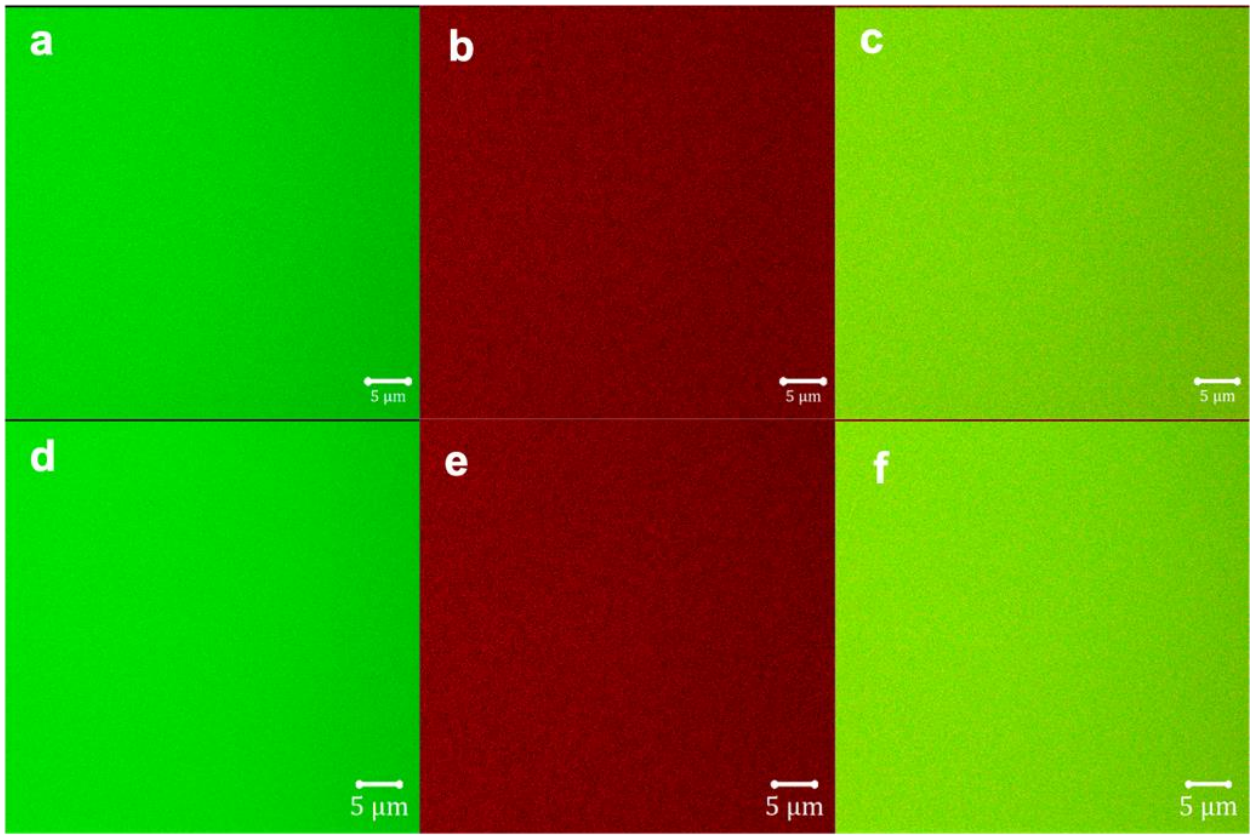

Figure 4.5 Confocal images of NaDC-CB[6] solutions tagged with berberine (green color) and rhodamine 6G (red color) (2 µM each) at CB[6]/NaDC ratios of 0 (a-c), 0.15 (d-f). Panels (a,d), (b,e) and (c,f) corresponds to the berberine channel, rhodamine 6G channel and merged channels, respectively.

Results for colocalization studies for berberine and rhodamine 6G in NaDC gels are summarized in Figure 4.6 and Figure C1. The aqueous phase in the gel has similar color coding as for the image obtained for solutions, whereas the spherical features constituting the gel structure are highlighted in yellow color. The scatter plot shows a relatively high contribution from the berberine channel to the image with little contribution from the rhodamine channel. These results indicate that the aqueous phase contains both the dyes while the gel structure is predominantly occupied by berberine.

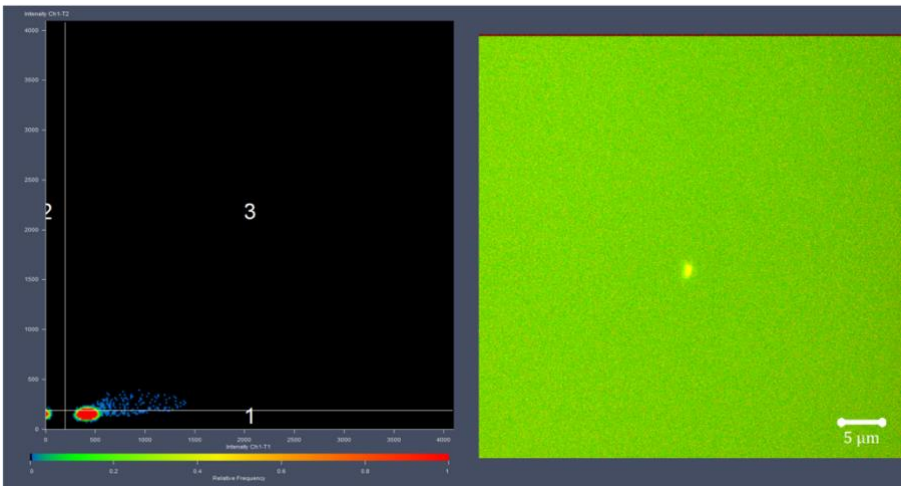

Figure 4.6 Scatter plot and merged confocal image of NaDC gel tagged with rhodamine 6G and berberine (2 µM each). The berberine channel is projected along the x-axis of the scatter plot. The rhodamine 6G channel is projected along the y-axis of the scatter plot.

In the case of NaDC-CB[6] gels, as seen in Figure 4.7 and Figure C2, the aqueous phase in the gel has similar color coding as the aqueous phase of the NaDC gel. Similar to the NaDC gel, the gel structure for NaDC-CB[6] has a yellow color coding. The scatter plot indicates that the majority of the contribution to the image is from the berberine channel with some contribution from the rhodamine 6G channel. The data points in quadrant 3 of the scatter plot suggest colocalization of dyes in the gel structure. In summary, results from colocalization studies show that CB[6] affects the distribution of the hydrophilic dye between the aqueous phase and gel structure. In the absence of CB[6], a hydrophilic dye is located mainly in the aqueous phase, whereas in the presence of CB[6], the hydrophilic dye is also located in the gel structure.

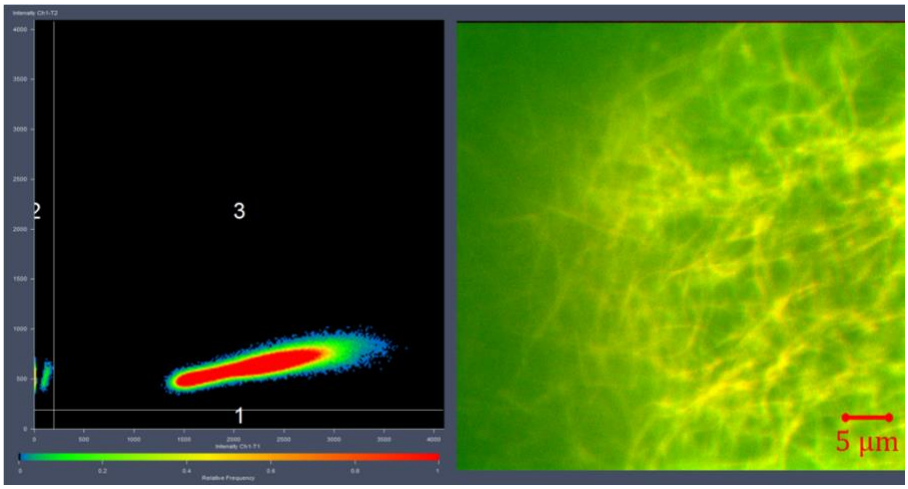

Figure 4.7 Scatter plot and merged confocal image of NaDC-CB[6] gel (0.15 CB[6]/NaDC ratio) tagged with rhodamine 6G and berberine (2 µM each). The berberine channel is projected along the x-axis of the scatter plot. The rhodamine 6G channel is projected along the y-axis of the scatter plot.

4.3.2 Colocalization studies with DSMI and berberine

The purpose of colocalization experiments with DSMI/berberine is to verify the hypothesis that CB[6] plays an active role in incorporating NaDC aggregates from the aqueous phase into the gel structure. Berberine and DSMI were chosen such that these dyes bind specific to NaDC aggregates and CB[6], respectively. Berberine was known to bind to the bile salt aggregates.[156] Studies showed that berberine can fit inside the CB[7] and CB[8] cavities, however, the size of berberine is too large to fit inside the CB[6] cavity.[175, 176] DSMI has a low quantum yield in water, but this dye exhibits strong fluorescence when bound inside the CB[6] cavity due to the inhibition of the TICT process.[157]

The emission spectra of berberine and DSMI are not well separated, and therefore a control experiment evaluating the cross talk of dyes between the emission channels was performed. The results in Figure 4.8 show the occurrence of cross talk between emission channels when both dyes are excited simultaneously.

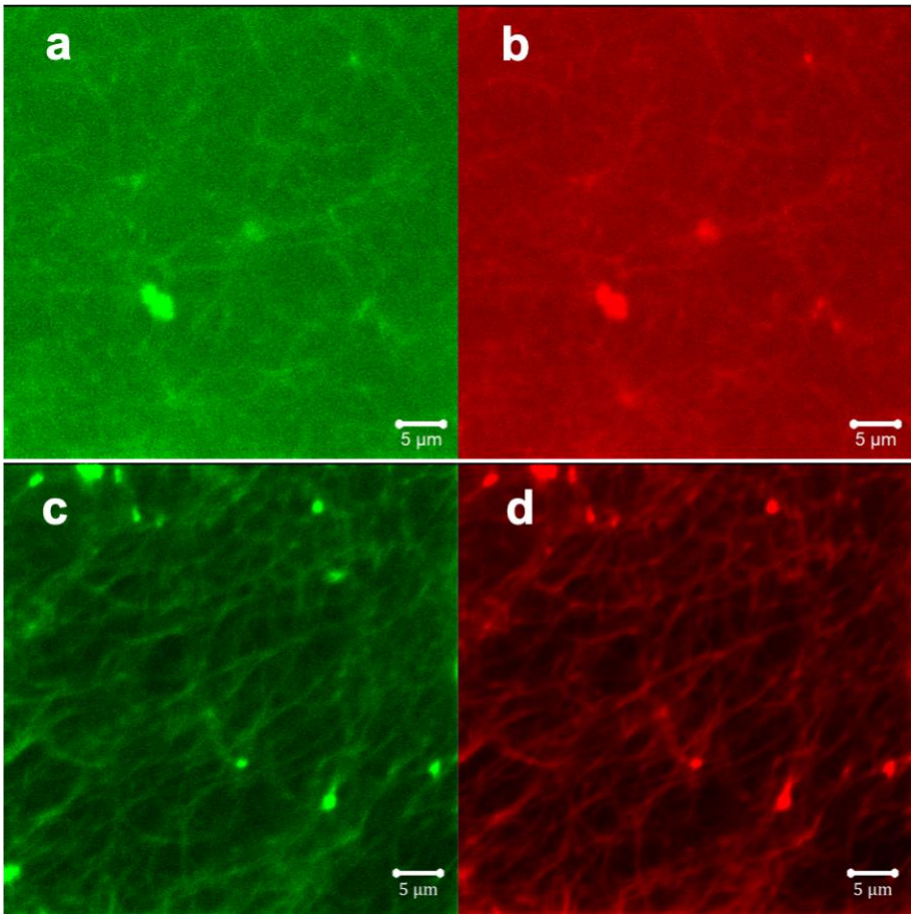

Figure 4.8 Confocal images of NaDC-CB[6] gel tagged with berberine (a,b) and DSMI (c,d). Left and right panels represent emission channels for berberine and DSMI, respectively.

Despite the cross talk between the dyes, the hypothesis stated above can still be verified by specifically exciting DSMI in the gels. The absence of any visible features in the NaDC gel (Figure 4.9a) showed that DSMI did not bind to NaDC aggregates. The fiber structures in Figure 4.9b show that DSMI was bound to CB[6]. DSMI localization in the fibers is an indication that CB[6] is a part of the fiber structure. These results suggest that CB[6] plays an active role in incorporating aggregates from the aqueous phase into the gel structure.

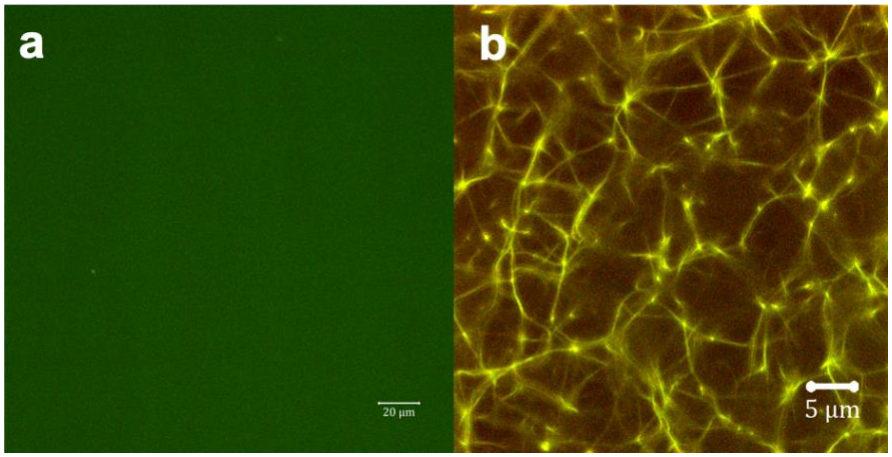

Figure 4.9 Confocal images of NaDC-CB[6] gels tagged with berberine and DSMI (2 µM each) at CB[6]/NaDC ratios of 0 (a), 0.15 (b). DSMI was specifically excited using 488 nm laser and the emissions in the red (berberine) and green (DSMI) channels were collected.

4.3.3 FRAP study

The purpose of the FRAP experiments is to study how the mobility within NaDC gels of small molecules, such as nile red, is affected with the addition of CB[6]. In the FRAP experiment, nile red molecules are bleached using a high-intensity laser power followed by monitoring the recovery of fluorescence to estimate the transport properties of nile red in different environments. FRAP experiments were performed for nile red in NaDC and 0.15 NaDC-CB[6] gels, both for the aqueous phase and gel structure, and in solutions. For each sample, three sets of FRAP experiments were performed on different regions of the sample and the experiments were repeated with independent samples to determine the reproducibility of these experiments.

To perform a FRAP experiment, three circular regions of interest (ROI) were chosen in an image.[177] ROI1 (highlighted in the white circle in Figure 4.10) corresponds to the ROI chosen for bleaching, ROI2 (highlighted in the green circle in Figure 4.10) corresponds to the total area covered by the gel structure enclosed by ROI1, and ROI3 (highlighted in the yellow circle in

Figure 4.10) corresponds to the background. While ROI1 is bleached, ROI1, ROI2 and ROI3 are analyzed. Although in the NaDC gel the entire gel structure is covered by ROI1 (Figure 4.10a), a similar circular area surrounding ROI1 as used for the NaDC-CB[6] gel (Figure 4.10b) was chosen as ROI2 to keep the conditions constant between the samples.

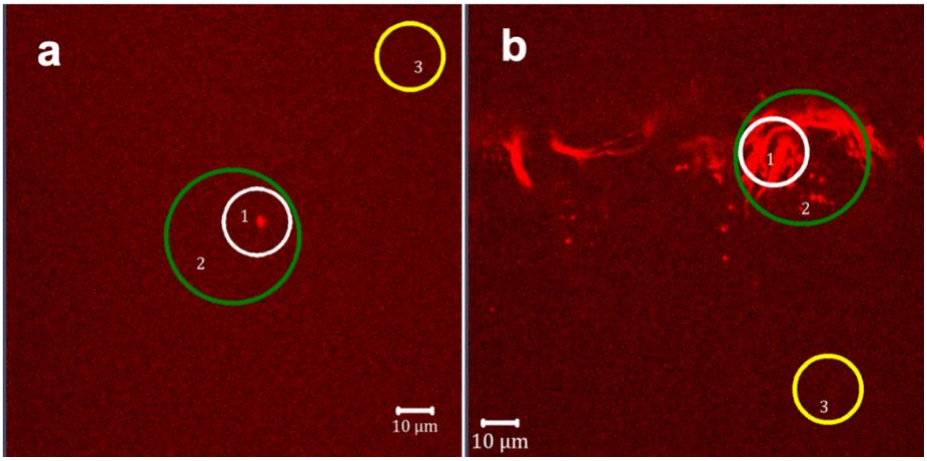

Figure 4.10 Confocal images of NaDC gel (a), NaDC-CB[6] gel (0.15 CB[6]/NaDC ratio) (b) tagged with nile red showing regions of interest for a FRAP experiment.

The radius of ROI1 (white circle), ROI2 (green circle) and ROI3 (yellow circle) in Figure 4.10 is 75 pixels (~7 µm), 150 pixels (~14 µm) and 75 pixels (~ 7 µm), respectively. Although the chosen ROIs are circular, the actual bleaching occurs in a cylindrical-like volume. A cylindrical bleached volume avoids any non-bleached dye molecules to enter the focal plane along the z-axis. Therefore, any influence from the diffusion along the z-axis can be neglected and diffusion can be simplified to two dimensions.

The FRAP experiment has three stages, i.e. pre-bleaching, bleaching and recovery stages (Figure 4.11). During the pre-bleaching stage, five reference images were acquired with a 10% laser intensity. Pre-bleach scans with low laser power serve as a control to determine that the sample is not bleached by the laser irradiation during the recovery phase.[178] During the bleaching stage, ROI1 was bleached with a 100% intensity of the laser intensity for 100

iterations corresponding to a total bleaching time of 38 s. The bleaching time period is kept minimal to avoid any melting of the gel due to the high intensity laser power and to minimize diffusion during the bleaching phase.[179] Finally, in the recovery stage, time scans (no time interval between scans) were collected at 10% laser intensity. The total experiment time was 2.2 min.

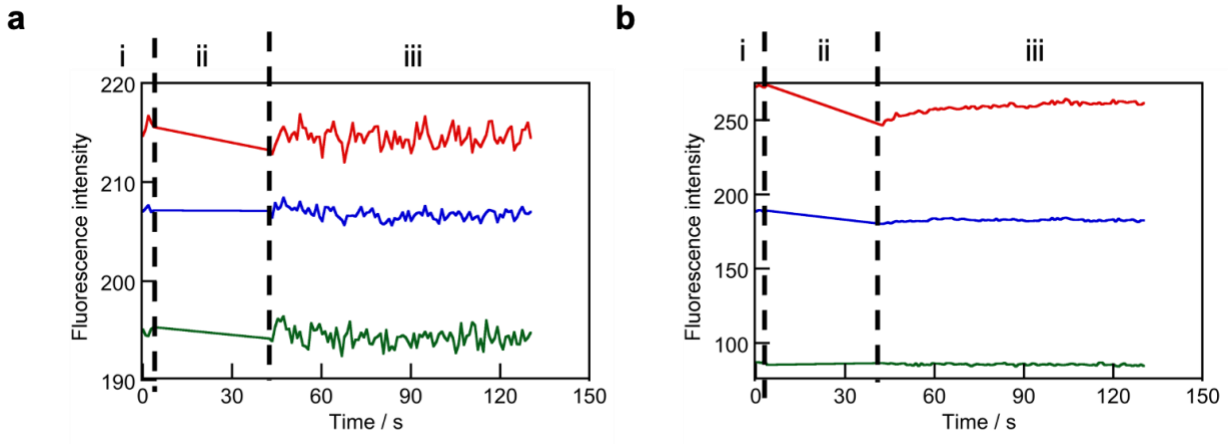

Figure 4.11 Fluorescence data for ROIs collected as a function of time in a. NaDC gel, b. NaDC-CB[6] (0.15) gel. i, ii, iii correspond to pre-bleaching, bleaching and recovery stages during the FRAP experiment. Red, blue, green traces correspond to the ROI1, ROI2, ROI3, respectively.

Studies in the literature discuss potential artefacts and pitfalls in the FRAP experiments.[155] For example, diffusion during the bleach period is often neglected in FRAP studies leading to an underestimation of diffusion coefficients. To avoid this artefact, the bleaching time period is kept minimal during FRAP experiments. Diffusion coefficients in FRAP are dependent on experimental conditions, such as the radius, shape of the bleaching spot and bleaching duration. Therefore, for the purpose of comparisons between chemically different environments, the bleaching conditions are kept constant for all studies.

FRAP data were analyzed using the easyFRAP web-based tool.[180, 181] In the first part of the analysis, at a given time, the intensities of the background (ROI3) were subtracted from the measured intensities (ROI1 and ROI2) to correct for noise (eq. 4.1).

$$I(t)_{ROI1'} = I(t)_{ROI1} - I(t)_{ROI3}$$

$$I(t)_{ROI2'} = I(t)_{ROI2} - I(t)_{ROI3}$$

Eq. 4.1

The data are normalized (Figure 4.12) using eq. 4.2 to correct for differences in fluorescence intensities in ROI1 and ROI2 as a result of the laser fluctuations. The parameter n_{pre} is the number of pre-bleaching steps. This correction is achieved by dividing corrected intensities for ROI1 and ROI2 at each time point with the average of the pre-bleach intensity for ROI1 and ROI2, respectively. Normalization also corrects for the loss in fluorescence due to possible bleaching during acquisition by dividing the fluorescence intensity for ROI1 by ROI2 for each time point. The normalization rescales recovery curves to a reference axis of arbitrary units between 0 and 1.

$$I(t) = \left(\frac{\frac{1}{n_{pre}} \cdot \sum_{t=1}^{n_{pre}} I(t)_{ROI2'}}{I(t)_{ROI2'}}\right) \cdot \left(\frac{I(t)_{ROI1'}}{\frac{1}{n_{pre}} \cdot \sum_{t=1}^{n_{pre}} I(t)_{ROI1'}}\right)$$

Eq. 4.2

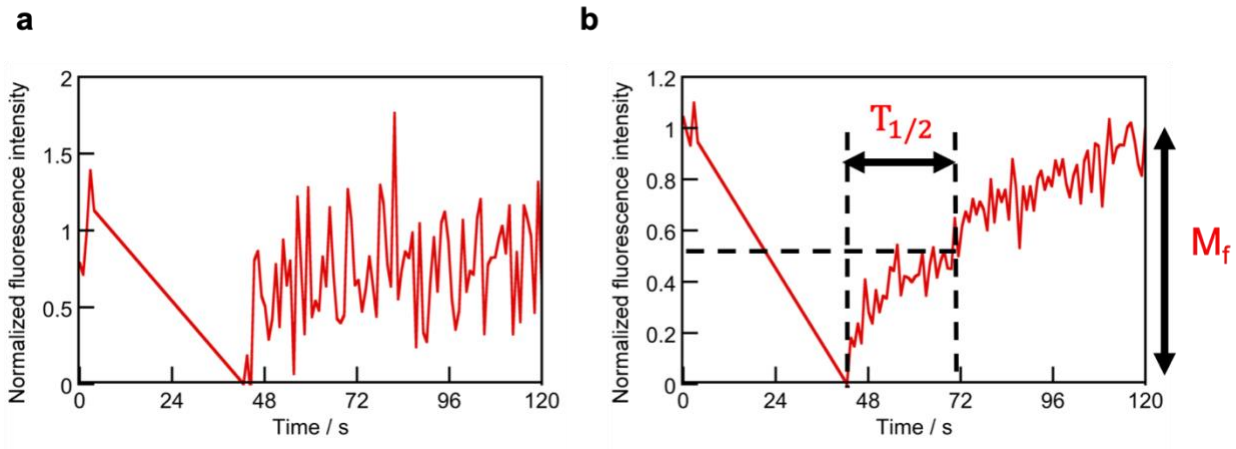

Figure 4.12 Normalized fluorescence recovery data of nile red in a. NaDC gel, b. NaDC-CB[6] (0.15) gel as a function of time. The observed $T_{1/2}$ for nile red in the NaDC-CB[6] gel structure for the shown experiment is 10±1 s.

The quantitative parameters $T_{1/2}$ and the mobile fraction were determined from the normalized curves, such as the one shown in Figure 4.12. The error in $T_{1/2}$ was determined from the normalization curve by considering the time at which the normalized intensity of the recovery curve is between 0.45 to 0.5.

The diffusion coefficient was calculated from $T_{1/2}$ using eq. 4.3 as proposed by Webb *et al.*[158]

$$D_{eff} = \frac{0.88 \times \omega^2}{4T_{1/2}}$$

Eq. 4.3

where, D_{eff} is the diffusion coefficient and ω is the radius of the bleached area.

The mobile fraction was observed to be 1 for solutions and the aqueous phase and gel structures of the NaDC and NaDC-CB[6] samples. The mobile fraction data suggest that complete recovery occurs, indicating that all the bleached nile red molecules are free to diffuse away from the bleached area and are substituted by nile red molecules diffusing from the surrounding area. Results in the aqueous phase (Figure C3, C4) and solutions (Figure C5, C6) showed that recovery is faster than 1 s, suggesting that D_{eff} is higher than 10 $\mu m^2 s^{-1}$. In the case of the NaDC gel structure, instant recovery is observed (< 1s) (Figure 4.12a). However, for the NaDC-CB[6] gel structure (Figure 4.12b, Figure C7, Figure C8), $T_{1/2}$ values in the range of 4-30 s corresponding to a D_{eff} range of 0.4-3 $\mu m^2 s^{-1}$ was observed, indicating a slower diffusion of nile red with the addition of CB[6]. The distribution of $T_{1/2}$ values obtained from the study of different NaDC-CB[6] gel structures show that these structures are heterogeneous, and thereby showing that analyzing different areas in the sample is required. In summary, FRAP results show that the diffusion of nile red molecules is different in the chemically different environments of the NaDC and NaDC-CB[6] gels.

4.4 Discussion

Colocalization studies with rhodamine 6G and berberine showed that the distribution of dye molecules between the aqueous phase and the gel structure was affected by CB[6]. Although my initial hypothesis based on the studies described in chapter 3 suggested that a hydrophilic dye and hydrophobic dye are located in the different regions of the gel, colocalization studies showed that this distinct separation of dyes based on hydrophobicity does not occur. The distribution in quadrant 3 of the scatter plot for NaDC-CB[6] gels (Figure 4.7) suggests that berberine and rhodamine 6G are colocalized in the image, whereas the distribution in quadrant 1 for NaDC gels (Figure 4.6) suggest the absence of colocalization in the image.

In the case of NaDC gels, for a hydrophilic dye, such as rhodamine 6G, green coding in the aqueous phase and the gel structure shows the interaction of rhodamine 6G with the NaDC aggregates (Figure 4.6), as the aggregates are present both in the aqueous phase and the gel structures. In Figure 4.6, the insignificant contribution from the y-axis channel (represented by rhodamine 6G) to the scatter plot suggests that the majority of the rhodamine 6G molecules is located in the aqueous phase and the emission appears as the background emission. In figure 4.6, the hydrophobic dye berberine, which corresponds to the x-axis in the scatter plot, suggest that the majority of berberine is located in the gel structure.

For the NaDC-CB[6] gels, the yellow color coding observed for the fibers and the contribution of the y-axis to the scatter plot (Figure 4.7) indicate that the distribution of rhodamine 6G between the aqueous phase and gel structure has changed with the addition of CB[6]. Since berberine is mainly localized in the NaDC aggregates, contribution of the x-axis to the scatter plot (Figure 4.7 compared to Figure 4.6) suggests that more NaDC aggregates are incorporated in the gel structure in the presence of CB[6].

The DLS and microscopy studies in chapter 2 provided evidence that NaDC aggregates from the aqueous phase are incorporated into the gel structure in the presence of CB[6]. However, the role CB[6] plays in this incorporation of aggregates remains unclear. Information on the role of CB[6] can be obtained using CLSM where the dyes are specifically designed to target NaDC and CB[6]. The results from colocalization studies with berberine and DSMI in NaDC and NaDC-CB[6] gels show that CB[6] molecules are a part of the gel structure (Figure 4.9). The incorporation of CB[6] molecules into the gel structure likely occurs because of the interactions between the negatively charged NaDC aggregates and CB[6] meditated by cations in the buffer, leading to the incorporation of NaDC aggregates from the aqueous phase into the gel structure.

Colocalization experiments showed that the dye molecules are distributed between different regions of the gel, which are the aqueous phase and the gel structure. Release studies in chapter 3 showed that the diffusion of a hydrophobic dye bound to NaDC aggregates is slowed down with the addition of CB[6], whereas the diffusion of a hydrophilic dye predominantly located in the aqueous phase is unaffected by the presence of CB[6]. The diffusion captured by these release studies is an overall measurement of dye release from the gels into the surrounding medium and regional differences in the diffusion of dye molecules within the gels as a result of their distribution between different regions of the gel are not evident from the release studies. Therefore, studies on the diffusion within the gels are necessary to bridge between dynamic information at the structural level from an overall effect for the release. FRAP studies were used to address the diffusion within the gels, which can then be related to bulk release properties.

Colocalization experiments showed that more aggregates are incorporated into the gel structure with the addition of CB[6]. Since nile red binds to NaDC aggregates, nile red is located

in the gel's structure and in the aggregates that are free in the aqueous phase of the gel. In the presence of CB[6], a larger fraction of nile red molecules resides in the gel structure as a larger proportion of the aggregates are located in these structures. As a result, when an area of the gel structure is bleached, I expect recovery in the gel structure to be fast as more nile red molecules are located in the gel structure surrounding the bleached area compared to the aqueous phase. However, FRAP studies showed that the recovery is slower in the gel structure compared to the aqueous phase. These results indicate that besides the availability of dye molecules surrounding the bleached area, the rate of mobility for these molecules is a crucial factor to determine the diffusion. The mobile fraction of 1 indicates that the slower recovery observed in the NaDC-CB[6] gels is not due to the presence of immobile dye molecules outside the bleached region in the gel structure. These results suggest that the viscosity in the gel structure is higher compared to the aqueous phase resulting in slower diffusion.

Viscosity changes in the gel structure with the addition of CB[6] could be tested in the future using molecular rotors like 9-(2,2-Dicyanovinyl) julolidine (DCVJ). When excited, molecular rotors undergo intramolecular rotation and return to the ground state through a non-radiative decay.[182] Any changes in the viscosity affect this rotation and therefore the fluorescence properties of these molecules. For example, an increase in the viscosity of the environment surrounding the probe hinders the intramolecular rotation leading to an increase in the emission fluorescence of the probe. The hydrophobic nature of DCVJ facilitates its localization in NaDC aggregates. Assuming that the viscosity in the aqueous phase in the gel will be similar to that in a solution, the emission fluorescence measured in solutions and gels for NaDC and NaDC-CB[6] (0.15) can be compared. If my hypothesis is valid, I predict that the emission fluorescence will

be higher for DCVJ in the NaDC-CB[6] gel compared to the emission fluorescence for this dye in the NaDC gel.

FRAP results showed correlations between the mobility of small molecules at a macroscopic and microscopic length scales. In solutions and the aqueous phase of the gel, the observed fluorescence recovery is instantaneous. The FRAP result supports the release studies, where the release of the dye that is predominantly in the gel's aqueous phase is not affected by the addition of CB[6]. However, the observed fluorescence recovery and half-life were slowed down in the gel with the addition of CB[6]. This result is consistent with the release studies, where the diffusion of the dye (pyrene) predominantly in the gel structure is affected by the addition of CB[6].

4.5 Conclusions

The colocalization experiments captured the distribution of dye molecules between different regions in the gel. The results from colocalization experiments complemented the information obtained on the regional differences in the diffusion within the gel as observed in FRAP studies. FRAP studies discussed in this chapter provided the proof of concept that length scale considerations go beyond the molecular structure and an emphasis on bulk release is not sufficient to understand the mobility in multicomponent gels.

Chapter 5 Summary

Gels have been investigated for many applications in materials science. However, application-based studies did not focus on the understanding of the complexity of gels. In this thesis, the properties of gels were studied from a mechanistic point of view. Additives in supramolecular gels are used as a strategy to change the distribution of small molecules between the compartments of the gel, thereby tuning the properties of this material, such as the release of small molecules from the gel. Based on the understanding developed in this thesis, the locations of the different dyes in the gels and how the dye localization is affected with the addition of CB[6] is highlighted in Figure 5.1.

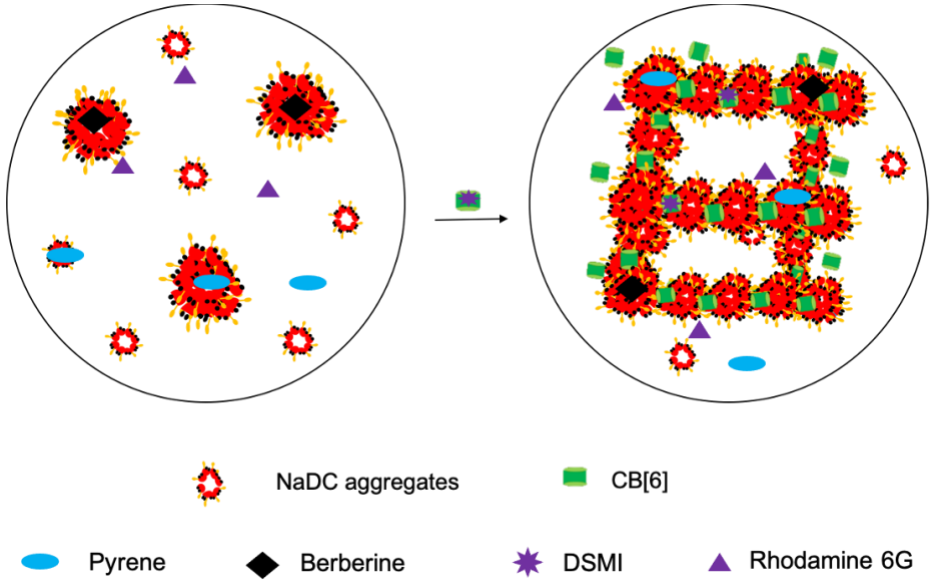

Figure 5.1 Schematic representation of dye localization in NaDC and NaDC-CB[6] gels.

CLSM studies are consistent with previous findings that the NaDC gel is made of aggregates in the aqueous phase and the gel structure. Structural studies for the NaDC-CB[6] gels showed that the effect of CB[6] on the structure of aggregates begins in solution and is translated into the sol and gel structures. Thermo-reversibility and kinetics of gel formation

indicate that the effect of CB[6] on NaDC gels extends beyond changes to the gel's structure. Release studies with dyes of different hydrophobicity revealed that the release of a hydrophilic dye and a hydrophobic dye was affected differently by CB[6]. While colocalization studies provided insights on the location of dyes of different hydrophobicity and CB[6] in the gels, dynamics using FRAP shed insights on the heterogeneity for the diffusion in gels. This work also highlights that structure, dynamics and release studies were equally important to understand the complexity of NaDC-CB[6] gels. For example, release studies alone did not reveal any information on the structural and dynamical heterogeneity inside the gels.

Structure, dynamics and release studies revealed complementary information and correlations were observed between these studies. Structural differences in gels (i.e. gel structure and aqueous phase) with the addition of CB[6] captured by DLS and CLSM were comparable to the observed diffusion differences between different regions in the gels. However, the arguments developed from structural studies were not enough to explain the dynamics studies, reflecting that the combination of two studies contributes to the better understanding of the functional properties of the gels. The differences in release of dyes was consistent with colocalization studies revealing the location of dyes in the gels. A correlation was seen between the colocalization studies showing the location of CB[6] in the gel and changes in gel structures of gels in the presence of CB[6]. The effect of CB[6] on the release of a hydrophobic dye from the gels is consistent with diffusion of the dye within the gel structure. The observation that diffusion in the aqueous phase of the gel is unaffected by the presence of CB[6] is consistent with the unaffected release of dye located in the aqueous phase, such as rhodamine 6G, during the release experiments. The combination of dynamics, structure and release led to non-trivial connections. For example, incorporation of aggregates from the aqueous phase of the gel into the gel's

structure led to formation of fibers. Diffusion of dyes in the fibers was slowed down eventually affecting the release properties.

The techniques and methods developed in this thesis presents a tool box when probing multicomponent gels. The tool box helps us to unlock the opportunity to control the properties in gels.

Bibliography

1. Lehn, J.-M., Towards complex matter: supramolecular chemistry and self-organization. *European Review* **2009,** *17* (2), 263-280.
2. Lehn, J.-M., Supramolecular chemistry. *Science* **1993,** *260* (5115), 1762-1763.
3. Lehn, J.-M., Toward self-organization and complex matter. *Science* **2002,** *295* (5564), 2400-2403.
4. Packwood, D. M.; Han, P.; Hitosugi, T., Chemical and entropic control on the molecular self-assembly process. *Nature Communications* **2017,** *8* (1), 14463-14463.
5. Adams, M.; Dogic, Z.; Keller, S. L.; Fraden, S., Entropically driven microphase transitions in mixtures of colloidal rods and spheres. *Nature* **1998,** *393* (6683), 349-352.
6. Capone, B.; Pierleoni, C.; Hansen, J. P.; Krakoviack, V., Entropic self-assembly of diblock copolymers into disordered and ordered micellar phases. *Journal of Physical Chemistry B* **2009,** *113* (12), 3629-3638.
7. Görl, D.; Würthner, F., Entropically driven self-assembly of bolaamphiphilic perylene dyes in water. *Angewandte Chemie International Edition* **2016,** *55* (39), 12094-12098.
8. Philp, D.; Stoddart, J. F., Self-assembly in natural and unnatural systems. *Angewandte Chemie International Edition* **1996,** *35* (11), 1154-1196.
9. Whitesides, G. M.; Mathias, J. P.; Seto, C. T., Molecular self-assembly and nanochemistry: a chemical strategy for the synthesis of nanostructures. *Science* **1991,** *254* (5036), 1312-1319.
10. Chayen, J., Micelles, monolayers and biomembranes. . *Cell Biochemistry and Function* **1996,** *14* (1), 75-78.
11. Desiraju, G. R., *Crystal engineering : the design of organic solids*. Elsevier: Amsterdam; New York, 1989.
12. Fendler, J. H., The colloidal domain: Where physics, chemistry, biology, and technology meet. *Advanced Materials* **1996,** *8* (3), 260-264.
13. Thomas, E. L., The ABCs of self-assembly. *Science* **1999,** *286* (5443), 1307-1308.
14. Kumar, A.; Abbott, N. L.; Biebuyck, H. A.; Kim, E.; Whitesides, G. M., Patterned self-assembled monolayers and meso-scale phenomena. *Accounts of Chemical Research* **1995,** *28* (5), 219-226.
15. Grzelczak, M.; Liz-Marzán, L. M.; Klajn, R., Stimuli-responsive self-assembly of nanoparticles. *Chemical Society Reviews* **2019,** *48* (5), 1342-1361.
16. Kean, Z. S.; Hawk, J. L.; Lin, S.; Zhao, X.; Sijbesma, R. P.; Craig, S. L., Increasing the maximum achievable strain of a covalent polymer gel through the addition of mechanically invisible cross-links. *Advanced Materials* **2014,** *26* (34), 6013-6018.
17. de Silva, A. P.; Gunaratne, H. Q. N.; Gunnlaugsson, T.; Nieuwenhuizen, M., Fluorescent switches with high selectivity towards sodium ions: correlation of ion-induced conformation switching with fluorescence function. *Chemical Communications* **1996,** (16), 1967-1968.
18. de Silva, A. P.; Sandanayake, K. R. A. S., Fluorescent PET (photo-induced electron transfer) sensors for alkali metal ions with improved selectivity against protons and with predictable binding constants. *Journal of the Chemical Society, Chemical Communications* **1989,** (16), 1183-1185.
19. Branco, M. C.; Schneider, J. P., Self-assembling materials for therapeutic delivery. *Acta Biomaterialia* **2009,** *5* (3), 817-831.

20. Kyle, S.; Aggeli, A.; Ingham, E.; McPherson, M. J., Production of self-assembling biomaterials for tissue engineering. *Trends in Biotechnology* **2009,** *27* (7), 423-433.
21. Aliabadi, H. M.; Landry, B.; Sun, C.; Tang, T.; Uludağ, H., Supramolecular assemblies in functional siRNA delivery: Where do we stand? *Biomaterials* **2012,** *33* (8), 2546-2569.
22. Tysseling, V. M.; Sahni, V.; Pashuck, E. T.; Birch, D.; Hebert, A.; Czeisler, C.; Stupp, S. I.; Kessler, J. A., Self-assembling peptide amphiphile promotes plasticity of serotonergic fibers following spinal cord injury. *Journal of Neuroscience Research* **2010,** *88* (14), 3161-3170.
23. Jones, C. D.; Steed, J. W., Gels with sense: supramolecular materials that respond to heat, light and sound. *Chemical Society Reviews* **2016,** *45* (23), 6546-6596.
24. Osada, Y.; Ping Gong, J.; Tanaka, Y., Polymer gels. *Journal of Macromolecular Science, Part C* **2004,** *44* (1), 87-112.
25. Terech, P.; Weiss, R. G., *Molecular gels : materials with self-assembled fibrillar networks*. Springer: Netherlands, 2006.
26. de Loos, M.; Feringa, B. L.; van Esch, J. H., Design and application of self-assembled low molecular weight hydrogels. *European Journal of Organic Chemistry* **2005,** *2005* (17), 3615-3631.
27. Estroff, L. A.; Hamilton, A. D., Water gelation by small organic molecules. *Chemical Reviews* **2004,** *104* (3), 1201-1218.
28. Steed, J. W., Supramolecular gel chemistry: developments over the last decade. *Chemical Communications* **2011,** *47* (5), 1379-1383.
29. Mohmeyer, N.; Schmidt, H. W., Synthesis and structure-property relationships of amphiphilic organogelators. *Chemistry* **2007,** *13* (16), 4499-4509.
30. Basit, H.; Pal, A.; Sen, S.; Bhattacharya, S., Two-component hydrogels comprising fatty acids and amines: structure, properties, and application as a template for the synthesis of metal nanoparticles. *Chemistry* **2008,** *14* (21), 6534-6545.
31. Suzuki, M.; Hanabusa, K., L-lysine-based low-molecular-weight gelators. *Chemical Society Reviews* **2009,** *38* (4), 967-975.
32. Naota, T.; Koori, H., Molecules that assemble by sound: an application to the instant gelation of stable organic fluids. *Journal of the American Chemical Society* **2005,** *127* (26), 9324-9325.
33. Piepenbrock, M.-O. M.; Clarke, N.; Steed, J. W., Shear induced gelation in a copper(ii) metallogel: new aspects of ion-tunable rheology and gel-reformation by external chemical stimuli. *Soft Matter* **2010,** *6* (15), 3541-3547.
34. Carretti, E.; Bonini, M.; Dei, L.; Berrie, B. H.; Angelova, L. V.; Baglioni, P.; Weiss, R. G., New frontiers in materials science for art conservation: responsive gels and beyond. *Accounts of Chemical Research* **2010,** *43* (6), 751-760.
35. Mukhopadhyay, P.; Fujita, N.; Takada, A.; Kishida, T.; Shirakawa, M.; Shinkai, S., Regulation of a real-time self-healing process in organogel tissues by molecular adhesives. *Angewandte Chemie International Edition* **2010,** *49* (36), 6338-6342.
36. Chivers, P. R. A.; Smith, D. K., Shaping and structuring supramolecular gels. *Nature Reviews Materials* **2019,** *4* (7), 463-478.
37. Raeburn, J.; Adams, D. J., Multicomponent low molecular weight gelators. *Chemical Communications* **2015,** *51* (25), 5170-5180.

38. Nanda, J.; Biswas, A.; Banerjee, A., Single amino acid based thixotropic hydrogel formation and pH-dependent morphological change of gel nanofibers. *Soft Matter* **2013,** *9* (16), 4198-4208.
39. Maeda, H., Anion-responsive supramolecular gels. *Chemistry – A European Journal* **2008,** *14* (36), 11274-11282.
40. Wu, J.-J.; Cao, M.-L.; Zhang, J.-Y.; Ye, B.-H., A nanocomposite gel based on 1D coordination polymers and nanoclusters reversibly gelate water upon heating. *RSC Advances* **2012,** *2* (33), 12718-12723.
41. Yagai, S.; Nakajima, T.; Kishikawa, K.; Kohmoto, S.; Karatsu, T.; Kitamura, A., Hierarchical organization of photoresponsive hydrogen-bonded rosettes. *Journal of American Chemical Society* **2005,** *127* (31), 11134-11139.
42. Murata, K.; Aoki, M.; Nishi, T.; Ikeda, A.; Shinkai, S., New cholesterol-based gelators with light- and metal-responsive functions. *Journal of the Chemical Society, Chemical Communications* **1991,** (24), 1715-1718.
43. Banerjee, S.; Das, R. K.; Maitra, U., Supramolecular gels 'in action'. *Journal of Materials Chemistry* **2009,** *19* (37), 6649-6687.
44. Sangeetha, N. M.; Maitra, U., Supramolecular gels: functions and uses. *Chemical Society Reviews* **2005,** *34* (10), 821-836.
45. Nakashima, T.; Kimizuka, N., Light-harvesting supramolecular hydrogels assembled from short-legged cationic L-Glutamate derivatives and anionic fluorophores. *Advanced Materials* **2002,** *14* (16), 1113-1116.
46. Koshima, H.; Matsusaka, W.; Yu, H., Preparation and photoreaction of organogels based on benzophenone. *Journal of Photochemistry and Photobiology A: Chemistry* **2003,** *156* (1), 83-90.
47. Bhattacharya, S.; Krishnan-Ghosh, Y., First report of phase selective gelation of oil from oil/water mixtures. Possible implications toward containing oil spills. *Chemical Communications* **2001,** (2), 185-186.
48. Vibhute, A. M.; Sureshan, K. M., How far are we in combating marine oil spills by using phase-selective organogelators? *ChemSusChem* **2020,** *13* (20), 5343-5360.
49. Mukhopadhyay, P.; Iwashita, Y.; Shirakawa, M.; Kawano, S.; Fujita, N.; Shinkai, S., Spontaneous colorimetric sensing of the positional isomers of dihydroxynaphthalene in a 1D organogel matrix. *Angewandte Chemie International Edition* **2006,** *45* (10), 1592-1595.
50. Moorthy, J.; Mensing, G. A.; Kim, D.; Mohanty, S.; Eddington, D. T.; Tepp, W. H.; Johnson, E. A.; Beebe, D. J., Microfluidic tectonics platform: A colorimetric, disposable botulinum toxin enzyme-linked immunosorbent assay system. *Electrophoresis* **2004,** *25* (10-11), 1705-1713.
51. Dasgupta, A.; Mondal, J. H.; Das, D., Peptide hydrogels. *RSC Advances* **2013,** *3* (24), 9117-9149.
52. Yan, N.; He, G.; Zhang, H.; Ding, L.; Fang, Y., Glucose-based fluorescent low-molecular mass compounds: creation of simple and versatile supramolecular gelators. *Langmuir* **2010,** *26* (8), 5909-5917.
53. Maitra, U.; Mukhopadhyay, S.; Sarkar, A.; Rao, P.; Indi, S. S., Hydrophobic pockets in a nonpolymeric aqueous gel: observation of such a gelation process by color change. *Angewandte Chemie International Edition* **2001,** *40* (12), 2281-2283.

54. van Bommel, K. J. C.; Stuart, M. C. A.; Feringa, B. L.; van Esch, J., Two-stage enzyme mediated drug release from LMWG hydrogels. *Organic & Biomolecular Chemistry* **2005,** *3* (16), 2917-2920.
55. Panda, J. J.; Mishra, A.; Basu, A.; Chauhan, V. S., Stimuli responsive self-assembled hydrogel of a low molecular weight free dipeptide with potential for tunable drug delivery. *Biomacromolecules* **2008,** *9* (8), 2244-2250.
56. Yang, Z.; Xu, B., A simple visual assay based on small molecule hydrogels for detecting inhibitors of enzymes. *Chemical Communications* **2004,** (21), 2424-2425.
57. Qiao, Y.; Lin, Y.; Wang, Y.; Yang, Z.; Liu, J.; Zhou, J.; Yan, Y.; Huang, J., Metal-driven hierarchical self-assembled one-dimensional nanohelices. *Nano Letters* **2009,** *9* (12), 4500-4504.
58. Blow, D. M.; Rich, A., Studies on the formation of helical deoxycholate complexes1,2. *Journal of the American Chemical Society* **1960,** *82* (14), 3566-3571.
59. Small, D. M.; Penkett, S. A.; Chapman, D., Studies on simple and mixed bile salt micelles by nuclear magnetic resonance spectroscopy. *Biochimica et Biophysica Acta* **1969,** *176* (1), 178-189.
60. Amundson, L. L.; Li, R.; Bohne, C., Effect of the guest size and shape on its binding dynamics with sodium cholate aggregates. *Langmuir* **2008,** *24* (16), 8491-8500.
61. Ju, C.; Bohne, C., Dynamics of probe complexation to bile salt aggregates. *The Journal of Physical Chemistry* **1996,** *100* (9), 3847-3854.
62. Rinco, O.; Nolet, M.-C.; Ovans, R.; Bohne, C., Probing the binding dynamics to sodium cholate aggregates using naphthalene derivatives as guests. *Photochemical & Photobiological Sciences* **2003,** *2* (11), 1140-1151.
63. Ju, C.; Bohne, C., Probing bile salt aggregates by fluorescence quenching. *Photochemistry and Photobiology* **1996,** *63* (1), 60-67.
64. Song, S.; Dong, R.; Wang, D.; Song, A.; Hao, J., Temperature regulated supramolecular structures via modifying the balance of multiple non-covalent interactions. *Soft Matter* **2013,** *9* (1), 4209-4218.
65. Li, R.; Santos, C. S.; Norsten, T. B.; Morimitsu, K.; Bohne, C., Aqueous solubilization of photochromic compounds by bile salt aggregates. *Chemical Communications* **2010,** *46* (11), 1941-1943.
66. Sobotka, H.; Czeczowiczka, N., The gelation of bile salt solutions. *Journal of Colloid Science* **1958,** *13* (2), 188-191.
67. Hofmann, A. F.; Mysels, K. J., Bile salts as biological surfactants. *Colloids and Surfaces* **1987,** *30* (1), 145-173.
68. Jover, A.; Meijide, F.; Rodríguez Núñez, E.; Vázquez Tato, J.; Mosquera, M.; Rodríguez Prieto, F., Unusual pyrene excimer formation during sodium deoxycholate gelation. *Langmuir* **1996,** *12* (7), 1789-1793.
69. Seyedalikhani, M. Exploring the binding of small guest molecules in sodium deoxycholate gels. PhD. Dissertation University of Victoria, http://hdl.handle.net/1828/7615, 2016.
70. Sun, X.; Du, Z.; Li, E.; Xin, X.; Tang, N.; Wang, L.; Yuan, J., Rheological properties of the gels of biological surfactant sodium deoxycholate/amino acids/halide salts systems. *Colloids and Surfaces A: Physicochemical and Engineering Aspects* **2014,** *457* (1), 345-353.

71. Sun, X.; Xin, X.; Tang, N.; Guo, L.; Wang, L.; Xu, G., Manipulation of the gel behavior of biological surfactant sodium deoxycholate by amino acids. *The Journal of Physical Chemistry B* **2014,** *118* (3), 824-832.
72. Jover, A.; Meijide, F.; Rodríguez Núñez, E., Dynamic rheology of sodium deoxycholate gels. *Langmuir* **2002,** *18* (4), 987-991.
73. Zhang, J.; Wang, H.; Li, X.; Song, S.; Song, A.; Hao, J., Two gelation mechanisms of deoxycholate with inorganic additives: hydrogen bonding and electrostatic interactions. *Journal of Physical Chemistry B* **2016,** *120* (27), 6812-6818.
74. Jover, A.; Meijide, F.; Rodríguez Núñez, E.; Vázquez Tato, J., Aggregation kinetics of sodium deoxycholate in aqueous solution. *Langmuir* **1998,** *14* (16), 4359-4363.
75. Murata, Y.; Sugihara, G.; Fukushima, K.; Tanaka, M.; Matsushita, K., Study of the micelle formation of sodium deoxycholate. Concentration dependence of carbon-13 nuclear magnetic resonance chemical shift. *The Journal of Physical Chemistry* **1982,** *86* (24), 4690-4694.
76. Song, S.; Feng, L.; Song, A.; Hao, J., Room-temperature super hydrogel as dye adsorption agent. *The Journal of Physical Chemistry B* **2012,** *116* (42), 12850-12856.
77. Song, S.; Wang, H.; Song, A.; Hao, J., Superhydrogels of nanotubes capable of capturing heavy-metal ions. *Chemistry – An Asian Journal* **2014,** *9* (1), 245-252.
78. Adhia, Y. J.; Schloemer, T. H.; Perez, M. T.; McNeil, A. J., Using polymeric additives to enhance molecular gelation: impact of poly(acrylic acid) on pyridine-based gelators. *Soft Matter* **2012,** *8* (2), 430-434.
79. Liu, X. Y.; Sawant, P. D., Micro/nanoengineering of the self-organized three-dimensional fibrous structure of functional materials. *Angewandte Chemie International Edition* **2002,** *41* (19), 3641-3645.
80. Cui, J.; Shen, Z.; Wan, X., Study on the gel to crystal transition of a novel sugar-appended gelator. *Langmuir* **2010,** *26* (1), 97-103.
81. Dasgupta, D.; Srinivasan, S.; Rochas, C.; Ajayaghosh, A.; Guenet, J. M., Hybrid thermoreversible gels from covalent polymers and organogels. *Langmuir* **2009,** *25* (15), 8593-8598.
82. Li, J. L.; Liu, X. Y.; Strom, C. S.; Xiong, J. Y., Engineering of small molecule organogels by design of the nanometer structure of fiber networks. *Advanced Materials* **2006,** *18* (19), 2574-2578.
83. Li, J.-L.; Liu, X.-Y., Architecture of supramolecular soft functional materials: from understanding to micro-/nanoscale engineering. *Advanced Functional Materials* **2010,** *20* (19), 3196-3216.
84. Hanabusa, K.; Itoh, A.; Kimura, M.; Shirai, H., Terephthaloyl derivatives as new gelators; excellent gelation ability and remarkable increase of gel strength by adding polymers. *Chemistry Letters* **1999,** *28* (8), 767-768.
85. Adhikari, B.; Banerjee, A., Short peptide based hydrogels: incorporation of graphene into the hydrogel. *Soft Matter* **2011,** *7* (19), 9259-9266.
86. Chen, L.; Revel, S.; Morris, K.; Spiller, D. G.; Serpell, L. C.; Adams, D. J., Low molecular weight gelator–dextran composites. *Chemical Communications* **2010,** *46* (36), 6738-6740.
87. Wang, C.; Zhang, D.; Zhu, D., A chiral low-molecular-weight gelator based on binaphthalene with two urea moieties: modulation of the CD spectrum after gel formation. *Langmuir* **2007,** *23* (3), 1478-1482.

88. Zhang, Y.; Gu, H.; Yang, Z.; Xu, B., Supramolecular hydrogels respond to ligand−receptor interaction. *Journal of the American Chemical Society* **2003,** *125* (45), 13680-13681.
89. Qiao, Y.; Lin, Y.; Zhang, S.; Huang, J., Lanthanide-containing photoluminescent materials: from hybrid hydrogel to inorganic nanotubes. *Chemistry – A European Journal* **2011,** *17* (18), 5180-5187.
90. Wang, Y. T.; Xin, X.; Li, W. Z.; Jia, C. Y.; Wang, L.; Shen, J. L.; Xu, G. Y., Studies on the gel behavior and luminescence properties of biological surfactant sodium deoxycholate/rare-earth salts mixed systems. *Journal of Colloid and Interface Science* **2014,** *431* (1), 82-89.
91. Wang, L.; Xin, X.; Yang, M.; Ma, X.; Shen, J.; Song, Z.; Yuan, S., Effects of graphene oxide and salinity on sodium deoxycholate hydrogels and their applications in dye absorption. *Colloids and Surfaces A: Physicochemical and Engineering Aspects* **2015,** *483* (1), 112-120.
92. Das, S.; de Rooy, S. L.; Jordan, A. N.; Chandler, L.; Negulescu, I. I.; El-Zahab, B.; Warner, I. M., Tunable size and spectral properties of fluorescent nanoGUMBOS in modified sodium deoxycholate hydrogels. *Langmuir* **2012,** *28* (1), 757-765.
93. McNeel, K. E.; Das, S.; Siraj, N.; Negulescu, I. I.; Warner, I. M., Sodium deoxycholate hydrogels: effects of modifications on gelation, drug release, and nanotemplating. *The Journal of Physical Chemistry B* **2015,** *119* (27), 8651-8659.
94. Guo, Y.; Wang, R.; Shang, Y.; Liu, H., Effects of polymers on the properties of hydrogels constructed using sodium deoxycholate and amino acid. *RSC Advances* **2018,** *8* (16), 8699-8708.
95. Steed, J. W.; Atwood, J. L., *Supramolecular chemistry*. Wiley: Chichester, UK, 2009.
96. Qi, Z.; Schalley, C. A., Exploring macrocycles in functional supramolecular gels: from stimuli responsiveness to systems chemistry. *Accounts of Chemical Research* **2014,** *47* (7), 2222-2233.
97. Masson, E.; Ling, X.; Joseph, R.; Kyeremeh-Mensah, L.; Lu, X., Cucurbituril chemistry: a tale of supramolecular success. *RSC Advances* **2012,** *2* (4), 1213-1247.
98. Cao, L.; Šekutor, M.; Zavalij, P. Y.; Mlinarić-Majerski, K.; Glaser, R.; Isaacs, L., Cucurbit[7]uril·guest pair with an attomolar dissociation constant. *Angewandte Chemie International Edition* **2014,** *53* (4), 988-993.
99. Yang, H.; Chen, H.; Tan, Y., Cucurbit[8]uril inducing supramolecular hydrogels by adjusting pH. *RSC Advances* **2013,** *3* (9), 3031-3037.
100. Yang, H.; Tan, Y.; Wang, Y., Fabrication and properties of cucurbit[6]uril induced thermo-responsive supramolecular hydrogels. *Soft Matter* **2009,** *5* (18), 3511-3516.
101. Hwang, I.; Jeon, W. S.; Kim, H. J.; Kim, D.; Kim, H.; Selvapalam, N.; Fujita, N.; Shinkai, S.; Kim, K., Cucurbit[7]uril: A simple macrocyclic, pH-triggered hydrogelator exhibiting guest-induced stimuli-responsive behavior. *Angewandte Chemie International Edition* **2007,** *46* (1-2), 210-213.
102. Appel, E. A.; Loh, X. J.; Jones, S. T.; Dreiss, C. A.; Scherman, O. A., Sustained release of proteins from high water content supramolecular polymer hydrogels. *Biomaterials* **2012,** *33* (18), 4646-4652.
103. Park, K. M.; Yang, J. A.; Jung, H.; Yeom, J.; Park, J. S.; Park, K. H.; Hoffman, A. S.; Hahn, S. K.; Kim, K., In situ supramolecular assembly and modular modification of hyaluronic acid hydrogels for 3D cellular engineering. *ACS Nano* **2012,** *6* (4), 2960-2968.

104. Dastidar, P., Supramolecular gelling agents: can they be designed? *Chemical Society Reviews* **2008,** *37* (12), 2699-2715.
105. Hirst, A. R.; Escuder, B.; Miravet, J. F.; Smith, D. K., High-tech applications of self-assembling supramolecular nanostructured gel-phase materials: from regenerative medicine to electronic devices. *Angewandte Chemie International Edition* **2008,** *47* (42), 8002-8018.
106. Colquhoun, C.; Draper, E. R.; Eden, E. G. B.; Cattoz, B. N.; Morris, K. L.; Chen, L.; McDonald, T. O.; Terry, A. E.; Griffiths, P. C.; Serpell, L. C.; Adams, D. J., The effect of self-sorting and co-assembly on the mechanical properties of low molecular weight hydrogels. *Nanoscale* **2014,** *6* (22), 13719-13725.
107. Yu, G.; Yan, X.; Han, C.; Huang, F., Characterization of supramolecular gels. *Chemical Society Reviews* **2013,** *42* (16), 6697-6722.
108. Escuder, B.; Llusar, M.; Miravet, J. F., Insight on the NMR study of supramolecular gels and its application to monitor molecular recognition on self-assembled fibers. *The Journal of Organic Chemistry* **2006,** *71* (20), 7747-7752.
109. Doniach, S., Changes in biomolecular conformation seen by small angle X-ray scattering. *Chemical Reviews* **2001,** *101* (6), 1763-1778.
110. Fuentealba, D.; Thurber, K.; Bovero, E.; Pace, T. C. S.; Bohne, C., Effect of sodium chloride on the binding of polyaromatic hydrocarbon guests with sodium cholate aggregates. *Photochemical & Photobiological Sciences* **2011,** *10* (9), 1420-1430.
111. Ramalhete, S. M.; Nartowski, K. P.; Sarathchandra, N.; Foster, J. S.; Round, A. N.; Angulo, J.; Lloyd, G. O.; Khimyak, Y. Z., Supramolecular amino acid based hydrogels: probing the contribution of additive molecules using NMR spectroscopy. *Chemistry* **2017,** *23* (33), 8014-8024.
112. Vivian, J. T.; Callis, P. R., Mechanisms of tryptophan fluorescence shifts in proteins. *Biophysical Journal* **2001,** *80* (5), 2093-2109.
113. Lakowicz, J. R., *Principles of fluorescence spectroscopy*. Springer: New York, 2006.
114. Kalyanasundaram, K.; Thomas, J. K., Environmental effects on vibronic band intensities in pyrene monomer fluorescence and their application in studies of micellar systems. *Journal of the American Chemical Society* **1977,** *99* (7), 2039-2044.
115. Weng, W.; Beck, J. B.; Jamieson, A. M.; Rowan, S. J., Understanding the mechanism of gelation and stimuli-responsive nature of a class of metallo-supramolecular gels. *Journal of the American Chemical Society* **2006,** *128* (35), 11663-11672.
116. Mears, L. L. E.; Draper, E. R.; Castilla, A. M.; Su, H.; Zhuola; Dietrich, B.; Nolan, M. C.; Smith, G. N.; Doutch, J.; Rogers, S.; Akhtar, R.; Cui, H.; Adams, D. J., Drying affects the fiber network in low molecular weight hydrogels. *Biomacromolecules* **2017,** *18* (11), 3531-3540.
117. Pawley, J. B., *Handbook of biological confocal microscopy*. Springer: New York, 2006.
118. Schmitz, K. S., *An introduction to dynamic light scattering by macromolecules*. Academic Press: New York, 1990.
119. Draper, E. R.; Adams, D. J., Low-molecular-weight gels: The state of the art. *Chem* **2017,** *3* (3), 390-410.
120. Draper, E. R.; Adams, D. J., How should multicomponent supramolecular gels be characterised? *Chemical Society Reviews* **2018,** *47* (10), 3395-3405.
121. Gupta, J. K.; Adams, D. J.; Berry, N. G., Will it gel? Successful computational prediction of peptide gelators using physicochemical properties and molecular fingerprints. *Chemical Science* **2016,** *7* (7), 4713-4719.

122. Ahearne, M.; Yang, Y.; El Haj, A. J.; Then, K. Y.; Liu, K.-K., Characterizing the viscoelastic properties of thin hydrogel-based constructs for tissue engineering applications. *Journal of The Royal Society Interface* **2005,** *2* (5), 455-463.
123. White, L. J.; Boles, J. E.; Allen, N.; Alesbrook, L. S.; Sutton, J. M.; Hind, C. K.; Hilton, K. L. F.; Blackholly, L. R.; Ellaby, R. J.; Williams, G. T.; Mulvihill, D. P.; Hiscock, J. R., Controllable hydrogen bonded self-association for the formation of multifunctional antimicrobial materials. *Journal of Materials Chemistry B* **2020,** *8* (21), 4694-4700.
124. Stetefeld, J.; McKenna, S. A.; Patel, T. R., Dynamic light scattering: a practical guide and applications in biomedical sciences. *Biophysical Reviews* **2016,** *8* (4), 409-427.
125. Liao, X.; Chen, G.; Liu, X.; Chen, W.; Chen, F.; Jiang, M., Photoresponsive pseudopolyrotaxane hydrogels based on competition of host–guest interactions. *Angewandte Chemie International Edition* **2010,** *49* (26), 4409-4413.
126. Mazer, N. A.; Carey, M. C.; Kwasnick, R. F.; Benedek, G. B., Quasielastic light scattering studies of aqueous biliary lipid systems. Size, shape, and thermodynamics of bile salt micelles. *Biochemistry* **1979,** *18* (14), 3064-3075.
127. Berthon, S.; Barbieri, O.; Ehrburger-Dolle, F.; Geissler, E.; Achard, P.; Bley, F.; Hecht, A.-M.; Livet, F.; Pajonk, G. M.; Pinto, N.; Rigacci, A.; Rochas, C., DLS and SAXS investigations of organic gels and aerogels. *Journal of Non-Crystalline Solids* **2001,** *285* (1), 154-161.
128. Martin, J. E.; Wilcoxon, J. P., Critical dynamics of the sol-gel transition. *Physical Review Letters* **1988,** *61* (3), 373-376.
129. Kohl, K., Comparison of dynamic light scattering and rheometrical methods to determine the gel point of a radically polymerized hydrogel under mechanical shear. *Micromachines* **2020,** *11* (5), 462-475.
130. Matsunaga, T.; Shibayama, M., Gel point determination of gelatin hydrogels by dynamic light scattering and rheological measurements. *Physical Review E* **2007,** *76* (3), 030401-030405.
131. Vashishat, R.; Sanan, R.; Mahajan, R. K., Bile salt-surface active ionic liquid mixtures: mixed micellization and solubilization of phenothiazine. *RSC Advances* **2015,** *5* (88), 72132-72141.
132. Sugihara, G.; Tanaka, M.; Matuura, R., The behavior of aqueous solution of sodium deoxycholate in capillary flow. *Bulletin of the Chemical Society of Japan* **1977,** *50* (10), 2542-2547.
133. Freeman, W. A.; Mock, W. L.; Shih, N. Y., Cucurbituril. *Journal of the American Chemical Society* **1981,** *103* (24), 7367-7368.
134. Laishram, R.; Maitra, U., Supramolecular gelation of europium and calcium cholates through the nucleation-elongation growth mechanism. *ChemPlusChem* **2019,** *84* (7), 853-861.
135. Swain, J.; Mishra, J.; Ghosh, G.; Mishra, A. K., Quantification of micropolarity and microviscosity of aggregation and salt-induced gelation of sodium deoxycholate (NaDC) using Nile red fluorescence. *Photochemical & Photobiological Sciences* **2019,** *18* (11), 2773-2781.
136. Ramalhete, S. M.; Nartowski, K. P.; Sarathchandra, N.; Foster, J. S.; Round, A. N.; Angulo, J.; Lloyd, G. O.; Khimyak, Y. Z., Supramolecular amino acid based hydrogels: probing the contribution of additive molecules using NMR spectroscopy. *Chemistry – A European Journal* **2017,** *23* (33), 8014-8024.
137. Li, J.; Mooney, D. J., Designing hydrogels for controlled drug delivery. *Nature Reviews Materials* **2016,** *1* (12), 16071-16088.

138. Mayr, J.; Saldías, C.; Díaz Díaz, D., Release of small bioactive molecules from physical gels. *Chemical Society Reviews* **2018,** *47* (4), 1484-1515.
139. Saboktakin, M. r.; Tabatabaei, R. M., Supramolecular hydrogels as drug delivery systems. *International Journal of Biological Macromolecules* **2015,** *75* (1), 426-436.
140. Zeng, F.; Shen, Y.; Chen, C.-F., Cross-linked supramolecular polymer networks with responsive and elastic gel properties via host–guest complexation: controlled release of squaraine dyes. *Soft Matter* **2013,** *9* (19), 4875-4882.
141. Ji, W.; Qin, M.; Feng, C., Photoresponsive coumarin-based supramolecular hydrogel for controllable dye release. *Macromolecular Chemistry and Physics* **2018,** *219* (2), 1700398-1700406.
142. Komatsu, H.; Matsumoto, S.; Tamaru, S.-i.; Kaneko, K.; Ikeda, M.; Hamachi, I., Supramolecular hydrogel exhibiting four basic logic gate functions to fine-tune substance release. *Journal of the American Chemical Society* **2009,** *131* (15), 5580-5585.
143. Vlachou, M. D.; Rekkas, D. M.; Dallas, P. P.; Choulis, N. H., Development and in vitro evaluation of griseofulvin gels using Franz diffusion cells. *International Journal of Pharmaceutics* **1992,** *82* (1), 47-52.
144. Hua, S., Comparison of in vitro dialysis release methods of loperamide-encapsulated liposomal gel for topical drug delivery. *International Journal of Nanomedicine* **2014,** *9* (1), 735-744.
145. Xu, W.; Demas, J. N.; DeGraff, B. A.; Whaley, M., Interactions of pyrene with cyclodextrins and polymeric cyclodextrins. *The Journal of Physical Chemistry* **1993,** *97* (24), 6546-6554.
146. Zana, R.; Guveli, D., Fluorescence probing study of the association of bile salts in aqueous solutions. *The Journal of Physical Chemistry* **1985,** *89* (9), 1687-1690.
147. Mohanty, J.; Nau, W. M., Ultrastable rhodamine with cucurbituril. *Angewandte Chemie International Edition* **2005,** *44* (24), 3750-3754.
148. Clifford, A.; Zhitomirsky, I., Aqueous electrophoretic deposition of drugs using bile acids as solubilizing, charging and film-forming agents. *Materials Letters* **2018,** *227* (1), 1-4.
149. Terdale, S.; Tantray, A., Spectroscopic study of the dimerization of rhodamine 6G in water and different organic solvents. *Journal of Molecular Liquids* **2017,** *225* (1), 662-671.
150. Shokry, D. S.; Waters, L. J.; Parkes, G. M. B.; Mitchell, J. C.; Snowden, M. J., Formation of a bile salt-drug hydrogel to predict human intestinal absorption. *Journal of Pharmaceutical Sciences* **2019,** *108* (1), 279-287.
151. Sueldo Occello, V. N.; de Rossi, R. H.; Veglia, A. V., Complexation (cucurbit[6]uril-pyrene): Thermodynamic and spectroscopic properties. *Journal of Luminescence* **2015,** *158* (1), 435-440.
152. Khan, F.; Bera, D.; Palchaudhuri, S.; Bera, R.; Mukhopadhyay, M.; Dey, A.; Goswami, S.; Das, S., Dual release kinetics in a single dosage from core–shell hydrogel scaffolds. *RSC Advances* **2018,** *8* (57), 32695-32706.
153. Onogi, S.; Shigemitsu, H.; Yoshii, T.; Tanida, T.; Ikeda, M.; Kubota, R.; Hamachi, I., In situ real-time imaging of self-sorted supramolecular nanofibres. *Nature Chemistry* **2016,** *8* (8), 743-752.
154. An, B.; Wang, X.; Cui, M.; Gui, X.; Mao, X.; Liu, Y.; Li, K.; Chu, C.; Pu, J.; Ren, S.; Wang, Y.; Zhong, G.; Lu, T. K.; Liu, C.; Zhong, C., Diverse supramolecular nanofiber networks assembled by functional low-complexity domains. *ACS Nano* **2017,** *11* (7), 6985-6995.

155. Kubota, R.; Nakamura, K.; Torigoe, S.; Hamachi, I., The power of confocal laser scanning microscopy in supramolecular chemistry: in situ real-time imaging of stimuli-responsive multicomponent supramolecular hydrogels. *ChemistryOpen* **2020,** *9* (1), 67-79.
156. Megyesi, M.; Biczók, L., Berberine alkaloid as a sensitive fluorescent probe for bile salt aggregates. *The Journal of Physical Chemistry B* **2007,** *111* (20), 5635-5639.
157. Li, Z.; Sun, S.; Liu, F.; Pang, Y.; Fan, J.; Song, F.; Peng, X., Large fluorescence enhancement of a hemicyanine by supramolecular interaction with cucurbit[6]uril and its application as resettable logic gates. *Dyes and Pigments* **2012,** *93* (1), 1401-1407.
158. Axelrod, D.; Koppel, D. E.; Schlessinger, J.; Elson, E.; Webb, W. W., Mobility measurement by analysis of fluorescence photobleaching recovery kinetics. *Biophysical Journal* **1976,** *16* (9), 1055-1069.
159. Lorén, N.; Hagman, J.; Jonasson, J. K.; Deschout, H.; Bernin, D.; Cella-Zanacchi, F.; Diaspro, A.; McNally, J. G.; Ameloot, M.; Smisdom, N.; Nydén, M.; Hermansson, A.-M.; Rudemo, M.; Braeckmans, K., Fluorescence recovery after photobleaching in material and life sciences: putting theory into practice. *Quarterly Reviews of Biophysics* **2015,** *48* (3), 323-387.
160. Levi, V.; Gratton, E., Exploring dynamics in living cells by tracking single particles. *Cell Biochemistry and Biophysics* **2007,** *48* (1), 1-15.
161. Saxton, M. J., Single-particle tracking: the distribution of diffusion coefficients. *Biophysical Journal* **1997,** *72* (4), 1744-1753.
162. Suh, J.; Dawson, M.; Hanes, J., Real-time multiple-particle tracking: applications to drug and gene delivery. *Advanced Drug Delivery Reviews* **2005,** *57* (1), 63-78.
163. Bausinger, R.; von Gersdorff, K.; Braeckmans, K.; Ogris, M.; Wagner, E.; Bräuchle, C.; Zumbusch, A., The transport of nanosized gene carriers unraveled by live-cell imaging. *Angewandte Chemie International Edition* **2006,** *45* (10), 1568-1572.
164. Carr, H. Y.; Purcell, E. M., Effects of diffusion on free precession in nuclear magnetic resonance experiments. *Physical Review* **1954,** *94* (3), 630-638.
165. Price, W. S., Pulsed-field gradient nuclear magnetic resonance as a tool for studying translational diffusion: part 1. Basic theory. *Concepts in Magnetic Resonance* **1997,** *9* (5), 299-336.
166. Deschout, H.; Raemdonck, K.; Demeester, J.; De Smedt, S. C.; Braeckmans, K., FRAP in pharmaceutical research: practical guidelines and applications in drug delivery. *Pharmaceutical Research* **2014,** *31* (2), 255-270.
167. Van Tomme, S. R.; De Geest, B. G.; Braeckmans, K.; De Smedt, S. C.; Siepmann, F.; Siepmann, J.; van Nostrum, C. F.; Hennink, W. E., Mobility of model proteins in hydrogels composed of oppositely charged dextran microspheres studied by protein release and fluorescence recovery after photobleaching. *Journal of Controlled Release* **2005,** *110* (1), 67-78.
168. Kosto, K. B.; Deen, W. M., Diffusivities of macromolecules in composite hydrogels. *American Institute of Chemical Engineers Journal* **2004,** *50* (11), 2648-2658.
169. Mueller, F.; Mazza, D.; Stasevich, T. J.; McNally, J. G., FRAP and kinetic modeling in the analysis of nuclear protein dynamics: what do we really know? *Current Opinion in Cell Biology* **2010,** *22* (3), 403-411.
170. Ishikawa-Ankerhold, H. C.; Ankerhold, R.; Drummen, G. P. C., Advanced fluorescence microscopy techniques--FRAP, FLIP, FLAP, FRET and FLIM. *Molecules* **2012,** *17* (4), 4047-4132.
171. Sarkar, N.; Das, K.; Nath, D. N.; Bhattacharyya, K., Twisted charge transfer processes of nile red in homogeneous solutions and in faujasite zeolite. *Langmuir* **1994,** *10* (1), 326-329.

172. Assaf, K. I.; Nau, W. M., Cucurbiturils: from synthesis to high-affinity binding and catalysis. *Chemical Society Reviews* **2015,** *44* (2), 394-418.
173. Wagner, B. D.; Boland, P. G.; Lagona, J.; Isaacs, L., A cucurbit[6]uril analogue: host properties monitored by fluorescence spectroscopy. *The Journal of Physical Chemistry B* **2005,** *109* (16), 7686-7691.
174. Zinchuk, V.; Zinchuk, O.; Okada, T., Quantitative colocalization analysis of multicolor confocal immunofluorescence microscopy images: pushing pixels to explore biological phenomena. *Acta Histochemica et Cytochemica* **2007,** *40* (4), 101-111.
175. Miskolczy, Z.; Biczók, L., Kinetics and thermodynamics of berberine inclusion in cucurbit[7]uril. *The Journal of Physical Chemistry B* **2014,** *118* (9), 2499-2505.
176. Miskolczy, Z.; Biczók, L., Sequential inclusion of two berberine cations in cucurbit[8]uril cavity: kinetic and thermodynamic studies. *Physical Chemistry Chemical Physics* **2014,** *16* (37), 20147-20156.
177. Markaki, Y.; Harz, H., *Light microscopy: methods and protocols*. Humana Press: Springer: New York, 2017.
178. Hagman, J.; Lorén, N.; Hermansson, A.-M., Effect of gelatin gelation kinetics on probe diffusion determined by FRAP and rheology. *Biomacromolecules* **2010,** *11* (12), 3359-3366.
179. Meyvis, T. K. L.; De Smedt, S. C.; Van Oostveldt, P.; Demeester, J., Fluorescence recovery after photobleaching: a versatile tool for mobility and interaction measurements in pharmaceutical research. *Pharmaceutical Research* **1999,** *16* (8), 1153-1162.
180. Rapsomaniki, M. A.; Kotsantis, P.; Symeonidou, I.-E.; Giakoumakis, N.-N.; Taraviras, S.; Lygerou, Z., easyFRAP: an interactive, easy-to-use tool for qualitative and quantitative analysis of FRAP data. *Bioinformatics* **2012,** *28* (13), 1800-1801.
181. Koulouras, G.; Panagopoulos, A.; Rapsomaniki, M. A.; Giakoumakis, N. N.; Taraviras, S.; Lygerou, Z., EasyFRAP-web: a web-based tool for the analysis of fluorescence recovery after photobleaching data. *Nucleic Acids Research* **2018,** *46* (W1), W467-W472.
182. Raeburn, J.; Chen, L.; Awhida, S.; Deller, R. C.; Vatish, M.; Gibson, M. I.; Adams, D. J., Using molecular rotors to probe gelation. *Soft Matter* **2015,** *11* (18), 3706-3713.

Appendix

Appendix A.

Table A-1 Resolution of the objective lenses used for imaging gel samples during CLSM experiments.

Objective lens type	Wavelength of laser / nm	Numerical aperture (NA) of the lens	Resolution / nm
63x	514	1.4	220
20x LWD	514	0.4	780

Determination of average size of gel structures in NaDC, NaDC-CB[6] gels using the ImageJ analysis:

1. Open tiff file of the image in ImageJ (Figure A-1).

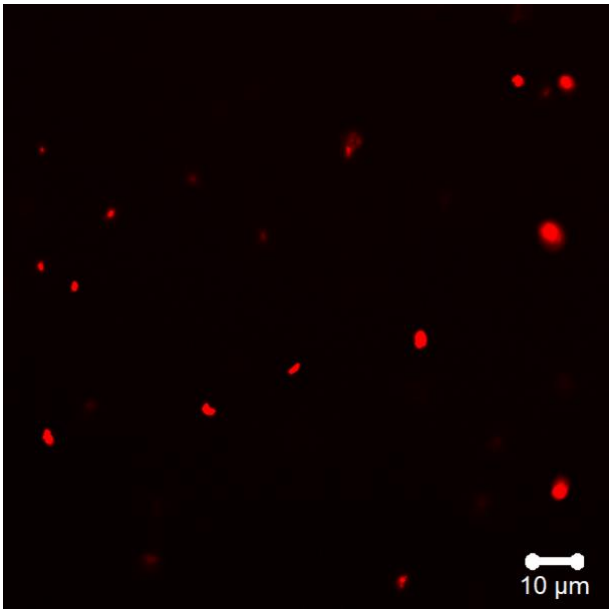

Figure A-1 Image of NaDC-CB6 gel tagged with rhodamine 6G (2 µM) at the CB[6]/NaDC ratio of 0.05. This image was taken after a 20 h resting period at room temperature. The concentration of NaDC in this sample is 50 mM.

2. The image dimensions in pixels need to be converted into µm. To set the image dimensions in µm, in Figure A-1, draw a line along the scale bar using “line icon” in the window, go to “analyse” -> “set scale”. Set the known distance and units (in Figure A-1 known distance is 10 µm) and click ok.

3. Chose an area in the image using the “rectangular box” icon. Go to “image” and click on “duplicate”.
4. Click “image” in the settings, select “type 8 bit” for analysis.
5. Click “image”-> “adjust”-> “threshold”. Adjust the min and max in the threshold such that all particles of interest in the image are selected (highlighted in white in Figure A2) and click apply.

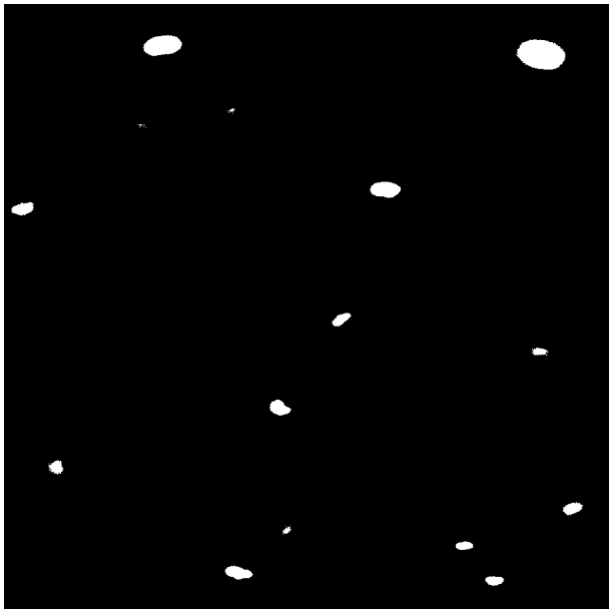

Figure A-2 Image of selected area in NaDC-CB6 gel tagged with rhodamine 6G (2 μM) at CB[6]/NaDC ratio of 0.05 after adjusting the threshold.

6. In the settings, choose “analyze”-> “set measurements”, select on the all required measurements, click ok.

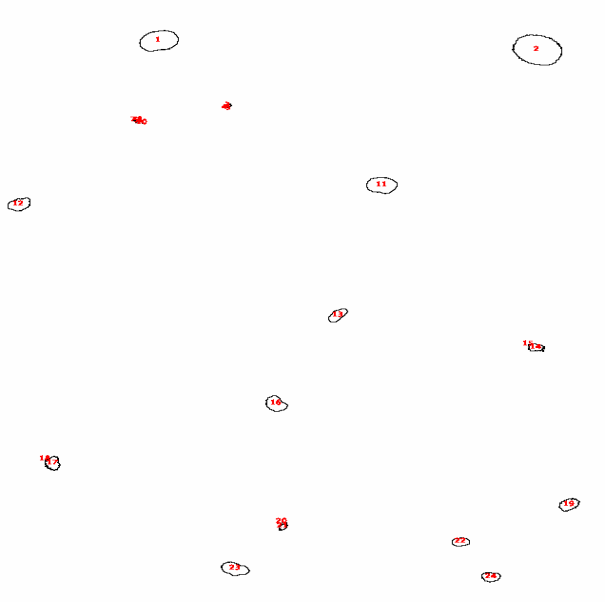

Figure A-3 Image of selected area in NaDC-CB6 gel tagged with rhodamine 6G (2 µM) at CB[6]/NaDC ratio of 0.05 that shows particles highlighted for size analysis.

7. Choose “analyze”-> “analyze particles”. Choose the particle size of interest (default: 0-infinity) and circularity between 0-1 (1 for perfect circle), show outlines. Enable display results, clear results, summarize and exclude on edges and click ok. Highlighted particles for analysis are shown in Figure A3. Average size of particles are summarized in Figure A4.

Summary

Slice	Count	Total Area	Average Size	%Area
SG171019LSM NaDC-CB6 63x-1.tif	24	124.048	5.169	0.997

Figure A-4 Summary of size analysis of selected area in NaDC-CB6 gel tagged with rhodamine 6G (2 µM) at the CB[6]/NaDC ratio of 0.05.

A DLS control experiment to verify the size distribution profile of NaDC solutions in the current study. Peaks ~ 1 nm and ~500 nm corresponds to primary and secondary aggregates of bile salts.

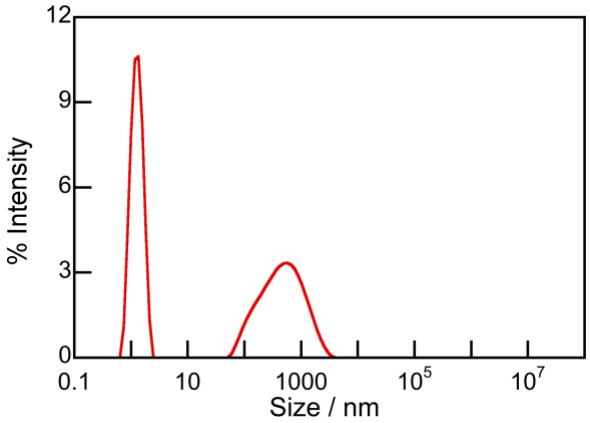

Figure A-5 Size distribution profile of 25 mM NaDC solution in water.

Appendix B.

B-1– B-5: Release experiments with NaDC-CB[6] gels tagged with 10 µM rhodamine 6G were performed to confirm the reproducibility of these experiments. As seen in Figure B-5, release of rhodamine 6G was unaffected by the presence of CB[6] in the gel. Time period to reach half the maximum release ($T_{1/2}$) was 100 min for all the gels irrespective of CB[6] concentration. The release pattern and $T_{1/2}$ is in agreement with the data in Figure 3.3.

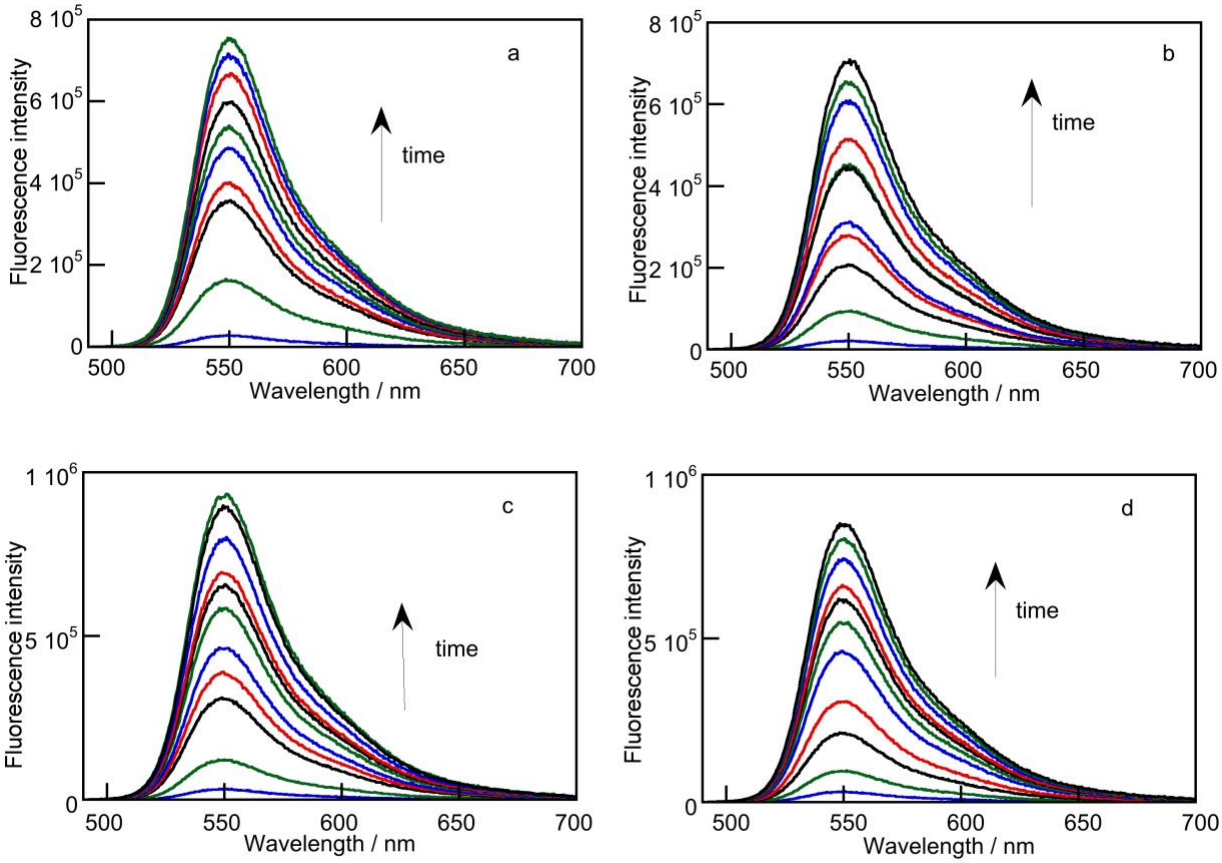

Figure B-1 Emission spectra of the surrounding medium collected at different time points during the release of rhodamine 6G (10 µM) dye from NaDC gels (50 mM) with different CB[6]/NaDC ratios: 0 (a), 0.05 (b), 0.1 (c), 0.15 (d).

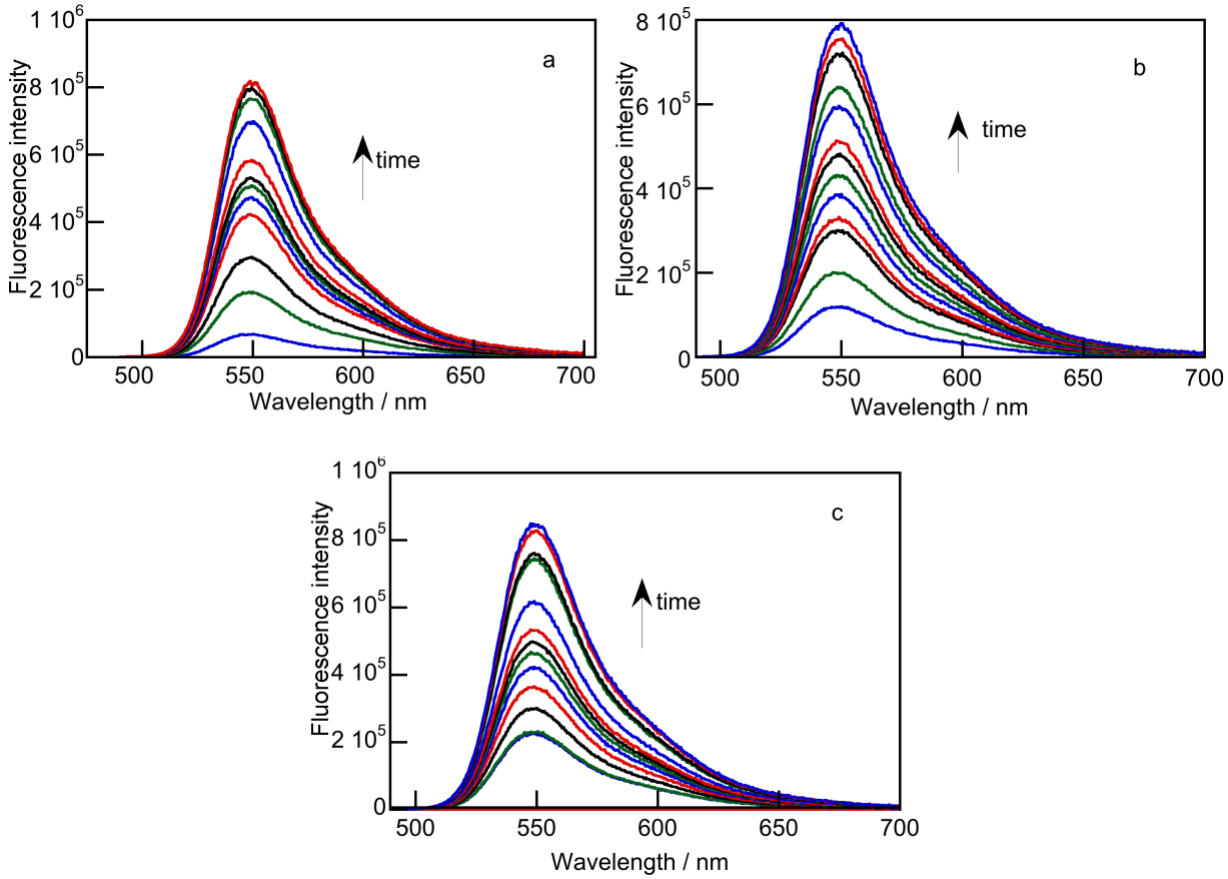

Figure B-2 Emission spectra of the surrounding medium collected at different time points during the release of rhodamine 6G (10 μM) dye from NaDC gels (50 mM) with different CB[6]/NaDC ratios: 0 (a), 0.05 (b), 0.1 (c).

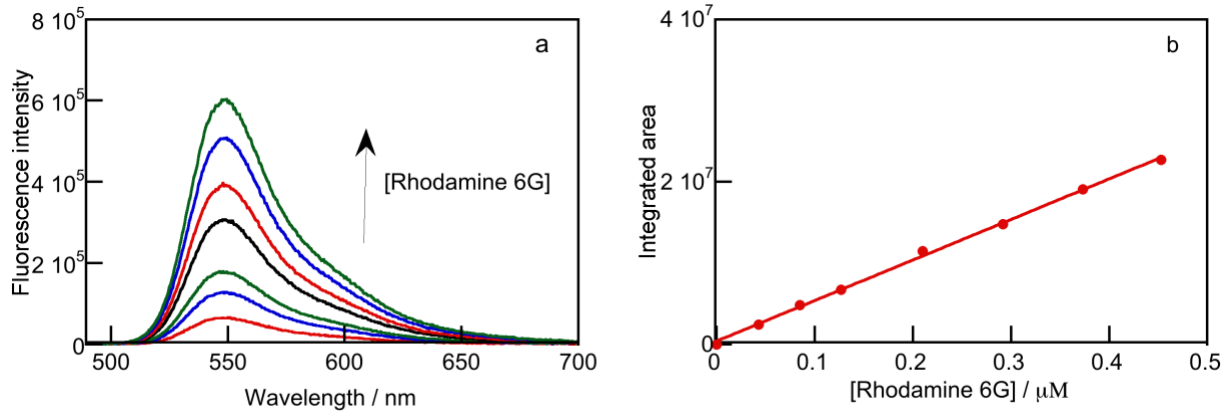

Figure B-3 a. Emission spectra of known concentrations of rhodamine 6G in phosphate buffer collected for the calibration curve. b. Calibration curve.

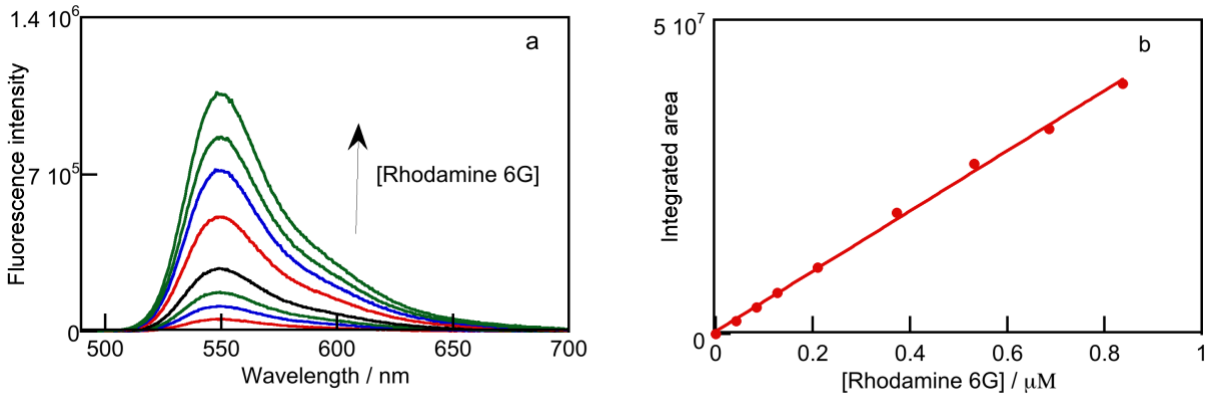

Figure B-4 a. Emission spectra of known concentrations of rhodamine 6G in phosphate buffer collected for the calibration curve. b. Calibration curve.

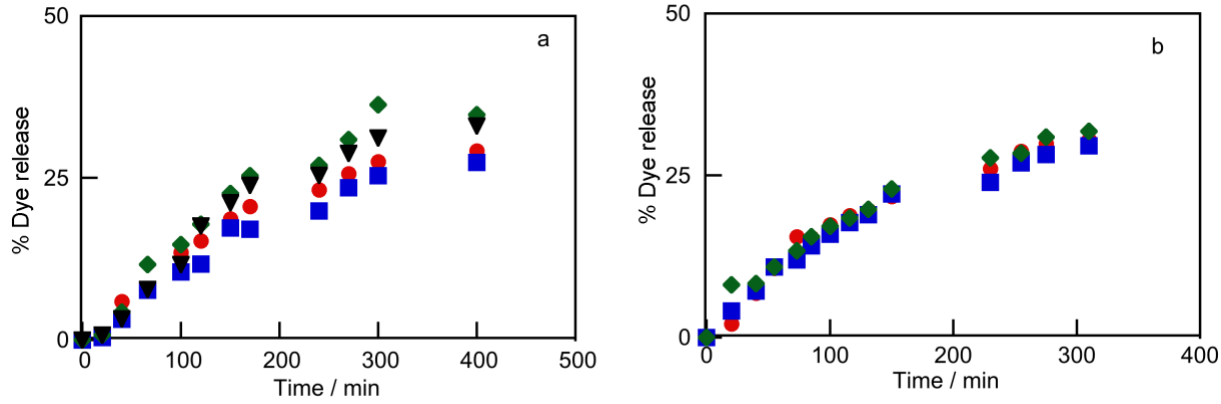

Figure B-5 Release profile for rhodamine 6G (10 μM) dye from NaDC gels (50 mM) with different CB[6]/NaDC ratios: 0 (red), 0.05 (blue), 0.1 (green), 0.15 (black). Panels a and b correspond to the data collected for two independent experiments on different days.

B-6 – B-7: Reproducibility of the release experiments of NaDC-CB[6] gels tagged with 1 mM rhodamine 6G was tested. As seen in Figure B-7, release pattern of the dye is similar for gels at CB[6]/NaDC ratios of 0, 0.05, 0.1. However for gels at CB[6]/NaDC ratios of 0.15, burst release pattern was observed where the percentage release reached maximum before the first reading collected at 60 min. The release pattern was observed to be consistent with Figure 3.6.

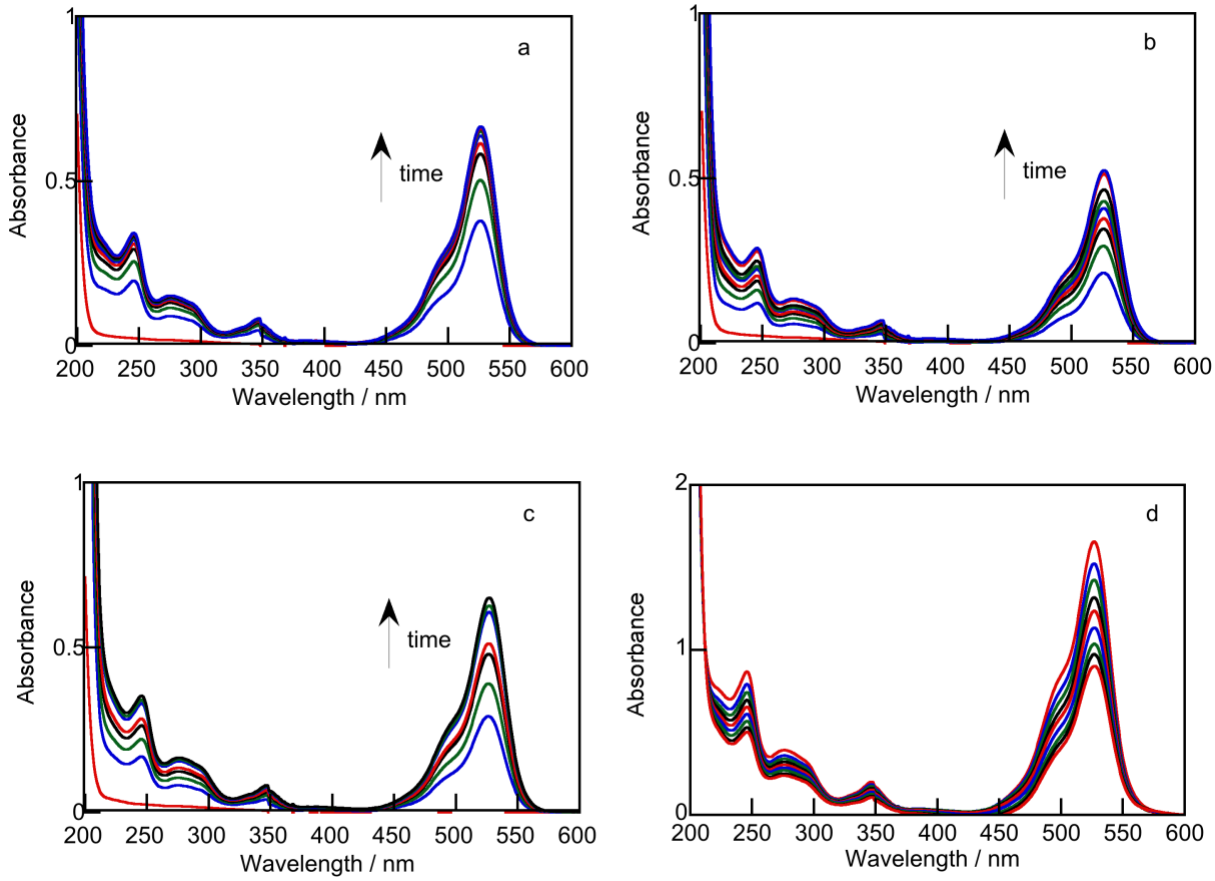

Figure B-6 Absorption spectra of the surrounding medium collected at different time points during the release of rhodamine 6G (1 mM) dye from NaDC gels (50 mM) with different CB[6]/NaDC ratios: 0 (a), 0.05 (b), 0.1 (c), 0.15 (d).

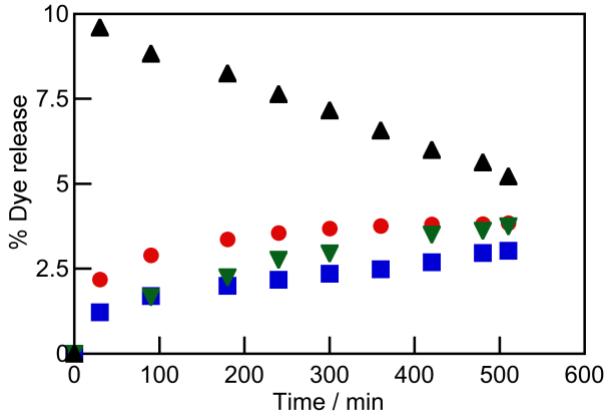

Figure B-7 Release profile for rhodamine 6G (1 mM) dye from NaDC gels (50 mM) with different CB[6]/NaDC ratios: 0 (red), 0.05 (blue), 0.1 (green), 0.15 (black).

B-8 – B-10: To confirm the reproducibility, release experiments with NaDC-CB[6] gels tagged with 5 µM pyrene were performed. As seen in Figure B-10, the amount of dye released from the gel into the surrounding media decreased with the increase in the CB[6]/NaDC ratio in the gel. The release pattern and $T_{1/2}$ (95 min) were in agreement with the data in Figure 3.9.

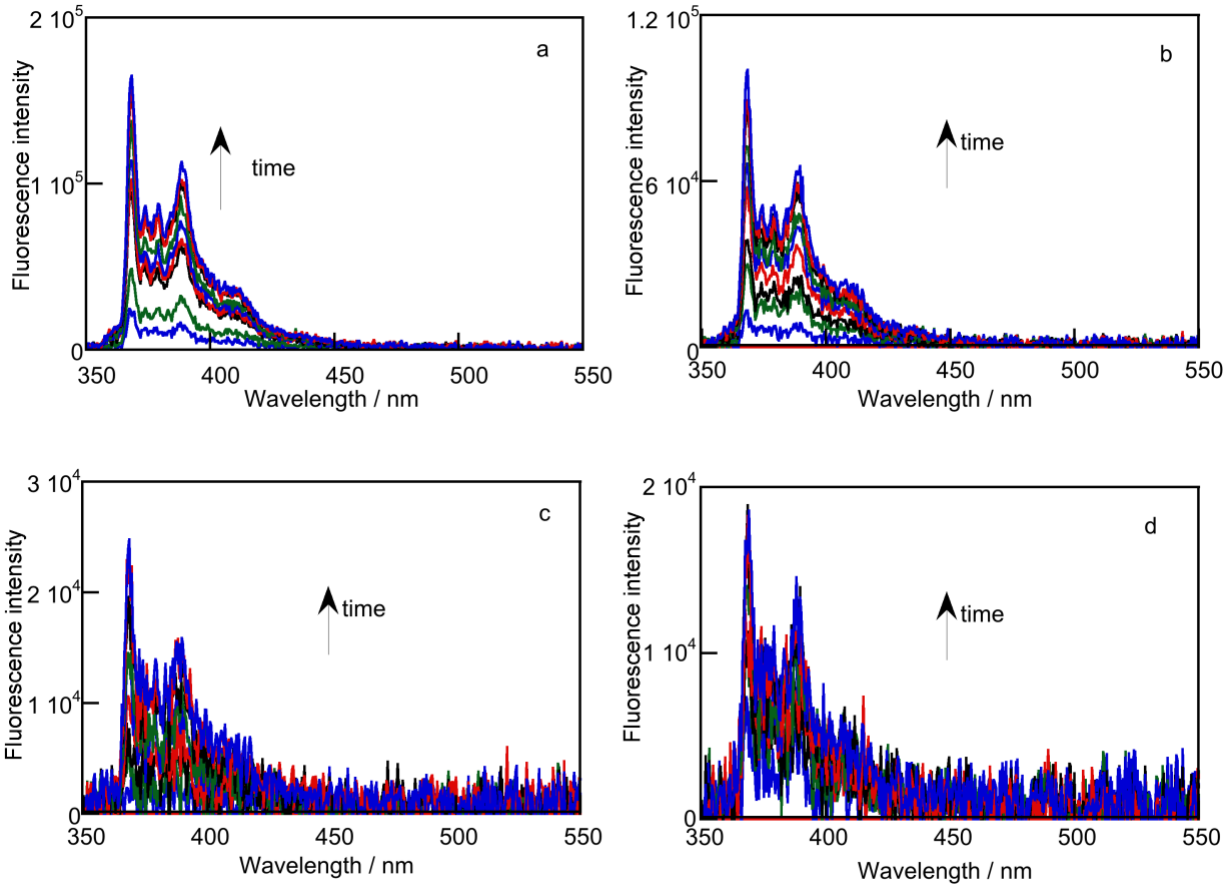

Figure B-8 Emission spectra of the surrounding medium collected at different time points during the release of pyrene (5 µM) dye from NaDC gels (50 mM) with different CB[6]/NaDC ratios: 0 (a), 0.05 (b), 0.1 (c), 0.15 (d).

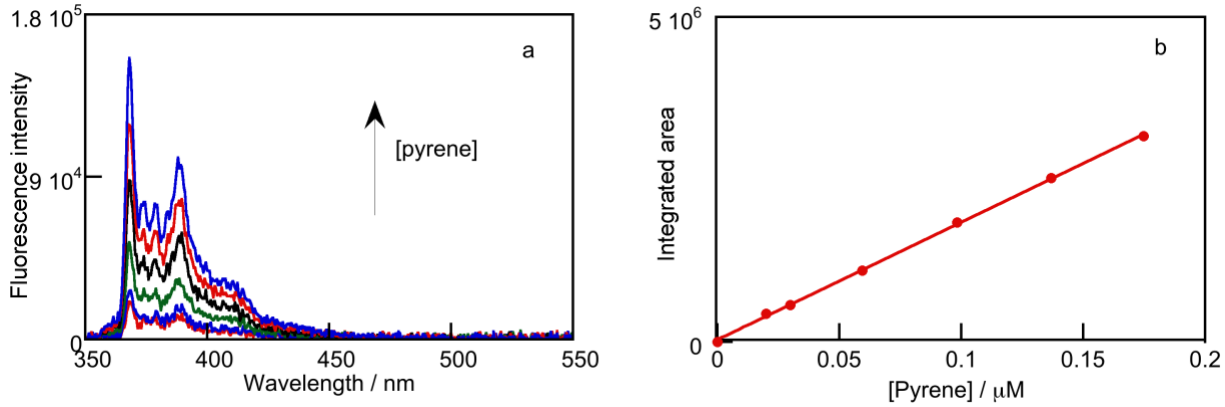

Figure B-9 a. Emission spectra of known concentrations of pyrene in phosphate buffer collected for the calibration curve. b. Calibration curve.

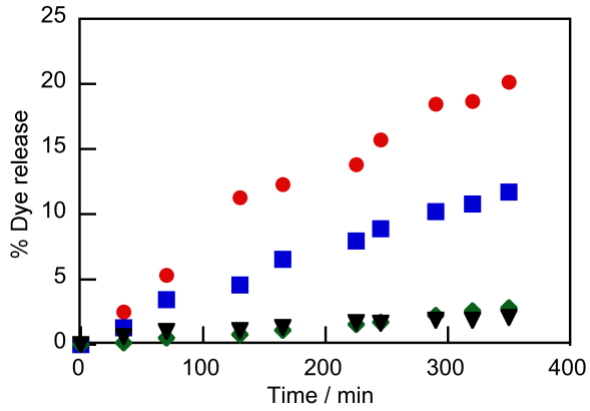

Figure B-10 Release profile for pyrene (5 μM) dye from NaDC gels (50 mM) with different CB[6]/NaDC ratios: 0 (red), 0.05 (blue), 0.1 (green), 0.15 (black).

B-11 – B-13: Loading experiments were performed to test the loss of any dye to the walls of sample vial while the gel was formed. As seen in Figure B-11 and B-13, scattering from sol samples was observed at the shorter wavelengths. Baseline corrections were performed on the raw data and LE% was determined using equation 3.4 (Table 3.1).

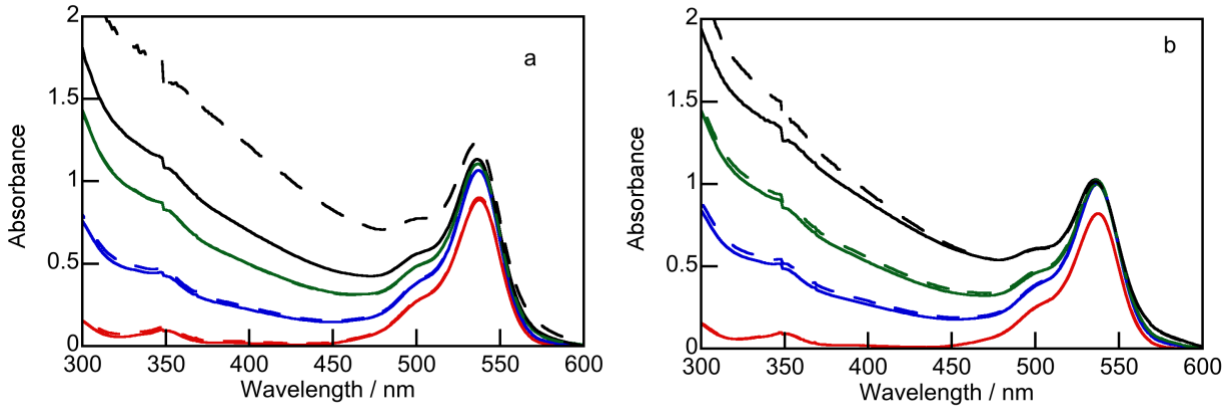

Figure B-11 Absorption spectra for rhodamine 6G (10 µM) in NaDC gels (50 mM) at different CB[6]/NaDC ratios: 0 (red), 0.05 (blue), 0.1 (green), 0.15 (black) collected at 0 h (solid lines) and 20 h (dashed lines) after sample preparation during different days (a,b).

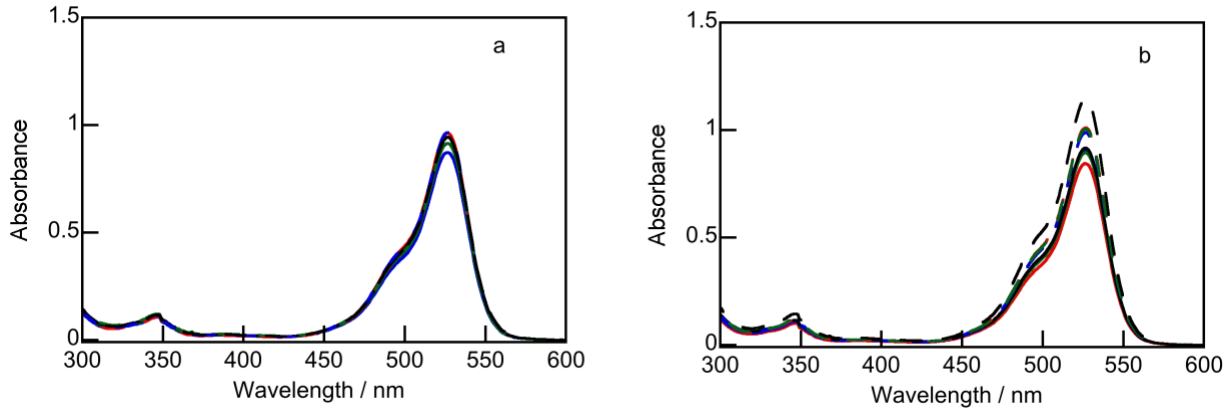

Figure B-12 Absorption spectra for rhodamine 6G (1 mM) in NaDC gels (50 mM) at different CB[6]/NaDC ratios: 0 (red), 0.05 (blue), 0.1 (green), 0.15 (black) collected at 0 h (solid lines) and 20 h (dashed lines) after sample preparation during different days (a,b).

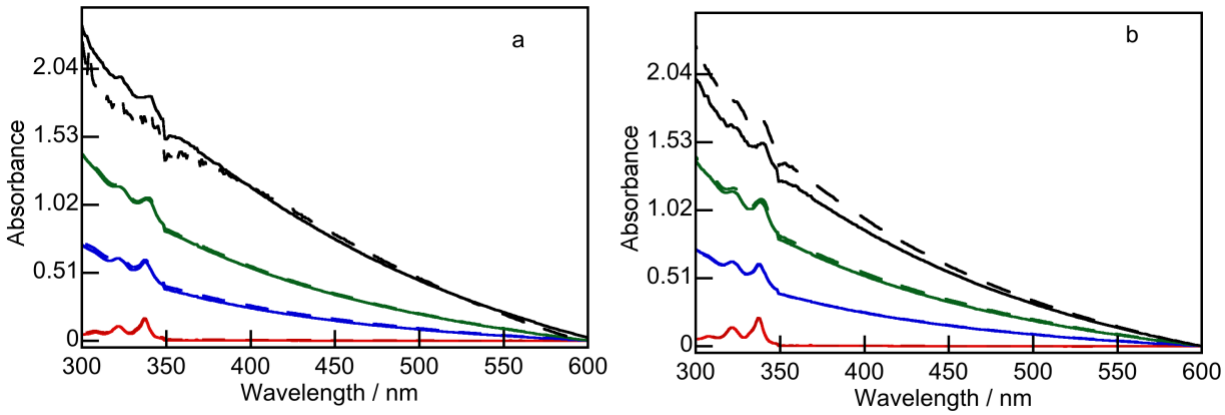

Figure B-13 Absorption spectra for pyrene (5 µM) in NaDC gels (50 mM) at different CB[6]/NaDC ratios: 0 (red), 0.05 (blue), 0.1 (green), 0.15 (black) collected at 0 h (solid lines) and 20 h (dashed lines) after sample preparation on different days (a,b).

B-14 – B-16: Mass balance experiments were performed to test the loss of any dye to the walls of sample vial during the release. As seen in Figure B-14 and B-16, scattering from sol samples was observed at the shorter wavelengths Baseline corrections were performed on the raw data and MB was determined using equation 3.3 (Table 3.1).

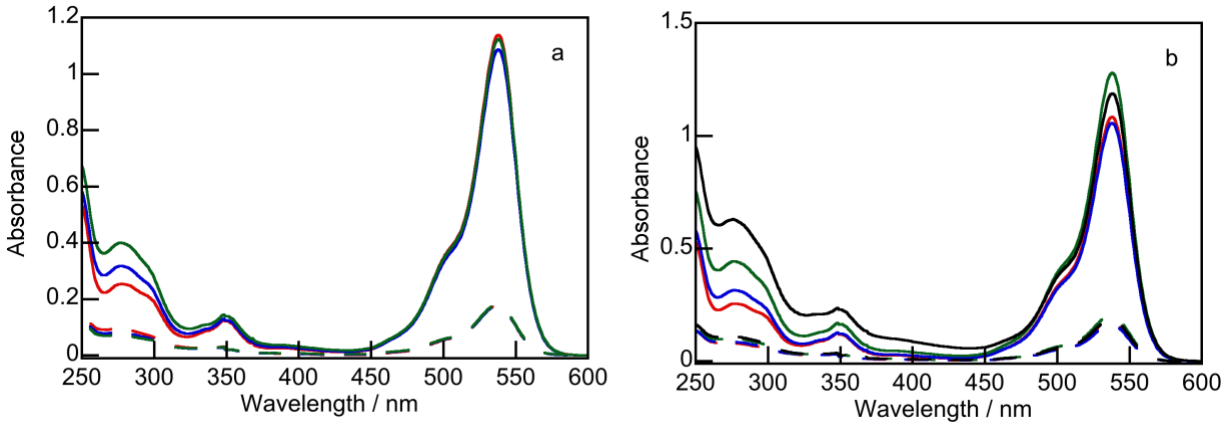

Figure B-14 Absorption spectra for rhodamine 6G (10 µM) in NaDC gels (50 mM) at different CB[6]/NaDC ratios: 0 (red), 0.05 (blue), 0.1 (green), 0.15 (black) collected at 0 h (solid lines) and end of the release studies (dashed lines) on different days (a,b).

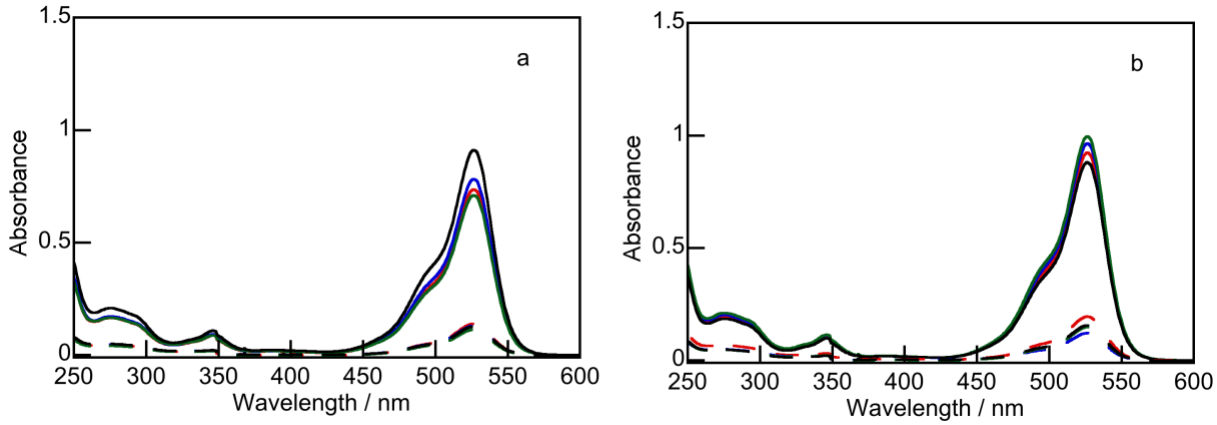

Figure B-15 Absorption spectra for rhodamine 6G (1 mM) in NaDC gels (50 mM) at different CB[6]/NaDC ratios: 0 (red), 0.05 (blue), 0.1 (green), 0.15 (black) collected at 0 h (solid lines) and end of the release studies (dashed lines) on different days (a,b).

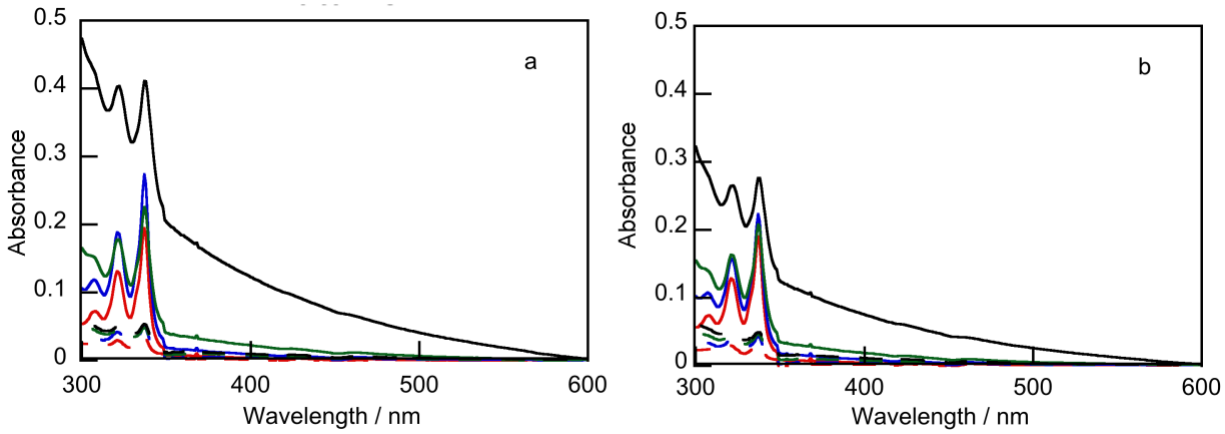

Figure B-16 Absorption spectra for pyrene (5 µM) in NaDC gels (50 mM) at different CB[6]/NaDC ratios: 0 (red), 0.05 (blue), 0.1 (green), 0.15 (black) collected at 0 h (solid lines) and end of the release studies (dashed lines) on different days (a,b).

B-17: A control experiment was performed in the absence of the dye with gels at CB[6]/NaDC ratios of 0, 0.05, 0.1, 0.15 to show the scattering from the sol. As seen in Figure B-17, scattering from the samples is dominant at shorter wavelengths and increased with the CB[6]/NaDC ratio in the gels.

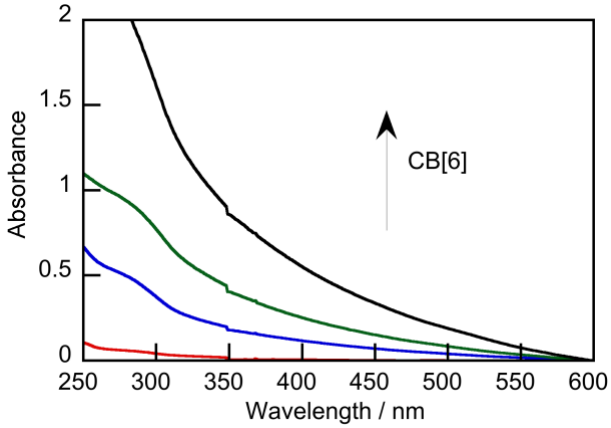

Figure B-17 Absorption spectra for NaDC gels (50 mM) at different CB[6]/NaDC ratios: 0 (red), 0.05 (blue), 0.1 (green), 0.15 (black) in the absence of the dye.

Appendix C.

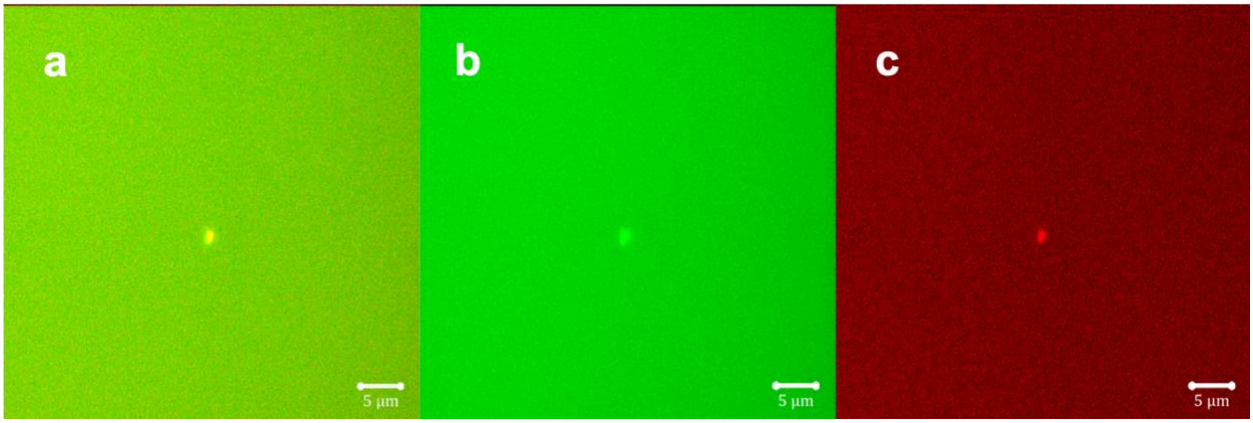

Figure C-1 Confocal images of NaDC gel tagged with berberine (2 µM) and rhodamine 6G (2 µM) collected using a 63× objective lens. Images a, b and c correspond to the merged, berberine and rhodamine 6G channels, respectively.

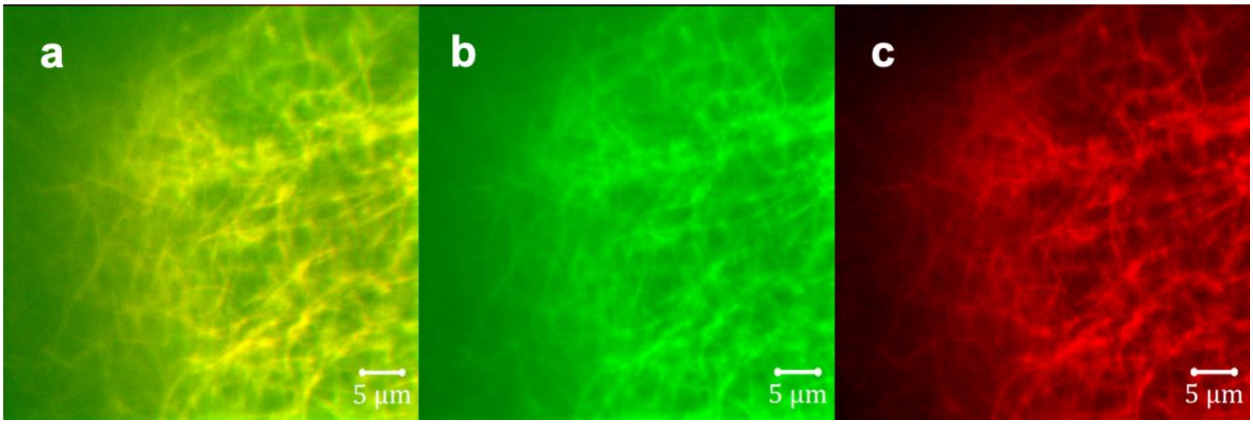

Figure C-2 Confocal images of NaDC-CB[6] gel (0.15 CB[6]/NaDC ratio) tagged with berberine (2 µM) and rhodamine 6G (2 µM) collected using a 63× objective lens. Images a, b and c correspond to the merged, berberine and rhodamine 6G channels, respectively.

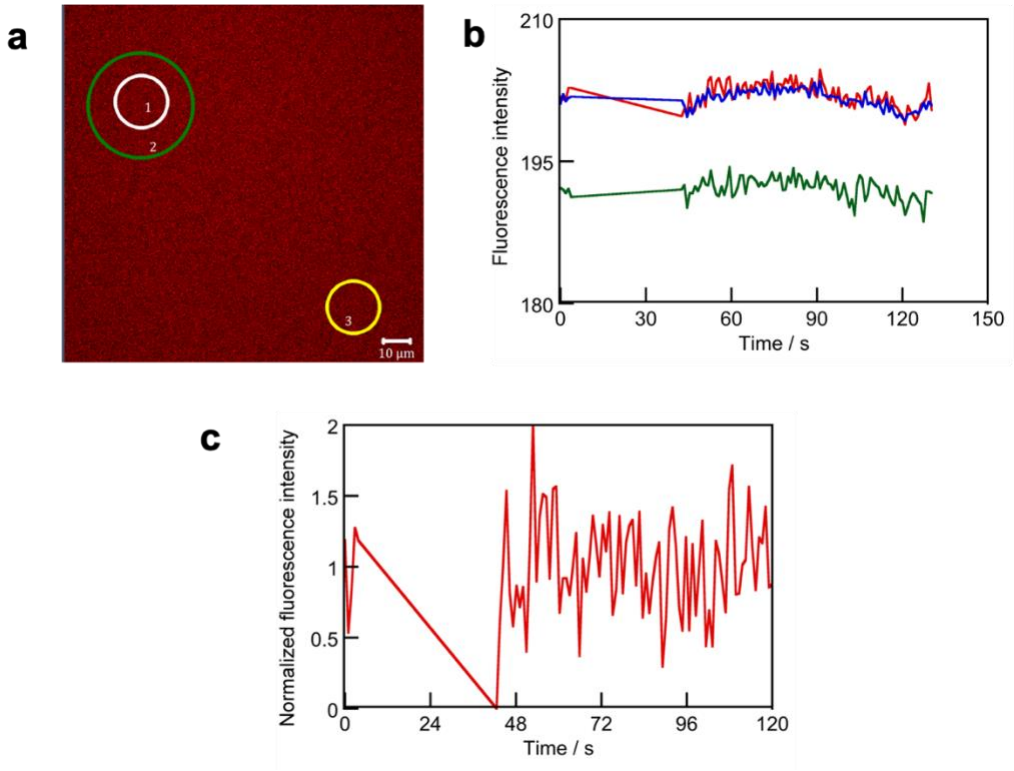

Figure C-3 FRAP analysis of the aqueous phase in the NaDC gel tagged with nile red showing a. Regions of interest bleached (white circle) and analyzed (white, green, yellow circles), b. Fluorescence recovery over time in the regions of interest with white, green and yellow circles representing ROI1, ROI2, ROI3, respectively. Red, blue and green traces correspond to ROI1, ROI2, ROI3, respectively, c. Normalized fluorescence recovery curve with time.

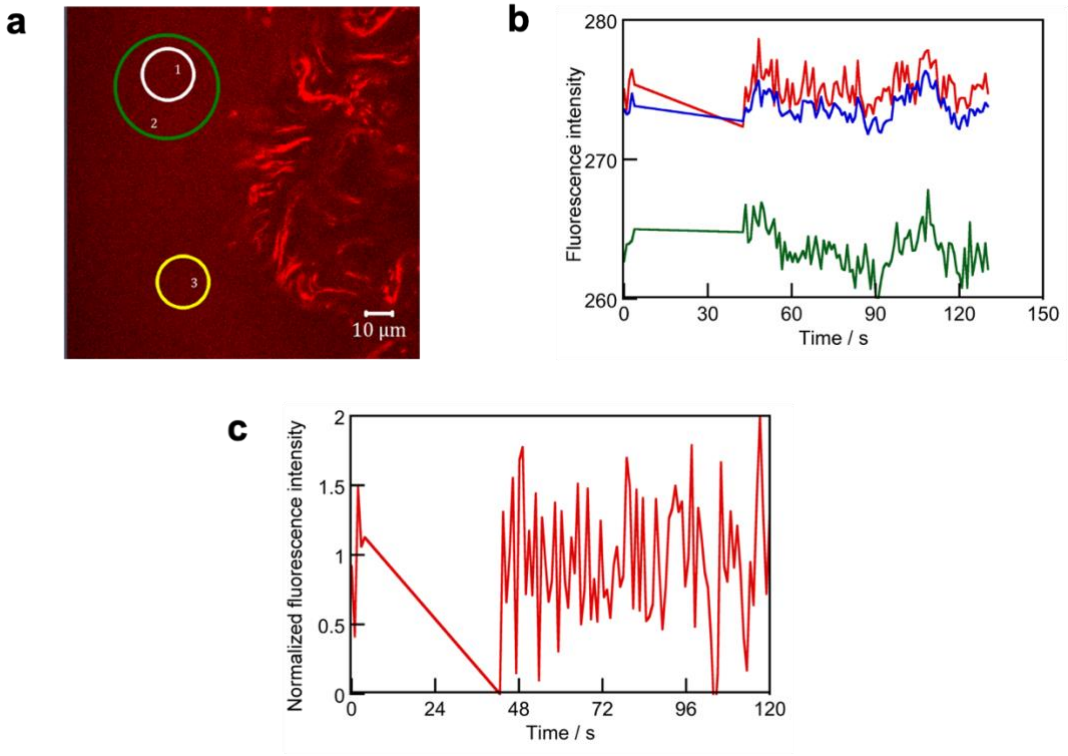

Figure C-4 FRAP analysis of the aqueous phase in the NaDC-CB[6] (0.15) gel tagged with nile red showing a. Regions of interest bleached (white circle) and analyzed (white, green and yellow circles), b. Fluorescence recovery over time in the regions of interest with white, green and yellow circles representing ROI1, ROI2, ROI3, respectively. Red, blue and green traces correspond in to ROI1, ROI2, ROI3, respectively, c. Normalized fluorescence recovery curve with time.

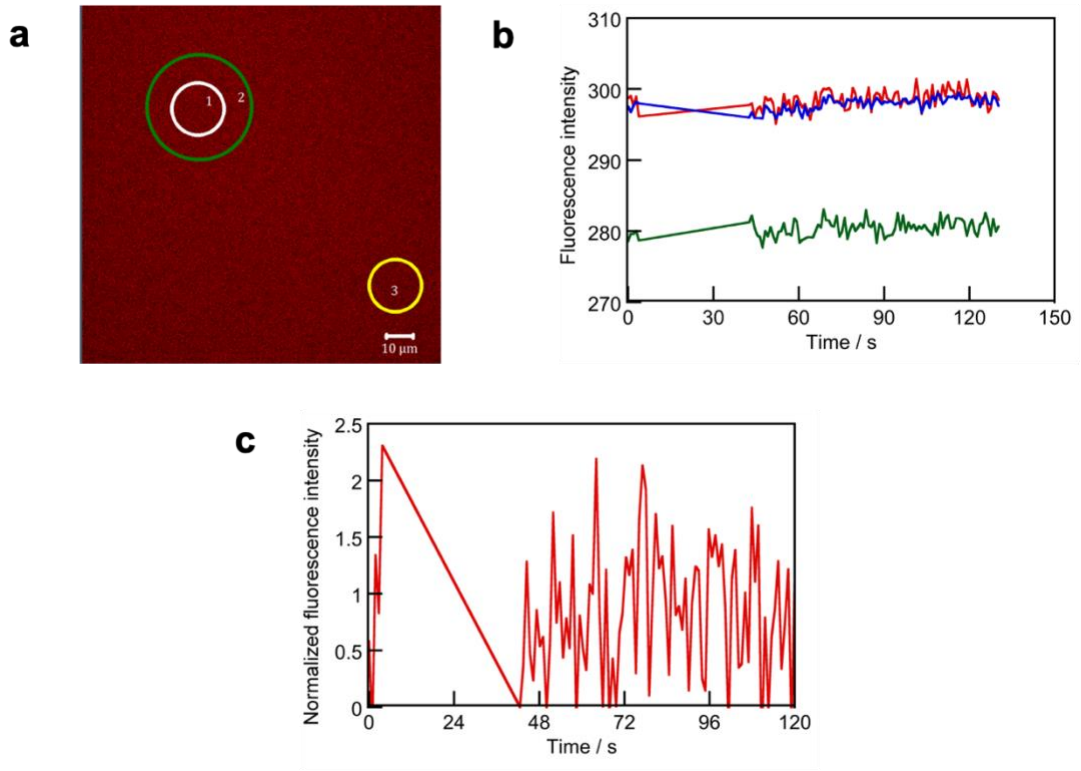

Figure C-5 FRAP analysis of the NaDC solution tagged with nile red showing a. Regions of interest bleached (white circle) and analyzed (white, green and yellow circles), b. Fluorescence recovery over time in the regions of interest with white, green and yellow circles representing ROI1, ROI2, ROI3, respectively. Red, blue and green traces correspond to ROI1, ROI2, ROI3, respectively, c. Normalized fluorescence recovery curve with time.

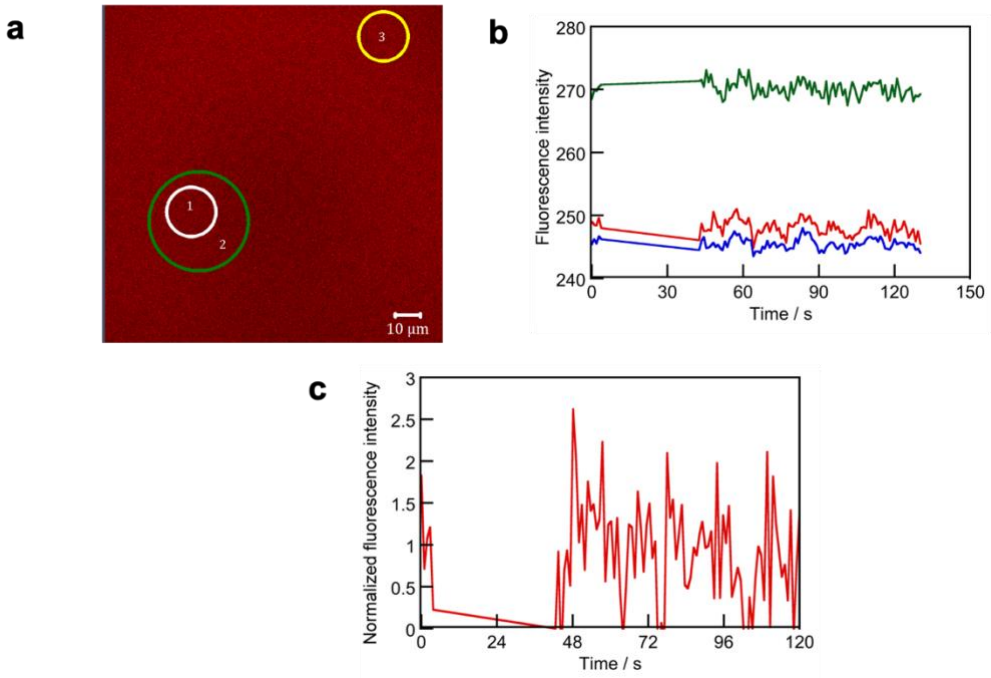

Figure C-6 FRAP analysis of NaDC-CB[6] (0.15) solution tagged with nile red showing a. Regions of interest bleached (white circle) and analyzed (white, green and yellow circles), b. Fluorescence recovery over time in the regions of interest with white, green, yellow circles representing ROI1, ROI2, ROI3, respectively. Red, blue and green traces correspond to ROI1, ROI2, ROI3, respectively, c. Normalized fluorescence recovery curve with time.

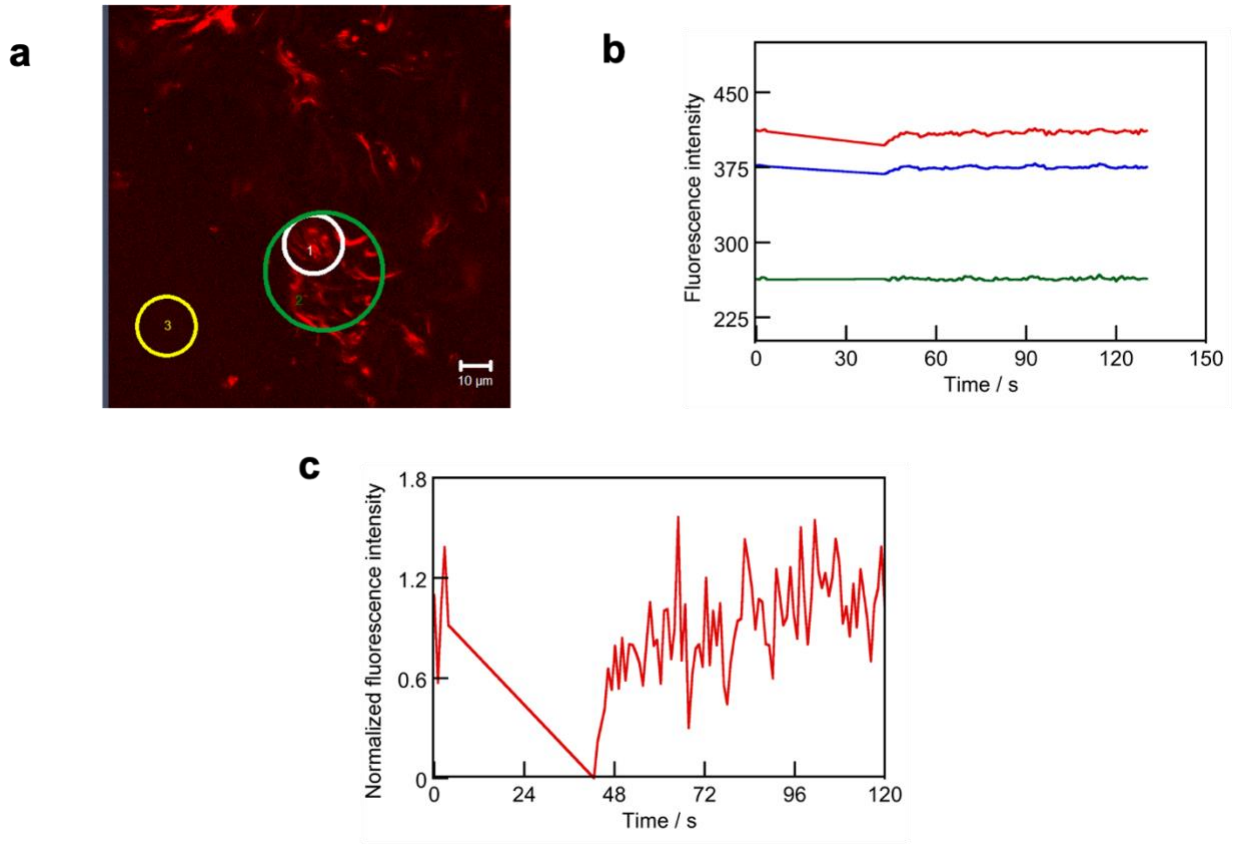

Figure C-7 FRAP analysis of NaDC-CB[6] (0.15) gel structure tagged with nile red showing a. Regions of interest bleached (white circle) and analyzed (white, green and yellow circles), b. Fluorescence recovery over time in the regions of interest with white, green and yellow circles representing ROI1, ROI2, ROI3, respectively. Red, blue andk green traces correspond to ROI1, ROI2, ROI3, respectively, c. Normalized fluorescence recovery curve with time. The observed $T_{1/2}$ for nile red in NaDC-CB[6] gel structure is 7±3 s.

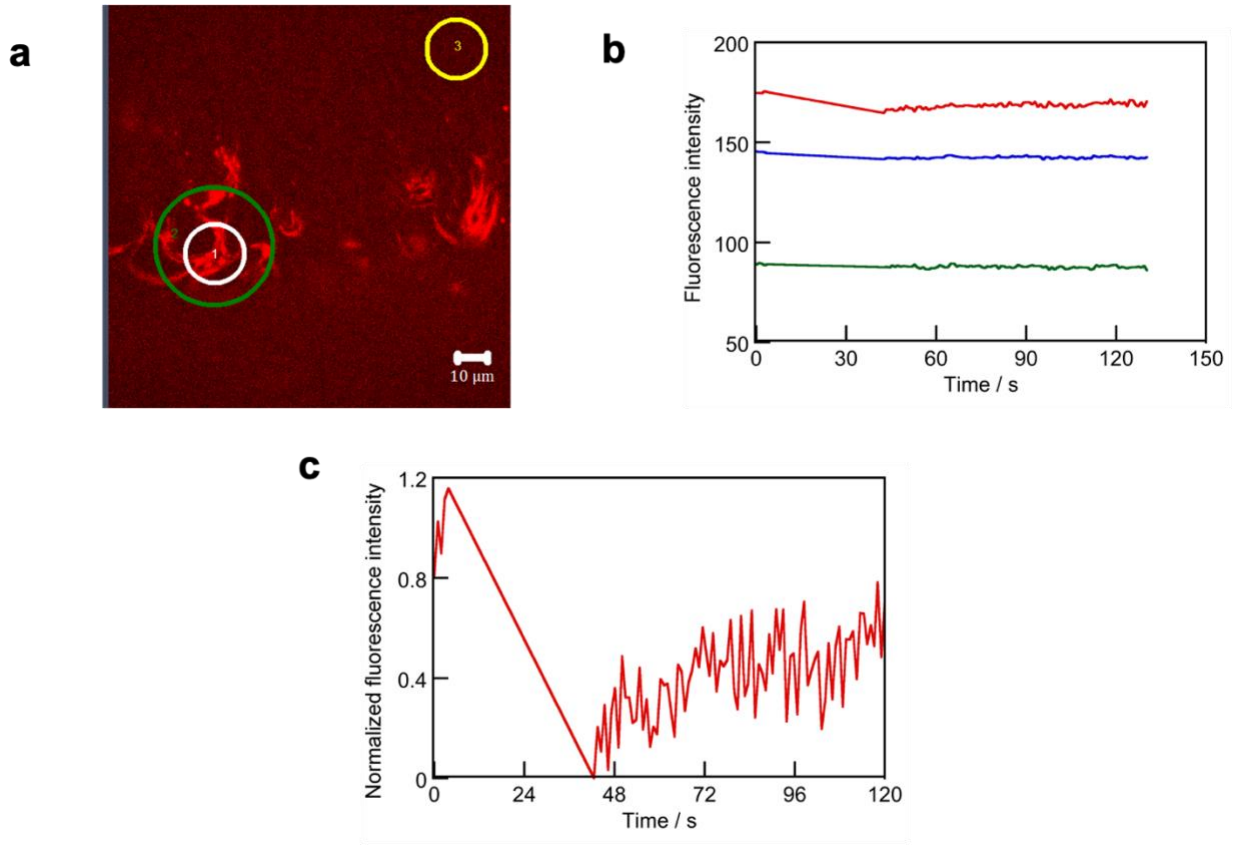

Figure C-8 FRAP analysis of NaDC-CB[6] (0.15) gel structure tagged with nile red showing a. Regions of interest bleached (white circle) and analyzed (white, green, yellow circles), b. Fluorescence recovery over time in the regions of interest with white, green and yellow circles representing ROI1, ROI2, ROI3, respectively. Red, blue and green traces correspond to ROI1, ROI2, ROI3, respectively, c. Normalized fluorescence recovery curve with time. The observed $T_{1/2}$ for nile red in NaDC-CB[6] gel structure is 20±10 s.